IOWA STATE UNIVERSITY
Digital Repository

2018

Evaluation of an innovative joint design for the adjacent box beam bridges

Zhengyu Liu
Iowa State University

Follow this and additional works at: https://lib.dr.iastate.edu/etd

Part of the Civil Engineering Commons

Evaluation of an innovative joint design for the adjacent box beam bridges

by

Zhengyu Liu

A dissertation submitted to the graduate faculty

in partial fulfillment of the requirements for the degree of

DOCTOR OF PHILOSOPHY

Major: Civil Engineering (Structural Engineering)

Program of Study Committee:
Brent M. Phares, Major Professor
Behrouz Shafei-Pamsari
Jiehua (Jay) Shen
Wei Hong
Jennifer Shane

The student author, whose presentation of the scholarship herein was approved by the program of study committee, is solely responsible for the content of this dissertation. The Graduate College will ensure this dissertation is globally accessible and will not permit alterations after a degree is conferred.

Iowa State University

Ames, Iowa

2018

TABLE OF CONTENTS

LIST OF FIGURES

LIST OF TABLES

ABSTRACT

Bridges constructed with adjacent precast prestressed concrete box beams have been in service for many years and provide an economical solution for short and medium span bridges. A recurring problem with this type of bridge is the cracking in the longitudinal joints between adjacent beams, resulting in reflective cracks forming in the asphalt wearing surface or concrete deck. AASHTO (2014) states that the differential shrinkage due to differences in age, concrete mix, environmental conditions etc., have been observed to cause internal force effects that are difficult to predict at the design phase. The objective of this research is to develop an innovative design of the connection used in adjacent precast concrete box beam bridges to eliminate cracking and leakage in the longitudinal joints between adjacent boxes.

To meet the research goal, a comprehensive review of relevant specifications and technical literature from the past twenty years has been conducted to study the design and construction attributes influencing the long-term performance of the box beam bridge joint and identify the reasons that cause cracking in the joint between the adjacent box beams. A three step evaluation of joint was conducted on the material level, small scale level and full scale level. In each level of evaluation, both experimental and analytical evaluation were conducted. The results indicated that the innovative connection can create a crack-free joint without the utilization of a shear key nor transverse post-tensioning. Both experimental and analytical results indicate that the innovative joint showed good performance in resisting joint cracks in both the early-age and the long-term service life of the bridge. The "compression-dominate-joint" created by the expansive joint material combined with transverse reinforcing steel across the interface is expected to overcome the difficulties in predicting the early-age internal forces during the design

phase stated by AASHTO (2014). To further investigate the performance of this joint detail, it is recommended that a field trial be completed. During this field trial, the bridge should be monitored and evaluated during early age concrete curing as well as for a period of at least two years following construction.

CHAPTER 1. INTRODUCTION

Bridges constructed with adjacent precast prestressed concrete box beams have been in service for many years and provide an economical solution for short and medium span bridges. A recurring problem with this type of bridge is the cracking in the longitudinal joints between adjacent beams, resulting in reflective cracks forming in the asphalt wearing surface or concrete deck. The cracking appears to be initiated by stresses induced by early-age shrinkage, temperature gradients, live loads, or a combination. Once the cracking has occurred, chloride-laden water can penetrate the cracks and cause corrosion of the reinforcement and prestressing strands. In the United States, there are three typically used generic partial depth joint geometries (Types I, II and III joints) and one full depth joint geometry (Type IV joint), all of which are shown in Figure 1-1. The typically used Japanese joint is a full depth joint (Type V) which is also shown in Figure 1-1. Lall et al. (1998) and Sang (2010) indicated that full depth joints show superior cracking prevention ability than the partial depth joint. El-Remaily et al. (1996) reported that longitudinal cracking was seldom found in adjacent box beam bridges with the Type V full depth joint.

1.1 Background

NCHRP Synthesis 39: Adjacent Precast Concrete Box Beam Bridges: Connection Details reported a wide variety of practices used by state highway agencies for the connection details between adjacent box beams. These practices include partial depth or full depth joints, joints grouted before or after transverse post-tensioning, prepackaged or non-prepackaged grout materials, post-tensioned or non-tensioned transverse ties, a wide range of applied transverse post-tensioning forces, and cast-in-place concrete decks or no decks. A few states reported that

their methods had reduced the longitudinal cracking, whereas others had not been successful using similar methods. NCHRP Synthesis 39 indicated that research to evaluate those practices at the design and construction phases could lead to connection details that prevent cracking and leakage at the joints and extend the service life of adjacent box beam bridges.

AASHTO (2014) states that the differential shrinkage due to differences in age, concrete mix, environmental conditions etc., have been observed to cause internal force effects that are difficult to predict at the design phase. To date, most researchers have analytically studied long-term joint behavior or experimentally investigated the early-age joint, but only a few have analytically studied the stress development during the early-age.
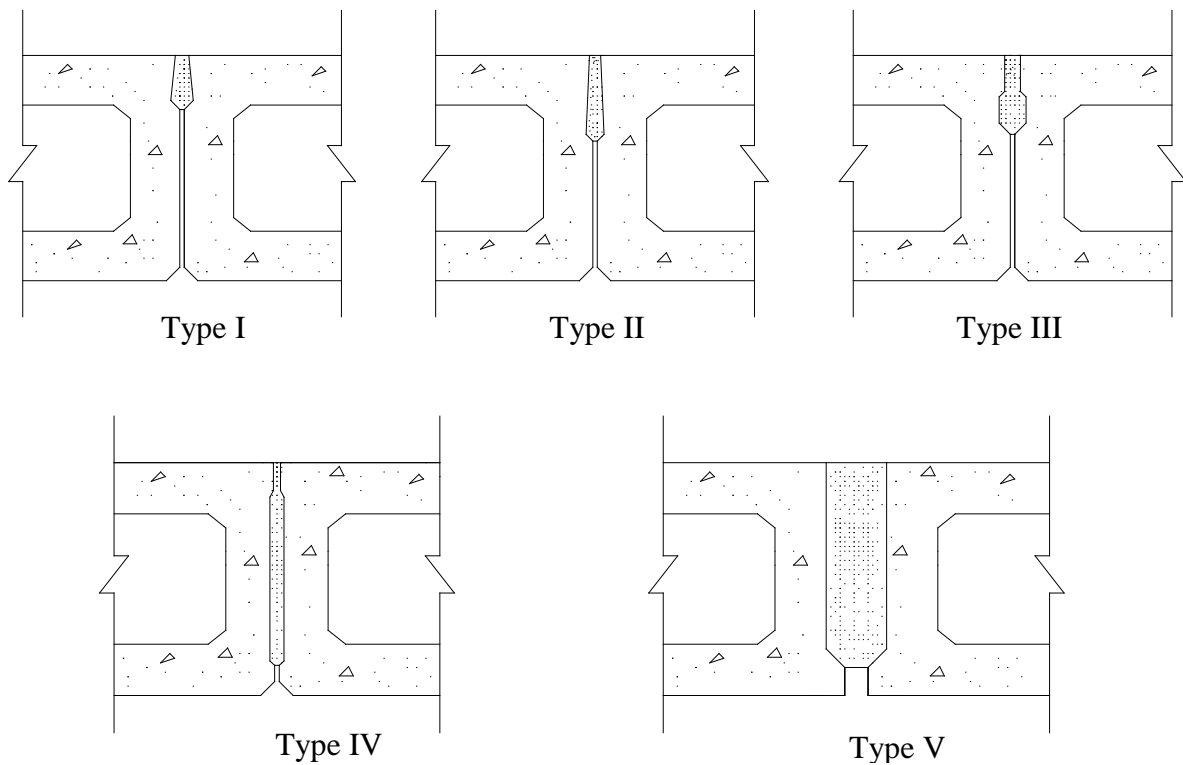
Figure 1-1 Basic Joint Geometries

1.2 Research objective and significances

The objective of this research is to develop an innovative design of the connection used in adjacent precast concrete box beam bridges to eliminate cracking and leakage in the longitudinal joints between adjacent boxes. This dissertation not only demonstrates the efficiency of an innovative joint detail but also provides details for the modeling of early-age joint between adjacent box beams and opens the door for predicting internal stress in fresh concrete on bridge structures.

1.3 Research outline

To meet the research goal which results in an adjacent box beam bridge that is crack and leak-free, a comprehensive review of relevant specifications and technical literature from the past twenty years has been conducted to study the design and construction attributes influencing the long-term performance of the box beam bridge joint and identify the reasons that cause cracking in the joint between the adjacent box beams. A three step experimental and analytical evaluation were then conducted with details as follows.

The objective of the first step is to select a better beam joint material that can resist early-age cracking in the joint between adjacent box beams. To achieve this objective, two phases of laboratory material characterization tests were conducted: Phase I, material selection and Phase II, time dependent material properties test. During Phase I, four different types of joint materials were tested: epoxy grout and (non-shrink) construction grout for the Type IV joint and shrinkage compensated concrete (mixed with Type K cement) and fiber reinforced concrete for the Type V joint. The materials were evaluated based upon shrinkage, flexural tensile strength and interfacial normal bond strength. During Phase II, time dependent material testing was conducted on the "best" materials from Phase I to characterize the nonlinear changes in bond strength,

compressive and tensile strength with time. Kanstad's (1990) time dependent material property equation was calibrated with the compressive strength and split cylinder tensile strength test data for the shrinkage compensated concrete. A finite element modeling approach capable of simulating the early-age joint behavior was developed and used for the further study. The objective of the finite element modeling was to calculate stress development in the joint during early-age and to evaluate the structural performance of both Type IV joint with epoxy grout and Type V joint with shrinkage compensated concrete subject to material self-volume change. Two finite element models were developed for a 4ft long beam-joint-beam structure and the calculated stress distribution in the joint was determined and analyzed.

In the second step, an innovative joint was designed based on the results from the literature review and the first step, and proposed to eliminate joint cracking. The design was evaluated with a series of small scale tests and analytical models. The small scale tests were conducted on four 3-ft. long specimens with different joint reinforcement ratios to study the effect of the joint reinforcement. The early-age joint behavior was monitored and an ultimate load test was performed. Finite element models were developed to calculate the time-dependent stress development in the joint and at the interface between the joint and the box beam concrete and validated with the experimental results. The behaviors of the joints with different reinforcement ratios were evaluated based on both the experimental and analytical results.

In the last step, the innovative joint design was further experimentally and analytically evaluated on a full-scale structure. A 31ft long specimen consisting of two box beams and one innovative joint was fabricated and tested in the laboratory. The early-age joint behavior subject to daily temperature change, heat of hydration, and material self-volume change was monitored. The joint was then tested under multiple levels of cyclic loadings and an ultimate horizontal

transverse loading. To investigate the early-age joint behavior and study the time-dependent stress development in the joint, a finite element model was developed based on the modeling approach proposed in the first step and validated with the early-age experimental test results.

The results from the comprehensive literature review is presented in Chapter 2. The research details and results of each step was summarized in paper format and presented in Chapter 3, 4 and 5. The general conclusion and the future study direction was summarized in Chapter 6.

1.4 References

El-Remaily, A., Tadros, M. K., Yamane, T., and Krause, G. (1996). "Transverse design of adjacent precast prestressed concrete box girder bridges." PCI Journal, 41, 96-113.

Kanstad, T., Hammer, T. A., Bjøntegaard, Ø., & Sellevold, E. J. (1999). Mechanical properties of young concrete: Evaluation of test methods for tensile strength and modulus of elasticity. Determination of model parameters. NOR-IPACS report STF22 A99762.

Lall, J., S. Alampalli, and E. F. DiCocco. (1998). "Performance of Full-Depth Shear Keys in Adjacent Prestressed Box Beam Bridges." PCI Journal, 43(2), 72-79.

Sang, Z. (2010). "A Numerical Analysis of the Shear Key Cracking Problem in Adjacent Box Beam Bridges." Doctoral dissertation, The Pennsylvania State University.

CHAPTER 2. LITERATURE REVIEW

A comprehensive literature search was conducted to collect information relevant to the research. These data were gathered, categorized, and summarized so as to study the design and construction attributes influencing the long-term performance of the box beam bridge joint and identify the reasons that cause cracking in the joint between the adjacent box beams. It is worth noting that a complete understanding of the current state-of-art and the state-of-practice is extremely important and invaluable at finalizing the plans for the analytical and experimental investigations It should be noted that NCHRP Synthesis 393 by Russell (2009) described current concrete box beam practices from multiple Departments of Transportation (DOT) at multiple levels and also provides extensive literature search results from before 2008.

The literature search was summarized as follows. First, NCHRP Synthesis 393 was summarized including the conclusions and recommendations. Second, literature published before 2008 will be reviewed to take note of the important information beneficial to the research. Third, literature published after 2008 was reviewed especially those with a connection to the results of NCHRP Synthesis 393. Finally, literature was summarized, synthesized, and then categorized as they relate to laboratory testing, field testing, and Finite Element analysis. Note that to provide a brief summary of each piece of literature, "Take Away" points for each are provided after each general summary (with the exception of NCHRP Synthesis 393).

2.1 NCHRP synthesis 393

The NCHRP Synthesis report by Russell (2009) summarized the observed types of distress associated with the joints used in adjacent box girder bridge systems including longitudinal cracking along the joint material and box beam interface, water and salt leakage

through the joint, cracking within the grout, spalling of the grout, spalling of the girder corners, differential vertical movement, corrosion of transverse ties and longitudinal prestressing strands, freeze-thaw damage to the grout and concrete near the joint. Note that the most common types of distress are longitudinal cracking along the grout and box beam interface, water and salt leakage through the joint, and reflective cracks that are commonly observed in the road surface.

Based on the survey of state DOTs and the literature search, Russell (2009) also began the process of identifying factors impacting the long-term performance of adjacent box beam bridge systems. In the synthesis, practices for structural design and detailing for adjacent box girder bridges from state DOTs and the literature were summarized as shown in Table 2-1. Specifications and construction practices for adjacent box girder bridges from state DOTs and the literature were also summarized as tabulated in Table 2-2. Finally, the recommended and not-recommended design and construction practices were summarized as tabulated in Table 2-3.

Russell (2009) indicated that keyway configurations consist of partial depth and full depth keyways. In the United States, three typically used generic partial depth keyway geometries are the Types I, II and III keyways and one generic full depth keyway geometry is the Type IV keyway as shown in Figure 2-1 (note that in Figure 2-1 the box beams have been shown to be in direct contact – this may or may not always be the case; however, sweep is typically removed with the application of post-tensioning). Conversely, the typically used Japanese keyway is the full depth keyway Type V shown in Figure 2-1. El-Remaily et al. (1996) reported that longitudinal cracking was seldom found in the adjacent box beam bridges with the Type V full-depth keyway.

Table 2-1 Structural Design and Details

Practices	Survey summary	Literature cited by Russell (2009)
Girder cross sections	Around 50% of states use AASHTO/PCI-shaped box beams	
Span lengths	Below 20 ft to above 80 ft	40 to 140 ft (PCI 1997; 2004)
Bridge skew	0º-60º; Most common: 30º	
Composite deck	• Most states use simple spans with composite deck (3-9 in. depth); • Bridges with multi-span and composite deck are usually designed continuous for live load.	The use of a deck does not eliminate differential rotation of girders and is not an economically and structurally efficient solution (El-Rmaily et al. 1996)
Keyway geometries	Most states use partial depth keyways; some use full depth keyways	• Longitudinal cracks were found in 54% of bridges with 12 in. partial depth keyway and 6 in. depth concrete deck and in 23% of the bridges with full depth keyways, concrete deck and more transverse ties (Lall et al. 1997; 1998). • No longitudinal cracks were found in Japanese bridges with 6 in. wide full depth keyway, cast-in-place concrete grout and 2-3 in. concrete or asphalt wearing surface (Remaily et al. 1996) • The full depth keyway hinders the joint from opening (Miller et al., 1999) • Wider full-depth keyways improves the interaction between adjacent girders and the contact between grout and girders, but forms are needed to contain the fresh grout during placement (Nottingham, 1995)
Transverse ties	• Most states use unbonded post-tensioned strands or bars; some states use bonded post-tensioned strands or bars; other states use non-presteressed reinforcements • The number of tie locations: 1-5 per span • Most states placed ties at mid-depth of girders (one tie per location) • Ties are typically placed at the third points when two ties are used at a single location	• Illinois DOT equation for the number ties per span (Anderson 2007): $N = \dfrac{\text{span}}{25} - 1 \geq 1$ • Less longitudinal cracking: Three transverse tie locations for the span less than 50 ft five for the span more than 50 ft (Lall et al. 1997; 1998) • Durable system in Japan: 4-7 evenly spaced transverse diaphragms with post-tensioning ties and post-tensioning is determined by flexural design (Yamane et al. 1994) • Partial depth keyway: Due to eccentricity of post-tensioning, cracks may be induced by post-tensioning ties at the girder mid-depth • Full depth keyway: Good with post-tensioning ties at the girder mid-depth
Post-tensioning force	• Most states specify the required post-tensioning force without extensive calculations • For 11 states: 0.5-12.5 kip/ft	• 4-14 kip/ft (El-Remaily et al. 1996) • 7-14 kip/ft (Hanna et al. 2007) • 27 kip/ft for 15 in. beam depth (Badwan and Liang et al. 2007) • 21 kip/ft per AASHTO LRFD specification (AASHTO 2007; 2008) • 4-11 kip/ft per PCI bridge design manual (PCI 1997; 2004) • Average of 11 kip/ft is Japanese practice (Yamane et al. 1994)
Exterior girders	• Most of states have the same design for exterior and interior girders	• No concrete barriers were used by Illinois DOT for box girder system because of the increased stiffness of exterior girders might cause increased differential deflections (Macioce et al. 2007) • The barrier load could be counteracted by the increased exterior girder section property (Harries 2006).

Table 2-2 Specifications and Construction Practices

Practices	Survey summary	Literature cited by Russell (2009)
Standard specifications (AASHTO 2002)		No guidelines are provided for the design and construction of the connection details of adjacent box girders
LRFD specifications (AASHTO 2007; 2008)		• A compression depth (≥7 in.) should be provided with a transverse post-tensioning ≥ 0.25 ksi • Post-tensioning ties are required to be placed at the centerline of the keyway
Bearing types	• Plain elastometic bearing: ¾ of respondents • Laminated elastomeric bearing: ¼ of respondents • Full-width support or full-point support on ends: 42% of states for each; Two-point support and one-point support: the other states • Uneven seating: half the respondents (especially for a full-width support)	
Construction sequence	• One stage construction: Erect all beams and connect them at one time • Two stage construction: a variety of sequences • Grout before/after post-tensioning: 50% of states for each • Grout after post-tensioning : higher cracking resistance • Construction sequence is affected by the skew of the bridge and intermediate diaphragm locations	Greuel et al. (2000) reported that spalling of beam bottom flanges occurred near the shear key for the two half bridges when the shear key was not grouted prior to post-tensioning
Differential camber	• Restrictions for differential camber: 1/3 of respondents • Maximum differential camber: 0.5 in. (½ of respondents) • Others: 0.25 in. in 10 ft; 0.75 in. maximum; 1 in. relative deflection for high and low beams in one span • Improving methods: load high beam before grouting and post-tensioning; adjust bearing seat elevations; concrete or asphalt topping; preassemble girders before shipment	
Keyway preparation	• Sandblast keyway: 45% of states • Sandblast and powerwash keyway:1/3 of respondents	• Poor adherence of keyway mortar (Attanayake and Aktan 2008)
Grout materials and practices	• Nonshrink grout: 40% of respondents; mortar: 25% of respondents; epoxy grout, epoxy resin, or concrete topping: other respondents • No curing: 40% of respondents; curing compounds: 5%; wet curing: around 45% of states • Most of states manually place the grout	• High-quality joint: prepackage mix with predetermined amount of water (e.g., prepackaged magnesium-ammonium-phosphate grout with pea gravel) (Nottingham 1995) • Improvements by West Virginia DOT (El-Remaily et al 1996): a pourable epoxy replacing a nonshrink grout; sandblasting surfaces; post-tensioning ties. • Andover Dam Bridge in Maine: wider shear key rapidly grouted with shrinkage-restrained self-consolidating concrete (Russell 2009) • Illinois DOT (2008): use a mechanical mixer for mixing nonshrink grout; place with a pencil vibrator; smooth surface; cover with the cotton mats for more than 7 days

Table 2-3 Recommended Practices

Practices	Recommended	Not recommended
Design practices	• Full depth keyway: grouted easily • Post-tensioning transverse ties: eliminating tensile stresses in the shear key • Cast-in-place reinforced concrete deck (compressive strength of more than 4 ksi and thickness of more than 5 in.): restrains longitudinal deck cracking	• Non-tensioned transverse ties: no crack resistant ability
Construction practices	• Form the void using stay-in-place expanded polystyrene • Sandblast the keyway surface before shipment: ensuring a better bonding surface for the grout • Powerwash the keyway surfaces (compressed air or water) before erection of girders: ensuring a better surface for the grout • Grout keyways before post-tensioning: the grout under compression • Grout with high bond strength: limit cracking • Provide suitable curing for the grout: developing desired strength and minimize shrinkage effects • Provide suitable wet curing for the concrete deck (more than 7 days): ensuring durable surface and minimize shrinkage cracks	• Use asphalt wearing surface with non-water proofing membrane: water gathers under the asphalt • Use non-prepackaged products for the keyway grout

2.2 Publications before 2008

Huckelbridge et al. (1995) revealed that precast prestressed adjacent box beams have been mostly used for the construction of bridges with short and medium spans ranging from 30ft to 100ft. The authors conducted field testing of several adjacent box girder bridges and the test results from two of these bridges were summarized in the 1995 report; one for a simply supported bridge and one for a four-span continuous bridge. A dump truck with a front axle weight of 12 kips and tandem axles weighing 38 kips was used to conduct on-site, controlled tests. During those tests, deflection transducers were installed on the bottom of adjacent beams near the keyway so as to record the relative deflections between those box beams; flexural strains were also measured on the girder bottom. The maximum relative deflection was found to be 0.2 and 0.15 in. for the two bridges, respectively. According to results from FE analysis (details of FE analysis were not given) and field tests, the authors pointed out that intact shear keys, should not permit relative deflection of more than 0.001 in. between adjacent girders. As they expected, reflective cracks were found around the shear keys on both bridges. Partially fractured shear keys were generally found close to the daily wheel positions and driving lanes with heavy truck traffic. However, they did note that the partially fractured shear keys still displayed adequate lateral live load distribution characteristics. The addition of lateral tie bars was found to have insignificant influence on shear key performance. Note that the transverse tie bars used in the tested bridges were made of 1 in. diameter mild steel and spaced at no more than 25ft and were not post-tensioned.

Take Away Points:

- Intact shear keys (i.e., crack free) should not permit relative deflection between adjacent box beams.

- Partially fractured shear keys still have adequate strength to distribute live loads laterally.

- Mild steel lateral tie-bars have insignificant influence on shear key performance.

In the experimental work by Gulyas et al. (1995), the performance of grouted keyways using non-shrink grouts and magnesium ammonium phosphate mortars were studied and compared. Three types of tests were conducted including a direct vertical shear test considering truck loads on the bridge, a direct transverse tension test considering transverse creep and shrinkage effects, and a direct longitudinal shear test considering longitudinal creep and shrinkage effects. All the 16 tested specimens had small dimensions and grout strengths ranging from 5.9 to 7.3 ksi. They found that the composite keyway specimens using magnesium ammonium phosphate mortars showed higher direct tensile bond strengths, vertical shear, and longitudinal shear than those of the non-shrink grout keyway specimens. They also found that magnesium ammonium phosphate mortars showed significantly lower chloride absorption ability, which is of benefit for roadways exposed to salts or sea sprays. Finally, the authors recommended not using non-shrink grouts for the keyway unless the tensile and shear strengths satisfy the requirements in their study.

Take Away Points:

- Mortars used in shearkeys consisting of ammonium phosphate displayed high bond and shear strengths and also had low chloride absorption.

El-Remaily, et al. (1996) compared the American and Japanese approaches to designing adjacent concrete box beam bridges primarily because longitudinal cracking was very rarely associated with Japanese box beam bridges. It was found that the primary differences between American and Japanese designs were: (1) the size and shape of longitudinal joints and (2) the

amount of transverse post-tensioning. After further review, the authors proposed a new precast prestressed box girder bridge design along with a design methodology suitable for U.S. practice. The proposed design methodology takes the transverse diaphragms as the only components which sustain the post-tensioning forces from the post-tensioning ties. The transverse diaphragms are connected at the joints and laterally distribute live loads among those box girders. A grillage analysis was performed using beam elements with common nodes for the diaphragms and beams and considering dead and live loads (including barriers). Working stress methodologies are used to compute the transverse stresses in the top and bottom of the diaphragms after the bending moments in the diaphragms are derived from the grillage model. The post-tensioning is determined to counteract the calculated stresses in the diaphragms such that no lateral tensile stress is induced in the diaphragms. The author's parametric studies indicated that the needed transverse post-tensioning remains constant per unit span length and varies significantly with the bridge width. This method was adopted by the Precast/Prestressed Concrete Institute (PCI) Bridge Design Manual (PCI 2003). The authors described a design example but provided no information on neither experimental validation nor analytical evaluations using a rigorous finite element approach.

Take Away Points:

- The primary differences between American and Japanese designs are: (1) the size and shape of longitudinal joints and (2) the amount of transverse post-tensioning.

- The amount of post-tensioning remains constant on a per foot basis (for constant width of bridge); the amount of post-tensioning needed varies with bridge width.

A study conducted in the State of Ohio examined the performance of the State's standard box beam shear key design, investigated the problem causing shear key failure and developed

new types of keyway connection details (Huckelbridge and El-Esnawi, 1997). Initially, a 3D finite element model of a three-box beam bridge with a length of 40ft and a width of 12ft was established. A concentrated load simulating a truck wheel load was applied on the center of the interior beam. The analytical results indicated that transverse tensile stresses in the bridge top flange are the main factor causing many shear key failures. To deal with the issue, a new type of shear key was proposed by placing the shear key at the neutral axis of the beam cross section. FE results showed that the proposed shear key sustained much smaller tensile stresses which would not cause shear key cracking nor failure. To complete the examination, small scale testing of a multi-beam bridge cross section was conducted. The small scale specimens are slices of the three-beam assembly with a length of 12 in., a width of 144 in., and a depth of 33 in. Static and cyclic loads were applied at the center of these specimens. The experimental results showed that the mid-depth shear key design (only the shear key was grouted instead of the whole keyway) had significantly improved the static load carrying capacity and provided a longer fatigue life than the previous shear key design. In the end, the authors also proposed a water-proofing shear key design with a mid-depth shear key, which uses water-proofing membrane, asphalt topping and foam filler above the shear key. The test results indicated that this shear key design maintained watertightness after fatigue testing in the laboratory environment. However, further evaluations at real bridge sites were noted to be needed.

Take Away Points:

- A shear key placed at mid-depth of the beam must resist much smaller tensile stresses than that which would cause cracking.

Research conducted by Lall et al. (1998) compared the long-term performance of a partial depth shear key system and a modified, full-depth shear key/transverse tie system based on a

survey of bridges in New York State. The modified full-depth shear key/transverse tie system was developed based on the results of bridge inspections in the State of New York and information from other states - in particular the State of Michigan. Note that the new system possesses two post-tensioning ties located at the third points of the girder depth instead of one tie at the girder mid-depth. Survey results indicated that the new full-depth shear key/transverse tendon system showed superior cracking prevention ability and reduced the frequency of reflective cracking in the deck. As a result of the work, the authors recommended using the new full-depth shear key for future adjacent box beam bridges. Additionally, the authors recommended the use of full-width bearing pads, more reinforcement in the concrete topping, higher transverse post-tensioning forces and two ties at each post-tensioning location.

Take Away Points:

- Two ties at each post-tensioning location are preferred to single ties.
- Full-depth shear keys show improved performance.
- Additional reinforcement in a cast-in-place topping also resulted in improved performance.
- Higher transverse post-tensioning also led to improved performance.

Miller et al. (1999) evaluated the performance of box girder shear keys with different shear key locations and different grouting materials. Three types of specimens, made of four box beams, were fabricated with a top shear key plus non-shrink grout, a mid-depth shear key plus non-shrink grout, and a top shear key plus epoxy grout. The specimens were fabricated and tested outside under real environmental conditions and thus experienced continuous temperature gradients. For each specimen a total of 1,000,000 cycles of load (20 kips) were applied on one interior beam and then moved to the other interior beam. The cracks that developed in the shear

keys were inspected using ultrasonic pulse velocity. A static load (20 kips) was also applied on the interior beams separately or simultaneously to check the live load distribution characteristics before and after the development of cracks caused by cyclic loads. The test results indicated that temperature induced stresses – when a shear key was located near the top of the beam – were consistently high enough to cause significant cracking of the shear key material. These cracks significantly propagated from the two ends near the supports to the bridge mid-span after cyclic loads. Conversely, when the shear key was placed at member mid-depth, the shear key did not experience significant cracking under neither thermal nor live loads. They also found that live loads would not cause new cracking but appeared to propagate existing thermal cracks. In addition, static load test results showed that the cracking in the shear key had no remarkable effect on the live load distributions among box beams, but did cause leakage in the joints. In the end, Miller et al. (1999) recommended the use of a grout material with high bond strength for the joints of the adjacent box girders even though this results in some concerns such as thermal compatibility due to the high thermal expansion coefficient of the epoxy, undesired failure in the concrete rather than the epoxy, inconvenience, and the use of poisonous methylethyketone (MEK) for the epoxy.

Take Away Points:
- Shear keys located near the top of the beam can experience stresses high enough to induced cracking from temperature changes.
- Cracking tends to start near the ends of the beams.
- Shear keys located near the beam mid-depth did not experience cracking of the joint material.

Follow-up work by Greuel et al. (2000) studied the field performance of a bridge constructed with a mid-depth shear key. Only the shear key was grouted and the gap above the shear key was filled with compacted sand with a sealant encapsulating the exposed longitudinal joint. Non-prestressed tie rods were used to connect the box beam together before grouting. Field testing was conducted using four Ohio DOT dump trucks - with a total weight ranging from 27 to 32 kips - at various transverse positions. In addition to the static load test, the bridge responses were continuously collected when trucks travels cross the bridge at a speed of around 50 miles per hour. The results indicated that there was no appreciable differential displacement between girders. The authors further concluded that the shear key and transverse rod system adequately resisted the applied live loads.

Take Away Points:

- A bridge with only the shear key grouted and non-tensioned transverse rods can result in a bridge that shows no differential displacement under live loads.

Issa et al. (2003) conducted small scale tests of keyway specimens to investigate the performance of four grout materials using direct shear, direct tension, and flexural tests. The chloride permeability and shrinkage of the four grouts were also measured. The test results indicated that the polymer concrete showed the highest shear, tensile and flexural strengths. The polymer concrete also had superior chloride resistance and less shrinkage compared to the other grouts while set grout had significant shrinkage due to its high water content. In addition, finite element analysis of tension test specimens showed that the polymer concrete specimens sustained the highest load with a minimum of cracking and crushing compared to others.

Take Away Points:

- Polymer concrete has good strength and chloride resistance characteristics.

Badwan and Liang (2007a) performed a grillage analysis to determine the needed transverse post-tensioning for a precast adjacent, solid, multi-beam deck. The grillage model was established using beam elements for the beams while also considering the stiffness at the keyway locations. Parametric studies were performed to investigate the importance of factors such as skew, deck width, thickness, and span length on the design of such a system. The results indicate that the required post-tensioning stress decreases with an increase in the deck width, deck thickness, and skew angles (especially for skew angles greater than 30 degrees). The authors note that the influence of skew is due to the fact that transverse bending in the skew direction decreases with skew angle. The span length affects the needed post-tensioning stress when the bridge skew is very large. In the end, they concluded that it is adequate to design the needed post-tensioning for such a system (especially with high skew) based on current AASHTO specifications.

Take Away Points:

- The amount of post-tensioning decreases with an increased deck width, thickness, and skew.

- Span length affects the needed post-tensioning when the skew is very large.

A literature search conducted by Badwan and Liang (2007b) revealed that little research has been conducted to study the performance of full depth keyways even though testing has been conducted to investigate the behavior of partial depth keyways. Thus, the authors implemented field testing and associated finite element analysis of a post-tensioned adjacent solid box girder bridge with full depth keyways, mid-depth shear keys, and transverse post-tensioning. The 3D finite element model was established using solid elements for the concrete and grout and link elements were used for the post-tensioning tendons. During testing, longitudinal strains in the

girders were recorded. The adequacy of the FE model was validated using the strain data. Based upon the testing and analytical results, the authors concluded that the lateral load distribution was not affected as long as no cracks were induced in the shear keys. It should be noted that serviceability issues caused by shear key cracking were not addressed by the authors.

Take Away Points:

- Lateral load distribution is not impacted by keyway geometry as long as no cracks are induced in the shear keys.

| (a) Joint A | (b) Joint B | (c) Joint C |
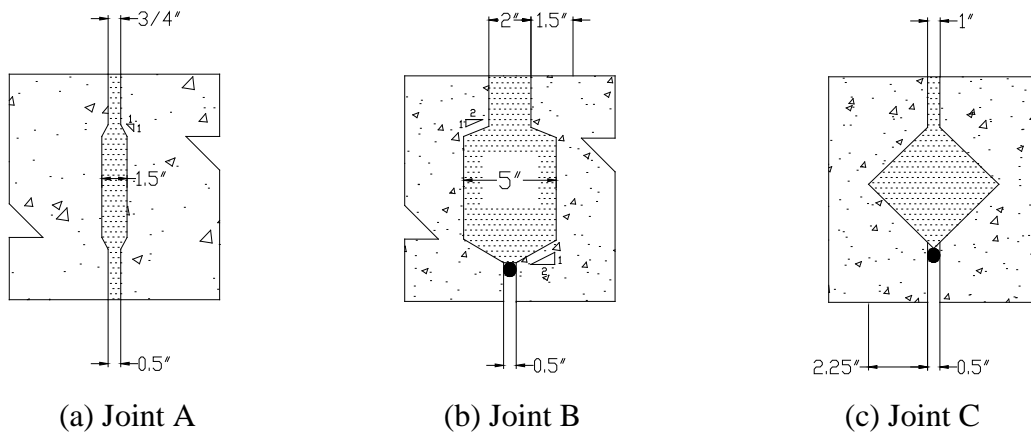
Figure 2-1 Basic Shear key Shapes

Dong et al. (2007) established 3D finite element models to investigate and compare the behavior of the three types of joints shown in Figure 2-1. Finite element models were established using solid elements for both the concrete and grout. Parametric studies were then conducted considering the three types of joints and three strengths of grouts. The results showed that no cracking was found in the finite element model of Joint A but significant stress concentrations and cracking occurred in Joints B and C. They concluded that cracks developed in Joints B and C were due to the significant change of the keyway shape. In addition, they also found that higher strength grout material does not reduce the cracks.

Take Away Points:

- Radical changes in shear key geometry (i.e., very sharp corners) may result in higher stress levels.

Sharpe (2007) conducted extensive FE element analysis of Precast/Prestressed Concrete Institute (PCI) style and Texas Department of Transportation (TxDOT) style box girder bridges to investigate the performances of the shear keys. FE models were established using solid elements for the beams, diaphragms, and keyways and elastomeric bearing pads were modeled using spring elements whose vertical and lateral stiffness were determined based on the material properties of the bearing pad and basic mechanics of materials. The AASHTO HS-25 truck load, strains due to shrinkage, and a temperature gradient were applied to those bridge models. Sharpe considered two types of failure in the shear keys: debonding and cracking (with different failure stresses). The finite element analysis results indicated that reflective cracking was due to high tensile stresses in the shear keys caused by temperature gradients and shrinkage strains instead of live loads. It was further found that these cracks usually developed near the supports instead of at the bridge mid-span. Analytical results showed that composite slabs are most effective at alleviating high tensile stresses in the shear keys although post-tensioning and full-depth keyways also reduce the tensile stresses. It should be noted that the full-depth keyways shown in Figure 2-2c and Figure 2-2d and examined by Sharpe extend the partial-depth keyways shown in Figure 2-2a and Figure 2-2b to the beam bottom.

Take Away Points:

- Cracking is due to shrinkage strains and temperature and not live loads.
- Cracks usually develop near the end of the bridge first.
- Composite slabs are the most effective means of alleviating high tensile stresses.

(a) PCI partial depth keyway   (b) AASHTO partial depth keyway

(c) Full depth keyway   (d) Full depth keyway
(revised from PCI partial depth keyway)   (revised from AASHTO partial depth keyway)
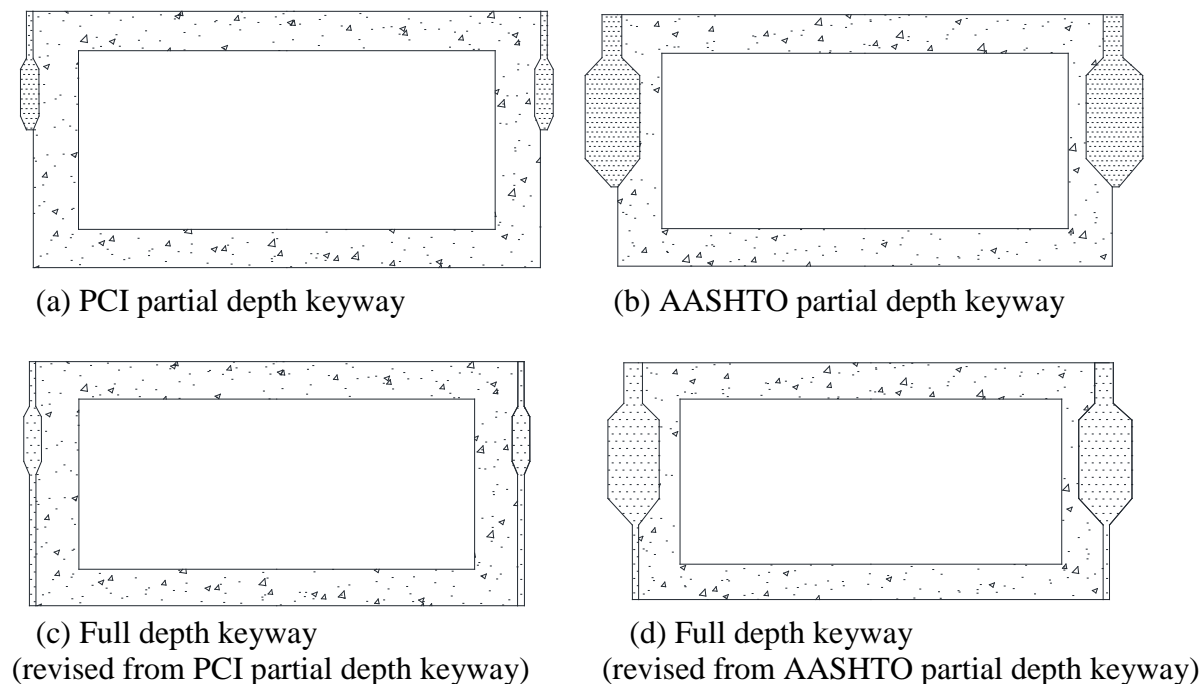
Figure 2-2 Keyway Geometries for PCI and TxDOT Style-Box Girder Bridges

2.3 Publications after 2008

The work done by Attanayake and Aktan (2008) summarized the evolution of the

Michigan design procedures for adjacent box-beam bridges and their performance since the

1950s. The Michigan Bridge Design Guide had adopted many recommended practices provided

in NCHRP Synthesis 393 such as higher transverse post-tensioning forces, full-depth keyways,

top shear keys, and using a 6 in. thick cast-in-place concrete deck as shown in Figure 2-3. They

found that reflective cracks were still found in the Michigan adjacent box-beam bridges. In order

to identify the main source of the formation of longitudinal reflective cracks, they monitored an

adjacent box-beam bridge starting from construction (note that the bridge has narrow, full depth

keyways with top shear keys). Inspection results revealed that cracks were found at the interfaces

between beams and keyways before and after the post-tensioning was applied. They also found

reflective cracks were found in the concrete deck (mostly near supports) 15 days after placement

even before construction the barrier or applying live loads. They concluded that reflective cracks are due to effects such as hydration heat and drying shrinkage.

Take Away Points:

- Cracking forms at the interface between the joint material and the box beam concrete.

- Reflective cracks are principally due to shrinkage.
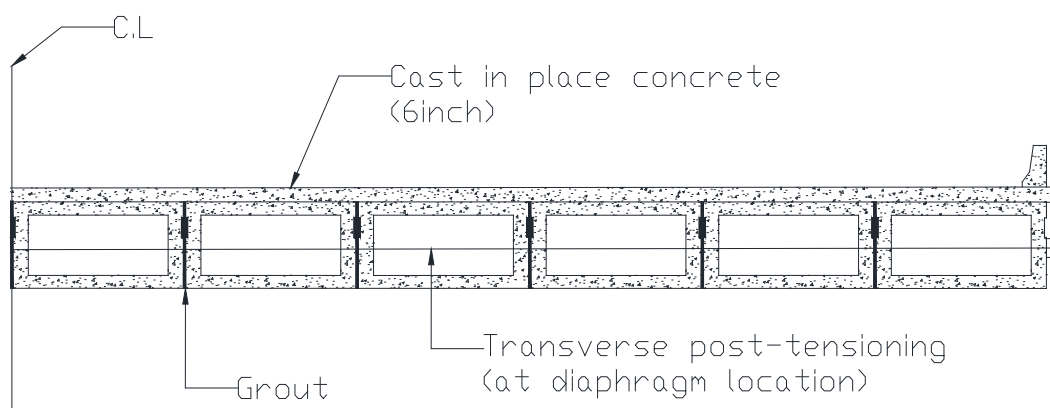
Figure 2-3 Typical Michigan Keyway Geometry and Post-tensioning

Kim et al. (2008) presented recent applications of precast adjacent box-beam bridges with full-depth keyways with mid-depth shear keys grouted with cast-in-place concrete and transverse post-tensioning in South Korea. The authors performed 2D finite element analysis of three box beam sections without transverse post-tensioning to investigate the performance of four placement conditions for the shear key (i.e., no shear key, top shear key, mid-depth shear key, and bottom shear key) as shown in Figure 2-4a, Figure 2-4b, Figure 2-4c, and Figure 2-4d. Various loading and boundary conditions were applied. Based on the beam differential deflections results, it was indicated that the top shear key, the mid-depth shear key, and the bottom shear keys all show superior performance than that of no shear key and the mid-depth shear key was the best of the four configurations. Sang (2010) confirmed their results and

concluded that the location of the shear key does not significantly affect the performance of full-depth keyways. To verify the feasibility of the proposed full depth keyway (with the mid-depth shear key grouted with cast-in-place concrete and high transverse post-tensioning), Kim et al. (2008) conducted flexural testing and 3D finite element modeling of a three box beam specimen. The failure and cracking loads both exceeded the ultimate load and service load based on the Korea design code which is similar to the AASHTO bridge design specifications. No longitudinal cracks were found in the joints when the specimen sustained service and ultimate loads. The measured relative displacements indicated that effective load transfer by the shear key connections was occurring. Kim et al. (2008) conducted fatigue testing (2 million cycles) of the three-box beam specimen. The test results indicated that no cracks were found in the longitudinal joints and the specimen exhibited excellent fatigue resistance with the residual deflection being recovered 24 hours after fatigue testing. Finally, Kim et al. (2008) applied the proposed full depth keyway to a real bridge. Field tests were conducted using static and moving dump trucks on the bridge. They concluded that the box-beam bridge performed well structurally under static and moving dump truck loads. Further, no longitudinal cracking in the keyway joints was reported by the authors. It should be pointed out that long term behavior of the three box beam specimens and the constructed bridge were not evaluated.

Take Away Points:

- Mid-depth shearkey placement results in the best performing joint – especially when used with high post-tensioning and cast-in-place concrete.

(a) No shear key   (b) Top shear key

(c) Mid-depth shear key   (d) Bottom shear key
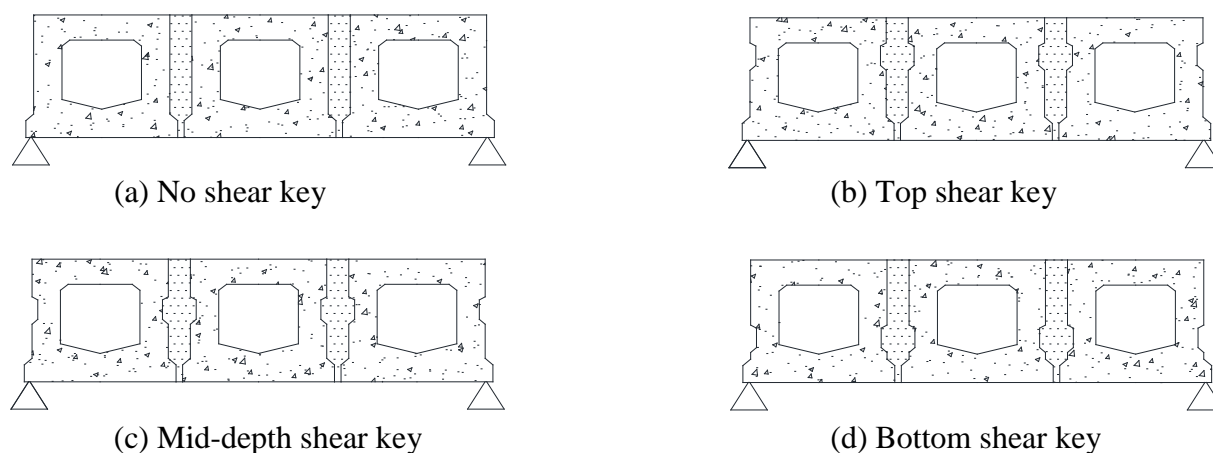
Figure 2-4 Common shear key locations

Attanayake and Aktan (2009) developed a simple analytical model consisting of plate elements based on the macromechanics concept. In this model, the plate element represents a combination of two half box-beam sections, one shear key and concrete deck. Namely, the cross-section of the plate element has the identical section properties as those of the combination cross-section. The stiffnesses of the box-beam sections, shear keys and concrete deck are calculated and then incorporated into the plate elements. The transverse moments along the longitudinal joints between the adjacent beams were determined from the macromechanical model based on the AAHSTO LRFD Bridge Design Specifications. These calculated moments were then used to determine the needed transverse post-tensioning. Further, the authors demonstrated a design example in their paper.

Take Away Points:

- Machromechanical modelling fails to simulate the interaction between the keyway and the beam.

Follow-up work by Ulku et al. (2010) proposed a rational design procedure utilizing the macromechanical model developed by Attanayake and Aktan (2009) to calculate the transverse moments along the transverse joints and thus determine the required transverse post-tensioning.

The concept is to use multi-stage post-tensioning to minimize the longitudinal cracking in the keyway and reflective cracking in the concrete deck. A 3D finite element model was established using solid elements for the beams, keyways, diaphragms and deck. Multi-stage post-tensioning after grouting the keyway and after the deck placement was simulated. They concluded that the two stage post-tensioning process is effective at reducing cracking issues for the bridge subjected to dead and live loads and temperature effects. However, in their designs, the tensile stresses in the deck near the fascia beams due to live loads are significant and may not be easily offset by two-stage post-tensioning. They also found that the temperature gradient is the main factor causing the cracks which developed at the interface of the top shear keys. Another cause of cracks is that the post-tensioning is not uniformly distributed at the keyway because of shear lag.

Take Away Points:

- Two stage post-tensioning may minimize longitudinal cracking.
- Temperature gradient is the main factor causing cracks to develop at the joint interface.

Sang (2010) performed grillage analysis of adjacent box girder bridges subjected to live loads so as to determine shear forces and moments that must be sustained by the shear keys. Subsequently, the performance of the keyway joint was investigated using a 2D finite element model which sustained the loads equivalent to the shear forces and moments derived from the grillage model. The finite element model was established using plane strain elements for the concrete and the grout which share common nodes at the interfaces. Shear tests were conducted to examine the failure modes of the keyway joints grouted with cementitious grout and epoxy. The test results were also used to validate the adequacy of the finite element model. Finally, parametric studies were performed using the validated FE models to investigate the influences of

keyway geometry, grouting materials, post-tensioning, and bearing locations on the performance of the shear key. Note that fiber reinforced cementitious material was recommended by the author to grout the shear key due to its high tensile strength and was also used in their finite element shear key models, although no previous research was found in the literature using fiber reinforced concrete for grouting the shear key. Based on the finite element analysis results, the authors concluded that cracks developed in both the full depth and partial depth keyways using cementitious grout while cracks was found in only the partial depth keyways but not in the full depth shear key using the epoxy grout and fiber reinforced cementitious grout. They also found that the vertical locations of the shear key did not affect its behavior. They recommended using a higher transverse post-tensioning force since they found the post-tensioning specified by the PennDOT was not enough to provide crack resistance. The finite element results indicated that the shared bearing pad (bearing under the shear key as shown in Figure 2-5(a)) reduces the cracks in the shear key relative to isolated bearing pads (bearing under the beam flanges as shown in Figure 2-5(b)).

Take Away Points:

- Epoxy grout and fiber reinforced cementitious materials perform well when used in a full-depth shear key.

- High post-tensioning may be needed to completely eliminate cracking.

(a) Isolated bearing pad   (b) shared bearing pad
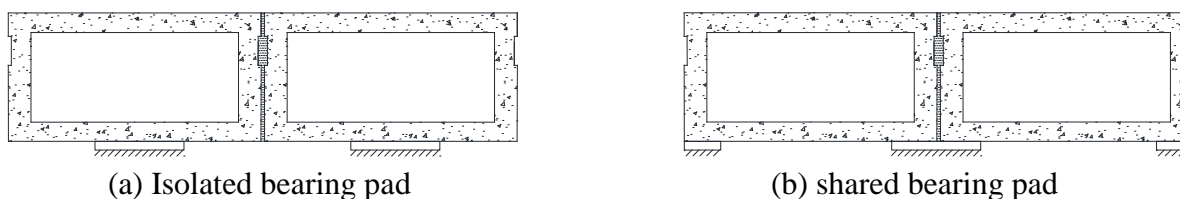
Figure 2-5 Common Bearing Pad Details

Fu et al. (2011) proposed an approach to designing the required post-tensioning for solid, multi-beam bridge system based on the shear friction concept and finite element modeling techniques. The FE models were established using solid elements, link elements, and contact elements for the beams, post-tensioning ties and interfaces between the shear key and the beam, respectively. The adequacy of the finite element models were validated against the strain data measured during field tests using an onsite controlled dump truck. Based on the finite element results, the author recommended different levels of post-tensioning for bridges with different span lengths. The authors found that the boundary conditions had great influence on the predicted bridge response. They found that the post-tensioning does not affect the live load distribution until cracks develop in the keyway and/or concrete topping. Finally, the authors gave some recommendations for improving the use of shear keys in Maryland (e.g., using a two-staged construction sequence {e.g., 16.7% and 100% of the designed post-tensioning of design level before and after grouting the keyways} and using full-depth shear keys).

Take Away Points:

- Bridges of different span lengths may require different amounts of post-tensioning.
- Two-stage post-tensioning may help reduce the development of cracks.

With the goal of achieving simple and economic fabrication and construction of precast adjacent box girder systems, Hanna et al. (2011) developed and evaluated two types of non-post-tensioned transverse connection details that don't use diaphragms nor a concrete deck (i.e., the wide joint system and the narrow joint system shown in Figure 2-6a and Figure 2-6b). The two systems were developed based on the AASHTO/PCI and the Illinois DOT box beam connection details, respectively. The wide joint system incorporates a wide full-depth keyway joint filled with cast-in-place concrete and utilizes top and bottom reinforcement placed in the top and

bottom flanges of the box beams to resist transverse tensile stresses. The narrow joint system incorporates a narrow joint with a partial depth keyway, top shear key and non-shrink grout and utilizes top and bottom threaded rods placed in the top and bottom flanges of the box beams to resist the transverse tensile stresses. 3D finite element models were established using shell elements for the beam flanges and webs and frame elements for the reinforcement and threaded rods. Design charts were developed for determining the needed tension force at the connection (i.e., the required amount of reinforcement or threaded rods). Two-beam specimens using the two systems were fabricated and tested under cyclic loads. Water dams were constructed on the top surface of the specimens so as to monitor for crack development and water leakage. Test results indicated that, for the two system specimens, neither cracks nor water leakage were found in the keyway after 2 million cycles and the differential deflections were found to be below 0.07 in. after 3 million cycles. However, in their study, no apparent consideration was given to performance under thermal loads.

Take Away Points:

- It may be possible to design a bridge without transverse post-tensioning that performs adequately.
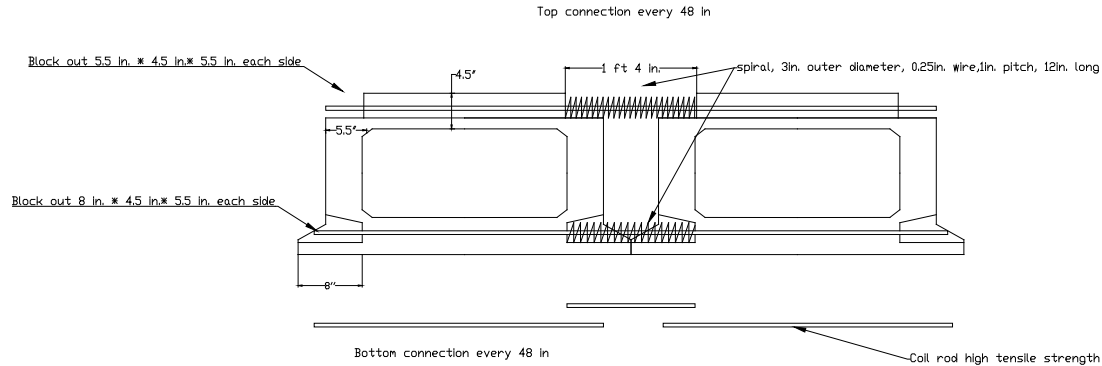
(a) Wide joint
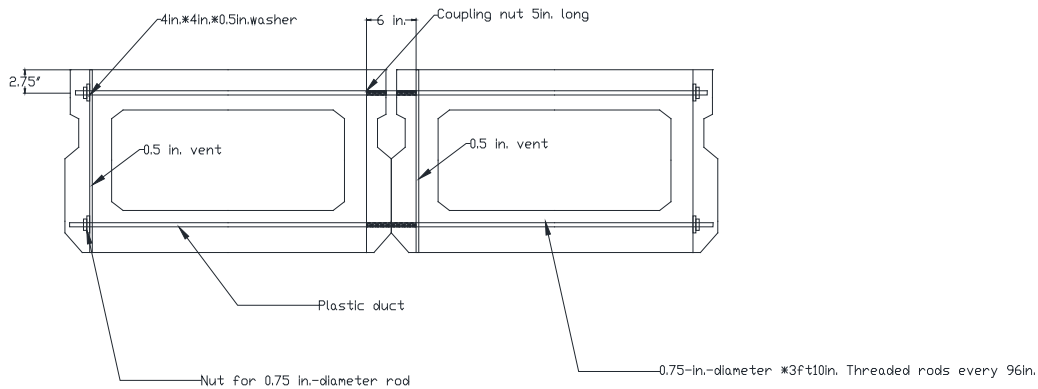
(b) Narrow joint

Figure 2-6 Connection Details Proposed by Hanna et al. (2011)

Follow-up work by Hansen et al. (2012) developed another joint system based on the

narrow joint system proposed by Hanna et al. (2011). This system was developed without using

diaphragms nor concrete topping and utilized post-tensioning to reduce the possibility of

cracking or leakage. As shown in Figure 2-7, the sleeves, located below the beam top flange and

above the bottom flange, are used to accommodate the duct, the post-tensioning rods and

couplers. The required post-tensioning was determined based upon the design chart for the

required tension force in the connection developed by Hanna et al. (2009). Experimental testing

was conducted for four box beam specimens placed in a cantilever and mid-span loading setups,

successively. In the cantilever setup, the specimen was supported at the transverse center and

edge and a load with 5 million cycles was applied on the joint. In the mid-span loading setup, the specimen was supported at the two transverse edges and the load was applied on the specimen center. Results indicated that no significant strain change, cracking, nor leakage near the shear key region occurred. The authors strongly recommend this system for real bridge construction. However, temperature gradient and shrinkage effects were not considered in their study.

Take Away Points:

- A cast-in-place topping may further improve the performance of a non-post-tensioned box beam bridge.
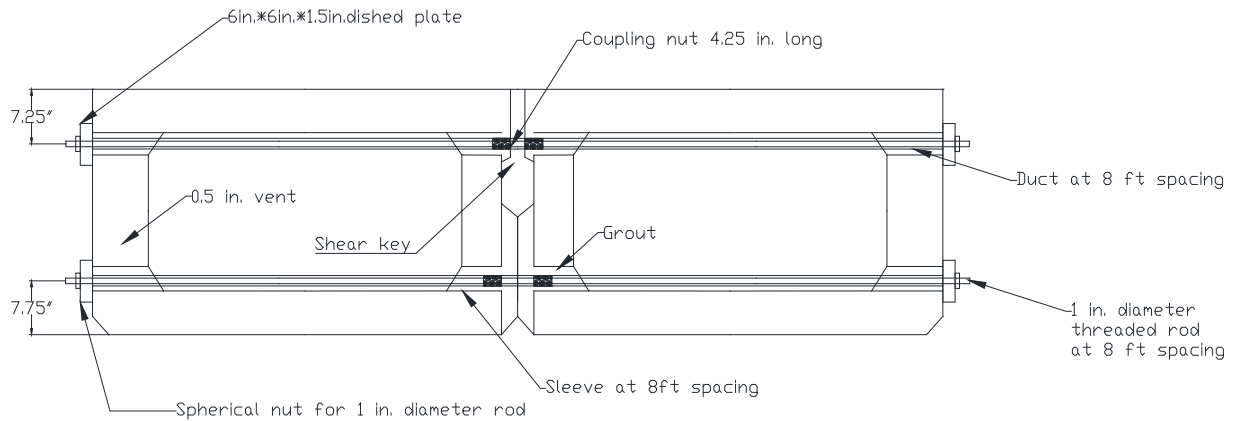
Figure 2-7 Connection Details Proposed by Hansen et al. (2012)

Grace et al. (2012) inspected a bridge in Michigan constructed based on recent Michigan design procedures. The bridge has two simply supported spans of 122.5ft, seven diaphragms with post-tensioning bars that were highly post-tensioned before grouting, and full depth keyways with a top shear key and a concrete deck. The inspection results found that significant longitudinal cracks were formed in the shear key and deck even though the traffic on that bridge is light and was judged to not likely have induced those cracks. In addition, inspection on some other adjacent box girder bridges in Michigan also revealed that reflective cracks had formed in the deck. To investigate the source of those cracks, the authors conducted an experimental test of a bridge specimen in the lab. A four-point concentrated load up to the service load of 80 kips was

applied on the specimen, and no reflective cracks in the deck were found even when the transverse post-tensioning decreased to zero. They concluded that the traffic loads are not the main condition causing reflective cracking in the deck. Thus, the authors considered temperature effects in subsequent finite element analyses. The finite element model was established using solid elements for the beams, diaphragms and deck, and link elements for the post-tensioning ties. After the finite element model was validated against the results from the experimental tests, finite element analyses of real bridges was performed considering dead and live loads and temperature gradients according to the AASHTO bridge design specifications. Based on the finite element results, the required amount of transverse post-tensioning required to mitigate reflective cracking for the real bridges was then established. For practical applications, the required number of diaphragms and the required amount of post-tensioning per diaphragm were given for the adjacent box-beam bridges in Michigan. The authors found that the post-tensioning effects are mainly localized at the diaphragm regions due to shear lag effects and the required amount of diaphragms for eliminating reflective cracks increases with an increase in span length, while the required post-tensioning increases with increased bridge width.

Take Away Points:

- Traffic loads are not the primary factor in the development of cracks.
- Temperature induced effects may be the primary source of crack development.

2.4 Literature search synthesis

A significant amount of information related to adjacent box beams was presented and summarized in the preceding pages. Although there are many important facts to take-away from these sources, the following synthesis and summary was formulated to provide a brief synopsis

of the information that had the greatest impact on the development of the research plan summarized in the following pages.

Cracking of the shearkey between adjacent box beams appears to principally be a service related problem as multiple sources indicate that even with a cracked joint, a bridge can continue to effectively distribute loads to the primary load carrying members. Consistent throughout the literature is the conclusion that joints that utilize full-depth keyways perform the best. The transverse post-tensioning seems to be effective only when high amounts of transverse post-tensioning were applied. However, there have been some reported instances where no post-tensioning was reported to perform well too. With regard to cracking, it appears that cracking tends to be most prominent at the interface between the joint material and the box beam. Further, cracking seems to first initiate near the ends of beams. Cracking does not seem to be first initiated by the application of live loads. There are, however, differing opinions on the relative contribution to cracking from shrinkage and temperature. Nevertheless, once cracking is initiated by either shrinkage and/or temperature, they can continue to grow with subsequent live load application.

To summarize information useful for the development of the analytical and testing plans, design/construction aspects and finite element analyses and testing on adjacent box beam bridges were grouped. Design and construction attributes for the adjacent box girder bridges in studies reported above are summarized in Table 2-4. Finite element analysis details are summarized in Table 2-5. Laboratory tests of small scale, medium scale, and full scale specimens are summarized in Table 2-6. Field testing of adjacent box girder bridges are summarized in Table 2-7. These four tables were found to be very helpful in developing the plan for the analytical and experimental evaluations.

Table 2-4 Design and Construction Attributes

Refs.	Keyway geometries	Transverse Tie details	Diaphragms	Grout	Keyway preparation	Bearing details	Construction sequence	Concrete Deck	FE analysis	Laboratory testing	Field testing
Huckelbridge [1995]	Partial depth keyway	Girder mid-height; Non-post-tension mild steel (1 in. diameter)	Yes	NG	NG	NG	NG	None	Yes	No	Yes
Gulyas et al. [1995]	Full depth keyway and top shear key; Narrow joint	No	No	Non-shrink grout; MAP mortars	Sandblast/wash off	NA	NA	NA	No	Yes	No
El-Remaily, et al. [1996]	Partial depth keyway and top shear key (pocket near diaphragms)	Post-tensioning (determined by design calculations)	5	NG	NG	NG	Post-tensing after grouting	No	Yes	No	No
Huckelbridge and El-Esnawi [1997]	Partial depth keyway and top and mid-depth shear keys	No	No	Non-shrink grout; MAP mortars; epoxy	Power grinder and wire brush; sand-blaster	NA	NA	No	Yes	Yes	No
Lall et al. [1998]	Full depth keyway and top shear key	Two post-tensioning ties at third points in depth	More than 3	NG	Sandblast, cleaned, and pre-wetted	Full width bearing	NA	Yes	No	No	No
Greuel et al. [2000]	Partial depth keyway and mid-depth shear key	Non-post-tensioned rods	5	NG	NG	Neoprene bearing pad	Grout after installing rods	2.5 in. asphalt wearing surface	No	No	Yes
Miller et al. [1999]	Partial depth keyway and mid-depth shear key (Pocket near diaphragms)	Slightly post-tensioned rods	5	Non-shrink grout; epoxy	NG	NG	Post-tensioning before grouting	No	No	No	Yes
Issa et al. [2003]	Full depth keyway and mid-depth shear key	No	No	Set 45; set 45 HW; set grout; polymer concrete	Sandblast; air pressure and high pressure washing	NA	NA	NA	Yes	Yes	No
Badwan and Liang [2007a]	Full depth and mid-depth shear key	Bonded post-tensioning tendons	No	NG	NG	NG	Post-tensioning before grouting	No	Yes	No	No
Badwan and Liang [2007b]	Full depth keyway and mid-depth shear key	Bonded post-tensioning tendons	No	NG	NG	NG	Post-tensioning before grouting	No	Yes	No	Yes
Dong et al. [2007]	Full depth and mid-depth shear key; partial depth keyway and mid- (bottom-) shear key	No	No	Yes	NG	NG	NA	No	Yes	No	No

MAP - Magnesium ammonium phosphate; NA - Not Applicable; CFRP - Carbon Fiber Reinforced Polymer; NG - Not Given

33

Table 2-4 (Continued)

Refs.	Keyway geometries	Transverse Tie details	Diaphragms	Grout	Keyway preparation	Bearing details	Construction sequence	Concrete Deck	FE analysis	Laboratory testing	Field testing
Sharpe [2007]	Partial depth keyway and top shear key; Full depth keyway and top shear key	Unbonded post-tensioning tendons	Spaced at 10 ft	Non-shrink grout	NG	Elastomeric bearing pads	NG	Yes	Yes	No	No
Attanayake and Aktan [2008]	Full depth keyway and top shear key (1.5-3 in.)	Bonded post-tensioning tendons	6	Type R-2, which is cement and fine aggregate mixture with 14 +/- 4% air	NG	NG	Post-tensioning after grouting	Yes	No	No	Yes
Kim et al. [2008]	FEA: Full depth keyway and no, top, mid-depth or bottom shear keys. Test: Full depth and mid-depth shear keys (2-4.8 in.)	Bonded post-tensioning tendons	5	Cast-in-place concrete	NG	Elastometric rubber pad	NG	Yes	No	No	Yes
Attanayake and Aktan [2009] and Ulku et al. [2010]	Full depth keyway and top shear key (1.5-3 in.)	Unbonded post-tensioning tendons	5-7	NG	NG	NG	Multi-staged construction: Post-tensioning after grouting and after deck placement	Yes	Yes	No	No
Sang [2010]	Full depth keyway and top shear key; Partial depth and top shear key	Post-tensioning tendons	NG	Fiber reinforced cememtitious material; cememtitious material; epoxy	NG	Placed under the keyway	Post-tensioning after grouting	Yes	Yes	Yes	No
Fu et al. [2011]	Full depth keyway and top shear key	Post-tensioning threaded rods	No	Non-shrink grout	NG	NG	Post-tensioning before grouting	Yes	Yes	No	Yes
Hanna et al. [2011]	Full depth keyway and no shear key; Partial depth and top shear key	Non-post-tensioning reinforcement; Non-post-tensioning threaded rods	No	Cast-in-place concrete; Non-shrink grout	Roughened	NG	NA	No	Yes	Yes	No
Jenna et al. [2012]	Partial depth keyway and top shear key	Non-post-tensioning threaded rods	No	Non-shrink grout	Roughened	Neoprene bearing pad	Post-tensioning after grouting	No	No	Yes	No
Grace et al. [2012]	Full depth keyway and top shear key	Unbonded post-tensioning CFRP	From FEA	Non-shrink grout	NG	Neoprene bearing pad	Post-tensioning after grouting	Yes	Yes	Yes	No

CFRP - Carbon Fiber Reinforced Polymer; MAP - Magnesium ammonium phosphate; NA - Not Applicable; NG - Not Given

Table 2-5 Summary of FE Analysis

Refs.	Type of Analysis	Software	Box Beam	Keyway	Interface	Diaphragm	Deck	Tie	Bearing	Load
Huckelbridge [1995]	NG	NG	NG	NG	NG	NG	NG	NG	NG	NG
El-Remaily, et al. [1996]	Grillage analysis	NG	Beam elements	Common nodes	Common nodes	beam elements	None	NA	Simply supported	Dead and live loads (including barriers)
Huckelbridge and El-Esnawi [1997]	3D	SAP	Solid elements	Solid elements	Common nodes	Solid elements	None	Directly apply forces	Simply supported	Concentrated load
	2D	SAP	Plane elements	Plane elements	Common nodes	None	None	None	Spring elements	Concentrated load
Issa et al. [2003]	3D	ANSYS	Solid elements	Solid elements	Common nodes	None	None	None	NA	Concentrated load
Badwan and Liang [2007a]	Grillage analysis	ANSYS	Beam elements	Common nodes	Common nodes	Beam elements	None	NA	Simply supported	HS-25 truck
Badwan and Liang [2007b]	3D	ANSYS	Solid elements	Solid elements	Common nodes	None	None	Link element	Simply supported	Dump truck
Dong et al. [2007]	3D	ABAQUS	Solid elements	Solid elements	Common nodes	None	None	None	NA	Concentrated load
Sharpe [2007]	3D	ANSYS	Solid elements	Solid elements	Common nodes	Solid elements	Solid elements	None	Spring elements	HS-25 truck; shrinkage; thermal gradient
Kim et al. [2008]	2D	DIANA	Plane elements	Plane elements	Common nodes	None	None	None	Simply supported	Concentrated load
	3D	DIANA	Solid elements	Solid elements	Common nodes	Solid elements	Solid elements	Bar elements	Simply supported	Concentrated load
Attanayake and Aktan [2009]	Maromechanical model	Programming	Integrated Plate elements	Integrated Plate elements	NONE	None	Integrated Plate elements	None	Simply supported	HL-93
Ulku et al. [2010]	3D	ABAQUS	Solid elements	Solid elements	NONE	Solid elements	Solid elements	Truss elements	Simply supported	HL-93
Sang [2010]	Grillage analysis	NG	Beam elements	Common nodes	Common nodes	Beam elements	None	NA	Simply supported	HS-25 truck
	2D	ABAQUS	Plane elements	Plane elements	Common nodes	None	None	None	NA	Concrentrated and distributed loads
Hanna et al. [2011]	3D	SAP2000	Shell elements	Common nodes	Common nodes	None	None	Frame elements	Simply supported	HL-93
Fu et al. [2011]	3D	ANSYS	Solid elements	Solid elements	Contact elements	None	None	Link elements	Simply supported	HL-93
Grace et al. [2012]	3D	NG	Brick elements	Brick elements	Contact elements	Brick elements	Brick elements	Truss elements	Simply supported	HL-93 and temperature gradient

NG - Not Given; NA - Not Applicable

Table 2-6 Summary of Laboratory Testing

References	Testing scale	Specimens	Length	Skew	Width	Depth	Number of beams	Grout strength	Concrete strength	Load	Temperature	Relative displacement	Strain	Crack detestion
Gulyas et al. [1995]	Small scale	Keyway specimens	3.25 in.	NA	6-6.5 in.	7-14 in.	NA	Non-shrink grout: 5.9 ksi; MAP mortars: 7.3 ksi	NG	Vertical shear; Direct tension; Longitudinal shear	No	NA	NA	Visually
Huckelbridge and El-Esnawi [1997]	Small scale	Multu-beam slices	12 in.	0º	144	33 in.	3	Non-shrink grout: 5.5 ksi; MAP mortars: 5 ksi; epoxy: 13 ksi	6 ksi	Cyclic concentrated load	No	Direct Current Differential Transducer (DCDT)	Foil-backed strain gages	Visually
Issa et al. [2003]	Small scale	Keyway specimens	5-6 in.	0	17-21 in.	17-26 in.	NA	Set 45: 5.8 ksi; set 45 HW: 5.6 ksi; set grout: 7.7 ksi; polymer concrete:10.8 ksi	6.5 ksi	Direct shear; Direct tension; Flexeral bending	No	NG	NG	Visually
Kim et al. [2008]	Full scale	Multi-box beam specimens	61 ft	0	95 in.	31.5 in	3	4.9 ksi	8 ksi	Static comcentrated load/ Cyclic concentrated load (Mid-span)	No	Linear variable differential transducers (LVDTs)	Strain gauges	Visually
Sang [2010]	Small scale	Keyway specimens	5 in.	0	7 in.	17 in.	NA	Cementitious grout: 4.5 ksi; epoxy: 10 ksi	11.3	Direct shear	No	NG	NG	Visually
Hanna et al. [2011]	Medium scale	Multi-box beam specimens	8 ft	0	8 ft	27 in.; 32 in.	2	6 ksi	8 ksi	Cyclic concentrated load	No	Yes	No	A water dam
Jenna et al. [2012]	Medium scale	Multi-box beam specimens	8 ft	0	16 ft	27 in.	4	Non-shrink grout: 10 ksi	8 ksi	Cyclic concentrated load	No	Yes	No	A water dam; Visually
Grace et al. [2012]	Full scale	Multi-box beam specimens	20 ft	0	75 in.	14 in.	4	Low-shrink grout: 8 ksi	Beam: 6 ksi; Deck: 5.7 ksi	Service concentrated load up to 80 kips	No (Recognize importance of temperature effects)	NG	No	Visually

NG - Not Given; NA - Not Applicable

Table 2-7 Summary of Field Testing

References	Bridge	Number of Span	Span (ft)	Skew (degree)	Width (ft)	Number of beams	Beam width × depth (in.)	Grout strength	Concrete strength (ksi)	Temperature	Load	Relative displacement	Strain	Crack detection
Huckelbridge et al. [1995]	No. 1	1	32.5	20	44	11	48 × 17	NA	NA	NG	50 kips Dump truck (12 +38 kips)	Relative displacement transducers (Own made)	Vibrating wire gage	Visually
	No. 2	4	40/54/54/40	17.4	68	17	48 × 27			NG				
Miller et al. [1999]	4 (with same girders, different grouting)	1	75	0	16	4	48 × 33	5 ksi	Beam: 9.4	Yealy range: -10-100 ºF; summer: 50-90 ºF	20 kips on the loaded interior beam	Direct current differential transducer (DCDT)	Transverse omega clip gauges; vibrating wire gauge	Ultrasonic pulse velocity
Greuel et al. [2000]	1	1	115.5	0	48	12	48 × 42	NG	Beam: 10	NG	Ohio DOT truck similar to HS-20 Truck	Linear variable differential transformer (LVDT)	Vibrating wire gauge; foil strain gages;	NG
Badwan and Liang [2007b]	1	2	29/29	30	44	6	87 × 15-18	NG	NG	NG	29 kips dump truck (9+20 kips)	No	Strain transducer	NG
Attanayake and Aktan [2008]	1	2	79/79	0	93.5	22	48 × 33	NG	Deck: 6.4	Early summer	No	No	No	Visually
Kim et al. [2008]	1	2	43/43	5	39	14	30 × 31.5	4.4 ksi	Beam: 7.3	NG	77.2 kips dump truck (16.7+60.5 kips)	Linear variable differential transducers (LVDTs)	Strain gauges	Visually
Grace et al. [2012]	1	1	35 ft	0	33	11	36 × 15	NG	Beam: 7.0; Deck: 4	NG	35 kips dump truck (10.8+24.2 kips)	No	Strain sensor	NG

NG - Not Given; NA - Not Applicable

2.5 References

Attanayake, U., and Aktan, H. (2008). "Issues with Reflective Deck Cracks in Side-by-Side Box Beam Bridges." Proceedings of the 2008 Concrete Bridge Conference, Federal Highway Administration, National Concrete Bridge Council, Missouri Department of Transportation, American Concrete Institute, 18p.

Attanayake, U., and Aktan, H. M. (2009). "Side-by-side Box-beam Bridge Superstructure: Rational Transverse Post-tension Design." Transportation Research Board Annual Meeting, Washington D.C.

Badwan, I. Z., and Liang, R. Y. (2007a). "Transverse Post-Tensioning Design of Precast Concrete Multi-beam Deck." PCI Journal, 52(4), 84-92.

Badwan, I. Z., and Liang, R. Y. (2007b). "Performance evaluation of precast post-tensioned concrete multibeam deck." Journal of Performance of Constructed Facilities, 21(5), 368-374.

Dong, H., Li Y., and Ahlborn T.M. (2007). "Performance of Joint Connections between Decked Prestressed Concrete Bridge Girders," PCI National Bridge Conference, Proceedings, Phoenix, Arizona.

El-Remaily, A., Tadros, M. K., Yamane, T., and Krause, G. (1996). "Transverse design of adjacent precast prestressed concrete box girder bridges." PCI Journal, 41, 96-113.

Fu, C. C., Pan, Z., and Ahmed, M. S. (2010). "Transverse Post-tensioning Design of Adjacent Precast Solid Multibeam Bridges." Journal of Performance of Constructed Facilities, 25(3), 223-230.

Grace, N. F., Jensen, E. A.,and Bebawy, M. R. (2012). "Transverse post-tensioning arrangement for side-by-side box-beam bridges." PCI Journal, 57(2), 48-63.

Greuel, A., Baseheart, T. M., Rogers, B. T., Miller, R. A., and Shahrooz, B. M. (2000). "Evaluation of a high performance concrete box girder bridge." PCI journal, 45(6), 60-71.

Gulyas, R. J., Wirthlin, G. J., & Champa, J. T. (1995). "Evaluation of keyway grout test methods for precast concrete bridges." PCI Journal, 40(1), 44-57.

Hanna, K. E. (2008). "Behavior of Adjacent Precast Prestressed Concrete Box Girder Bridges." PhD diss., University of Nebraska, Lincoln, NE.

Hanna, K.E., G. Morcous, and M. K. Tadros (2007). "Transverse Design and Detailing of Adjacent Box Beam Bridges," PCI National Bridge Conference, Proceedings, Phoenix, Ariz.

Hanna, K. E., Morcous, G., & Tadros, M. K. (2009). Transverse post-tensioning design and detailing of precast, prestressed concrete adjacent-box-girder bridges. PCI journal, 54(4), 160-174.

Hanna, K., Morcous, G., & Tadros, M. K. (2011). Adjacent box girders without internal diaphragms or post-tensioned joints. PCI journal, 56(4), 51-64.

Hansen, J., Hanna, K., and Tadros, M. K. (2012). "Simplified transverse post-tensioning construction and maintenance of adjacent box girders." PCI journal, 57(2), 64-79.

Harries K.A. (2006). "Full-scale Testing Program on De-commissioned Girders from the Lake View Drive Bridge," Report No. FHWA-PA-2006-008-EMG001, Pennsylvania Department of Transportation, Harrisburg.

Huckelbridge Jr, A. A., and El-Esnawi, H. H. (1997). "Evaluation of Improved Shear Key Designs for Multi-beam Box Girder Bridges." No. FHWA/OH-97/009, report to Ohio Department of Transportation, Case Western Reserve University, Cleveland, OH.

Huckelbridge Jr, A. A., El-Esnawi, H., and Moses, F. (1995). "Shear key performance in multibeam box girder bridges." Journal of Performance of Constructed Facilities, 9(4), 271-285.

Illinois DOT (2008). "Concrete Deck Beams," Guide Bridge Special Provisions (GBSP), No. 62, Illinois Department of Transportation, Springfield.

Issa, M. A., do Valle, C. L. R., Abdalla, H. A., Islam, S., and Issa, M. A. (2003). "Performance of transverse joint grout materials in full-depth precast concrete bridge deck systems." PCI Journal, 48(4), 92-103.

Kim, J. H. J., Nam, J. W., Kim, H. J., Kim, J. H., & KEUN, J. B. (2008). "Overview and applications of precast, prestressed concrete adjacent box-beam bridges in South Korea." PCI Journal, 53(4), 83-107.

Lall, J., E.F. DiCocco, and S. Alampalli (1997). "Full-Depth Shear-Key Performance in Adjacent Prestressed-Beam Bridges." Special Report No. 124, Transportation Research and Development Bureau, New York State Department of Transportation, Albany.

Lall, J., S. Alampalli, and E. F. DiCocco. (1998). "Performance of Full-Depth Shear Keys in Adjacent Prestressed Box Beam Bridges." PCI Journal, 43(2), 72-79.

Macioce, T.P., H.C. Rogers, R. Anderson, and D.C. Puzey (2007). "Prestressed Concrete Box Beam Bridges—Two DOTs'Experience," PCI National Concrete Bridge Conference, Proceedings, Phoenix, Ariz.

Miller, R. A., Hlavacs, G. M., Long, T., and Greuel, A. (1999). Full-scale testing of shear keys for adjacent box girder bridges. PCI Journal, 44(6), 80-90.

Nottingham, D. (1995). Discussion of "Evaluation of Keyway Grout Test Methods for Precast Concrete Bridges," by R.J. Gulyas, G.J. Wirthlin, and J.T. Champa, PCI Journal, 40(4), 98–103.

Precast/Prestressed Concrete Institute (PCI) (1997; 2004), PCI Bridge Design Manual, Precast/Prestressed Concrete Institute, Chicago, IL, 1997 (updated July 2004).

Precast/Prestressed Concrete Institute (PCI). (2003). PCI bridge design manual, 2nd Ed., Precast/Prestressed Concrete Institute, Chicago, IL.

Russell, H. G. (2009). Adjacent Precast Concrete Box Beam Bridges: Connection Details (Vol. 393). Transportation Research Board.

Sang, Z. (2010). "A Numerical Analysis of the Shear Key Cracking Problem in Adjacent Box Beam Bridges." Doctoral dissertation, The Pennsylvania State University.

Sharpe, G. P. (2007). "Reflective cracking of shear keys in multi-beam bridges", Doctoral dissertation, Texas A&M University.

Ulku, E., Attanayake, U., and Aktan, H. M. (2010). "Rationally Designed Staged Post-tensioning to Abate Reflective Cracking on Side-by-Side Box-Beam Bridge Decks." Transportation Research Record: Journal of the Transportation Research Board, 2172(-1), 87-95.

Yamane, T., M.K. Tadros, and P. Arumugasaamy (1994). "Short to Medium Span Precast Prestressed Concrete Bridges in Japan," PCI Journal, 39(2), 74–100.

CHAPTER 3. MATERIAL SELECTION FOR THE JOINT BETWEEN ADJACENT BOX

BEAMS

Liu, Zhengyu[1]; Phares, Brent M[2];

3.1 Abstract

Bridges constructed with adjacent precast concrete box beams have been in service for

many years. A recurring problem with this type of bridge is the cracking in the longitudinal

joints between adjacent beams. Many past research results pointed to the fact that an efficient

joint material should have small or zero shrinkage at the early-age and achieve sufficient bond

strength at the interface between the joint and the box beam. The objective of this paper is to

select a better material for the joint between the adjacent box beams to resist cracking. To

achieve this objective, two phases of laboratory material characterization tests were performed.

During Phase I, four potential joint materials were tested and evaluated based upon the

shrinkage, flexural tensile strength and normal bond strength. During Phase II, time dependent

material testing was conducted on the selected materials from Phase I to characterize the

nonlinear changes in bond strength, compressive and tensile strength with time. The compressive

strength and tensile strength data of shrinkage compensated concrete were used to calibrate

Kanstad's (1990) time dependent material property equation. Finite element modeling approach

was adopted to calculate the early-age joint stress distribution and evaluate the structural

performance of both Type IV joint grouted by epoxy grout and Type V joint filled by shrinkage

compensated concrete. A finite element modeling approach which is capable of simulating the

---

[1] Liu, Zhengyu, Ph.D. Candidate, Graduate Research Assistant, Department of Civil, Construction and Environment Engineering, Iowa State University, Ames, Iowa 50010, zhengyu@iastate.edu.
[2] Phares, Brent M., PhD, P.E., Director, Bridge Engineering Center, Iowa State University, Ames, Iowa 50010, bphares@iastate.edu.

early-age joint behavior was illustrated and the models were developed for 4ft long beam-joint-beam structures. The analytical results indicated that the Type V joint filled with shrinkage compensated concrete is expected to perform superior to the Type IV joint filled with epoxy in resisting joint cracking. Although the FEM results indicates that Type V joint filled with shrinkage compensated concrete still induces tensile stress near the exterior of the interface, the placement of reinforcement near the edge will have sufficient capacity to resist the debonding at the interface during the early-age period when initial cracking has been found to occur. A further evaluation on the performance of shrinkage compensated concrete associate with Type V joint on resisting the joint cracking was recommended. More researches should be conducted experimentally and analytically with consideration of early-age thermal load and live load etc.

Keywords: Adjacent box beam bridges; Finite element modeling; Early-age shrinkage-compensated concrete; Joint cracking.

3.2 Introduction

Bridges constructed with adjacent precast prestressed concrete box beams have been in service for many years and can provide an economical solution for short and medium span bridges. A recurring problem with this type of bridge is cracking in the longitudinal joints between adjacent beams, resulting in reflective cracks forming in the wearing surface. In United States, there are three typically used generic partial depth joint geometries (Types I, II and III joints) and one full depth joint geometry (Type IV joint), all of which are shown in Figure 3-1. The typically used Japanese joint is a full depth joint (Type V) which is also shown in Figure 3-1. Lall et al. (1998) and Sang (2010) indicated that full depth joints show superior cracking prevention ability than the partial depth joint. El-Remaily et al. (1996) reported that longitudinal cracking was seldom found in adjacent box beam bridges with the Type V full depth joint.

Ramakrishnan et al. (1999) evaluated the performance of three types of specimens, fabricated with 1) a top shear key with non-shrink grout, 2) a mid-depth shear key with non-shrink grout, and 3) a top shear key with epoxy grout. The test specimens consisted of four box beams, fabricated and tested outside under real environmental conditions. Both cyclic load tests and live load tests were performed. The test results indicated that temperature induced stresses were consistently high enough to cause significant cracking of the shear key material. These cracks propagated from the two ends near the supports toward the bridge mid-span after cyclic loads. They also found that live loads did not cause new cracking but appeared to propagate cracks initiated under thermal changes. In addition, static load test results showed that the cracking in the shear key had no remarkable effect on the live load distribution characteristics but did cause leakage in the joints. A grout material with high bond strength for the joints of the adjacent box girders was recommended.

Sharpe (2007) conducted extensive finite element analysis of Precast/Prestressed Concrete Institute (PCI) style and Texas Department of Transportation (TxDOT) style box girder bridges to investigate the performances of the shear keys. Finite element models were established using solid elements for the beams, diaphragms, and joints and spring elements for the elastomeric bearing pads. The AASHTO HS-25 truck load, strains due to shrinkage, and a temperature gradient were applied to those bridge models. Two types of failure in the shear keys were considered: debonding and cracking. The finite element analysis results indicated that reflective cracking was the resulted high tensile stresses in the shear keys caused by temperature gradients and shrinkage instead of live loads.

Dong et al. (2007) established 3D finite element models to investigate and compare the behavior of the three different types of joints with different shear key geometry. The results

showed that radical changes in shear key geometry (i.e., sharp corners) may result in higher stress levels. In addition, they also found that higher strength grout materials do not reduce the cracks.

Work conducted by Attanayake and Aktan (2008) summarized the evolution of the Michigan design procedures for adjacent box-beam bridges and their performance since the 1950s. The Michigan Bridge Design Guide had adopted many recommended practices provided in NCHRP Synthesis 393 (Russell, 2009) such as higher transverse post-tensioning forces, full-depth joints, top shear keys, and a 6 in. thick cast-in-place concrete deck. They found that reflective cracks were still found in the Michigan adjacent box-beam bridges. In order to identify the main source of the formation of longitudinal reflective cracks, an adjacent box beam bridge was monitored starting from construction (note that the bridge had narrow, full depth joints with top shear keys). Inspection results revealed that cracks were found at the interfaces between beams and joints three days after placing the joint material and before post-tensioning and live load were applied. They concluded that reflective cracks are due to effects such as hydration heat and drying shrinkage.

Ulku et al. (2010) proposed a rational design procedure to calculate the transverse moments along the transverse joints to determine the required transverse post-tensioning. A 3D finite element model was established using solid elements for the beams, joints, diaphragms and deck. They found that temperature gradient is the main factor causing the cracks which developed at the interface of the shear keys.

Grace et al. (2012) inspected a bridge in Michigan and conducted a laboratory test to find the source of longitudinal reflective cracks in the joint. They concluded that the traffic loads are not the main cause of reflective cracking in the deck. A 3D finite element model was established

and validated against the results from the experimental tests. Finite element analyses of real bridges were performed considering dead and live loads and temperature gradients. The authors found that temperature induced effects may be the primary source of crack development.

It appears that cracking tends to be most prominent at the interface between the joint material and the box beam. Cracking does not seem to be first initiated by the application of live loads. There are, however, differing opinions on the relative contribution to cracking from shrinkage and temperature. Nevertheless, once cracking is initiated during the early-age of the joint, they will likely continue to grow with live load application. It was also been found that a full depth joint shows better performance than a partial depth joint. Based upon the results of research conducted on box beam bridges during the past twenty years, it can confidently be stated that a well performing joint material should have small or zero shrinkage at the early-age and small temperature induced volume change. The material should attain high bond strength at the interface between the joint and the box beam from an early-age and remain through the entire bridge service life.

The objective of this work is to select a better beam joint material that can resist early-age cracking in the joint between adjacent box beams. To achieve this objective, two phases of laboratory material characterization tests were conducted: Phase I, material selection and Phase II, time dependent material properties test. During Phase I, four different types of joint materials were tested: epoxy grout and (non-shrink) construction grout for the Type IV joint and shrinkage compensated concrete (mixed with Type K cement) and fiber reinforced concrete for the Type V joint. The materials were evaluated based upon shrinkage, flexural tensile strength and interfacial normal bond strength. During Phase II, time dependent material testing was conducted on the "best" materials from Phase I to characterize the nonlinear changes in bond strength,

compressive and tensile strength with time. Kanstad's (1990) time dependent material property equation was calibrated with the compressive strength and split cylinder tensile strength test data for the shrinkage compensated concrete. A finite element modeling approach capable of simulating the early-age joint behavior was developed and used for the further study. The objective of the finite element modeling was to calculate the stress development in the joint during early-age and to evaluate the structural performance of both Type IV joint with epoxy grout and Type V joint with shrinkage compensated concrete subject to the material self-volume change. Two finite element models were developed for a 4ft long beam-joint-beam structure and the calculated stress distribution in the joint was determined and analyzed.

3.3 Material test

3.3.1 Phase I: initial material testing and selection

The objective of the Phase I test is to perform laboratory material characterization tests which will allow for the selection of the most viable joint material. The joint materials tested were selected based upon previous experience and information collected during an extensive literature review and include: epoxy grout and (non-shrink) construction grout for the Type IV joints and shrinkage compensated concrete (Type K cement added) and fiber reinforced concrete for the Type V joints (shown in Figure 3-1). The joint materials were evaluated based on three basic material properties: shrinkage, flexural tensile strength, and interfacial normal bond strength between precast concrete and the joint material. The mix designs for shrinkage compensated concrete and fiber reinforced concrete were adapted from the standard Iowa DOT C4 concrete as shown in Table 3-1. For the shrinkage compensated concrete, 15% of the traditional Portland cement was replaced by Type K cement.

Shrinkage testing was conducted following the provisions outlined in ASTM C157. This test method determines changes in length in hardened hydraulic cement mortar and concrete that are produced by causes other than from externally applied forces and temperature changes. For each type of material, three specimens (shown in Figure 3-2a and b) were cast and then cured under room temperature (about 75°F) with 100% humidity. For each test, the mold was removed 24 hours after pouring and the first data were measured immediately after removal of the mold. The shrinkage data were collected each day for the 28 days following casting. The results for all four type of materials shown are in Figure 3-3. The construction grout expanded about 750 microstrain during the first 14 days and shrank back to about 200 microstrain at about the 28th day, while the shrinkage compensated concrete expanded only 80 microstrain during the first seven days. It should be noted that the magnitude of expansion of shrinkage compensated concrete can be controlled by adjusting the proportion of the Type K cement. The epoxy grout shrank to about 250 microstrain at 10th day while the fiber reinforced concrete started to shrink at the 14th day and achieved 600 microstrain shrinkage at 28th day.

The flexural strength tests were conducted based on ASTM C580-02 for the epoxy grout (shown in Figure 3-2 c) and ASTM C78 for the other three materials (shown in Figure 3-2 d). All specimens were cured as specified for 28 days and tested at the 28th day. Based on ASTM C580-02, which covers the determination of flexural strength and modulus of elasticity in flexure of cured chemical resistant materials in the form of molded rectangular beams, six 1"×1"×12" specimens were cast and tested with the two-point load approach. The flexural strength of the shrinkage compensated concrete and fiber reinforced concrete were tested based on ASTM 78, which covers the determination of the flexural strength of concrete by the use of a simple beam with third-point loading. Three 6"×6"×21" specimen were casted and tested for each material.

The flexural strength testing of the construction grout also followed ASTM 78, except the specimen size was reduced into 3"×3"×11.25". In all tests, fracture initiated on the tension surface within the middle third of the span length. Figure 3-4 shows the tensile stress at failure for all specimens. The results indicates that the epoxy grout has a high flexural tensile strength (about 4.8ksi), while the other three materials show similar flexural tensile strengths of about 1ksi.

The interfacial bond strength between the joint materials and the precast concrete were tested based on ASTM C1583M. For each type of material, two type of surface treatments (water blasted surface and sand blasted surface) were prepared on traditional concrete block specimens, each being about 6in. by 21in. The sand blasted surface had aggregate extending beyond the hardened cement paste by about ¼ in. The water blasted surface had no significant visible difference from the untreated condition. After placement and curing of the joint material, three 2in. diameter specimens were created on each test block by coring through the joint material and through the bond surface (shown in Figure 3-2e). All specimens were cured under sprayed water with 100% humidity and room temperature (about 75°F) for 28 days and cored and tested at the 28th day. All the specimen failed either at the interfacial surface or in the base concrete (box girder concrete). The test results shown in Figure 3-4 indicates that the interfacial normal bond strength for all four materials is spreading between 0.25ksi to 0.4ksi. No significant difference were observed between water blasted surface and sand blasted surface.

Comparing the construction grout with the epoxy grout, both materials show a similar bond strength at the 28th day but complete opposite self-volume change during the first 28days. Since, one of the approaches to prevent cracking in the joint is to increase the material tensile strength and the epoxy grout shows an extremely large flexural tensile strength (about 5ksi.)

compared to that of the construction grout which is around 1ksi, the epoxy grout was selected for the consideration in Type IV joint geometry. The fiber reinforced concrete and the shrinkage compensated concrete show similar flexural strength and bond strength. However, the shrinkage compensated concrete expanded during the early-age while the fiber reinforced concrete had a shrinkage of approximately 600 microstrain. Since shrinkage is considered to be one of the main causes of early joint crack developing, the shrinkage compensated concrete was selected for the consideration in Type V joint. For the epoxy grout and shrinkage compensated concrete, a sand blasted surface did provide a slightly higher bond strength than the water blasted surface (shown in Figure 3-3).

3.3.2 Phase II: time dependent material properties

In Phase II, time dependent material testing was conducted on the materials selected in Phase I, shrinkage compensated concrete and epoxy grout, to characterize the early-age time dependent nonlinear changes in compressive strength, tensile strength, and normal bond strength. The tensile strength in Phase II was tested following ASTM C580-02 for epoxy grout, and following both ASTM C78 and ASTM C496 for shrinkage compensated concrete to capture the difference between the flexural tensile strength and split cylinder tensile strength. The test results shown in Figure 3-5a indicate that the epoxy grout quickly developed a high tensile strength (about 5ksi.) during the first day and was almost constant during the next 27 days. Both split cylinder test and flexural test show very similar tensile strengths (0.7ksi) at the 28th day, while it seems that the flexural tensile strength developed earlier than the split cylinder tensile strength during the first 7 days. The compressive strength was tested following ASTM 1583 for epoxy grout and ASTM C39 for the shrinkage compensated concrete. The results in Figure 3-5b shows a similar trend as tensile strength development that epoxy grout developed a earlier and higher

strength in compression than the shrinkage compensated concrete. Kanstad's (1990) developed Eq. 1 and 2 to represent the time dependent change of the compressive strength and tensile strength for concrete material, in which, t^0 is the time when the concrete starts develop strength and stiffness and is usually assumed to be 0.25 day (6hr). The compressive strength and split cylinder tensile strength test data of the shrinkage-compensated concrete were used to calibrate two parameters s, and n_t and equal to 0.34 and 0.8, respectively (see Figure 3-5a and b for a comparison with test data).

$$f_t(t) = f_{t28}\{\exp\left[s * \left(1 - \sqrt{\frac{28}{t - t^0}}\right)\right]\}^{n_t} \tag{1}$$

$$f_c(t) = f_{c28}\{\exp\left[s * \left(1 - \sqrt{\frac{28}{t - t^0}}\right)\right]\} \tag{2}$$

The bond strength between the normal concrete and shrinkage compensated concrete was tested with various interface treatments: (1) no treatment; (2) sand blasted with aggregate exposed about 1/4 in.; (3) form retarder 1 roughened with aggregate exposed about 5/8 in.; (4) form retarder 2 roughened with aggregate exposed about 3/4 in. (5) no surface treatment but reinforced by No.4 rebar; Two test approaches were used: direct Pull-off test following ASTM C1583M for treatment (2) and split cylinder test following ASTM C496 (shown in Figure 3-2f) for treatment (1), (3), (4) and (5). The bond strength between the epoxy and normal concrete was tested following ASTM C1583M and the interface was sand blasted with aggregate exposed about 1/4 in. The results in Figure 3-5c indicates that the bond strength developed during the first three days and tends to be constant after that. Both joint materials shows similar bond strength while the specimens reinforced with steel have a higher normal bond strength than the others at both the early-age and 28 days.

3.4 Prediction of early-age joint stress

A finite element model was established to simulate the stress development in the joint from the 24hr after material placement to the 7th day to evaluate the structural performance of both the Type IV joint with epoxy grout and Type V joint with shrinkage compensated concrete subject to material self-volume changes. Since joint material shrinkage/expansion induced cracking is known to be a local phenomenon, the finite element model was developed for portion of a joint consisting of two 4ft long box girders and one joint. The cross sectional geometry for the Type IV and Type V joints are shown in Figure 3-6. The finite element model was established using three dimensional solid elements for both the box girder and the joint as shown in Figure 3-7. The element size for both models are about 1in. except in the Type IV joint model where 1/3in. elements were used to mesh the narrow joint. In general, the aspect ratio in all models is less than 3. Since the structure is symmetric in both the transverse and longitudinal directions, the model was created for only a quarter of the structure to improve computational efficiency. The joint element and box beam element shared the same nodes at the interface. Sliding at the interface was not included in the model. A trial analytical study indicated that a transverse tensile stress in the joint is induced by the expansion of the joint material due to "edge effects". It was found, as a result, that the model without sliding at the interface results in a higher transverse tensile stress in the joint and is, therefore, more conservative.

The total strain in the early-age ageing material (cement-based grout, epoxy grout and concrete), which includes stress induced (ε_σ) strain and stress independent strain (ε^o), can be expressed as (L'Hermite, 1988):

$$\varepsilon(t) = \varepsilon_\sigma(t) + \varepsilon^o(t) = \varepsilon_E(t) + \varepsilon_C(t) + \varepsilon_S(t) + \varepsilon_T(t) \tag{3}$$

where stress induced strain (ε_E) discussed here includes only instantaneous elastic strain (ε_E) and creep strain (ε_C). The stress independent strain (ε^o) discussed in this paper includes only shrinkage strain (ε_S) and temperature induced strain (ε_T).

Before a bridge is subjected to live load, ε_σ can be caused by concrete hardening, creep, shrinkage, and temperature change (induced by heat of hydration and daily environmental temperature change). In this analysis the shrinkage loading is the only loading considered as the effects from temperature changes as independent of the material utilized. The shrinkage test results shown in Figure 3-3 indicated that the epoxy grout experienced a 200 microstrain shrinkage from 24hr to 7th day and the shrinkage compensated concrete experienced an 80 microstrain expansion during the same period. Therefore, the 200 microstrain shrinkage and 80 microstrain expansion was applied on Type IV and Type V joint, respectively, by creating an artificial temperature loading that resulted in the same shrinkage/expansion.

The reinforcement in the box beam was smeared into the concrete by increasing the effective Young's modulus, since they contribute minimally to the transverse stress in the joint and at the interface. The time dependent Young's modulus was estimated based on the compressive strength test results in Figure 3-5b using Eqn.4.

$$E(t) = 57{,}000\sqrt{f_c{'}(t)} \quad (psi) \tag{4}$$

The results are shown in Figure 3-8 for epoxy grout and shrinkage compensated concrete. Since the box beams are usually precast before the construction, the time dependent effect of the box beams was not included in the model. The compressive strength of the box beams were assumed to be 5ksi and 4,030ksi was used as the Young's modulus of box beam. Since the Young's modulus of epoxy kept almost constant during the 24hr to 7th day (see Figure 3-8), a linear elastic analysis was performed on the Type IV joint model with a constant Young's

moduli 5,600ksi for the joint material. Since the shrinkage compensated concrete experienced a significant increase in Young's modulus from 2000ksi to 4300ksi, a time dependent analysis based on the superposition approach was performed on the Type V joint model.

At the early-age of concrete, the strength hardening and creep behavior can be simplified using an aging viscoelastic model. Bazant (1988) indicates that the strain induced by stress in an aging viscoelastic concrete material can be calculated based on the principal of supposition and expressed as,

$$\varepsilon_\sigma(t) = \int_0^t J(t, t') \, d\sigma(t') \tag{5}$$

where, $J(t, t')$ is a creep compliances which represent the strain induced by a unit constant stress imposed at time t'. The $J(t, t')$ compliance, which accounts for both the aging instantaneous effect and the viscoelastic effect, can be expressed as

$$J(t, t') = \frac{1}{E(t')} + C(t, t') \tag{6}$$

where $E(t')$ is elastic modulus characterizing the instantaneous deformation at age t' and $C(t, t')$ is the creep compliance. Concrete creep is a very complicated mechanism and can be influenced by various factors (such as mix design, temperature, load level, shrinkage, humidity, etc.). There is not consistent agreements in available literature about how much effect comes from each factor or from the combination of different factors. The model developed in this paper does not include the creep effect since the joint stress tends to be in relaxation form and reduces with time when it subject to constant loading. Further, model without creep results in a higher stress in the joint and is more conservative.

The constitutive relationship in Eqn.5 can be expressed in three dimensions as (Bazant, 1988),

$$\boldsymbol{\varepsilon}(t) = \int_0^t \boldsymbol{B} J(t, t') \, d\boldsymbol{\sigma}(t') + \boldsymbol{\varepsilon}^0(t) \tag{7}$$

in which,

$$\boldsymbol{\sigma} = (\sigma_{11}, \sigma_{22}, \sigma_{33}, \sigma_{12}, \sigma_{23}, \sigma_{31})^T$$

$$\boldsymbol{\varepsilon} = (\varepsilon_{11}, \varepsilon_{22}, \varepsilon_{33}, \varepsilon_{12}, \varepsilon_{23}, \varepsilon_{31})^T$$

$$\boldsymbol{\varepsilon}^0 = (\varepsilon^0, \varepsilon^0, \varepsilon^0, 0,0,0)^T$$

and

$$\boldsymbol{B} = \begin{bmatrix} 1 & -\nu & -\nu & 0 & 0 & 0 \\ -\nu & 1 & -\nu & 0 & 0 & 0 \\ -\nu & -\nu & 1 & 0 & 0 & 0 \\ 0 & 0 & 0 & 1+\nu & 0 & 0 \\ 0 & 0 & 0 & 0 & 1+\nu & 0 \\ 0 & 0 & 0 & 0 & 0 & 1+\nu \end{bmatrix} \tag{8}$$

where σ_{ij} and ε_{ij} are the stress and strain components in Cartesian coordinate; ε^0 is the stress independent strain including the strain caused by temperature and shrinkage; superscript T donates the transpose of a matrix and ν is the Poisson's ratio.

The time dependent early-age ageing finite element structural analysis was performed using the commercial software ABAQUS and a custom MATLAB script. Figure 3-9 shows a flow chart that describes the process to perform a time dependent structural analysis with ageing concrete. The first step is to divide the loading (joint material expansion for Type V joint) into load increments (ΔP). In this analysis, a time stepped 0.05day (1.2hr.) was used. At each load increment (ΔP), a linear elastic analysis was performed using the Young's Modulus value at the time of the load increment. The strength hardening of the fresh concrete was modeled by updating the Young's Modulus $E(t)$ in each analysis. The total structural response at a certain time point (t) can be obtained by summing the results from all the elastic analysis before time (t) based on the superposition approach mentioned previously.

3.4.1 Type IV joint

Figure 3-10 shows the stress distribution on the Type IV joint. Figure 3-10a and c show the first principal stress in the joint and indicate that most of the joint material is subject to tensile stress caused by shrinkage of the epoxy grout. Figure 3-10b and d show the contour plot for the transverse stress. The results indicate that most of the joint is subject to tension in the transverse direction except near the exterior and formed a "tension-domain" joint, which shows an agreement with the analytical results in Sharp (2007). All four contour plots in Figure 3-10 show that stress concentration at the vicinity of shear key, which is consistent with the findings by Dong (2007).

3.4.2 Type V joint

Figure 3-11 shows the stress distribution in the Type V joint. Figure 3-11a, b, c and d show the transverse stress from the four layer elements in the joint (see Figure 3-7b). It is obvious the majority of the joint is subject to compressive stress in the transverse direction except at the exterior region and therefore formed a "compression-domain" joint. This is opposite to the results from Type IV joint since the shrinkage compensated concrete in the Type V joint expanded. Figure 3-11e and f plot the shear stress distribution at the interface elements (Layer 1 from Figure 3-7b). It can be seen that the expansion of the joint material induces shear stress at the interface which results in the tension at the exterior region due to the "edge effect". Considering the bond strength test results that showed that the steel reinforcement significantly increases the normal bond strength, it is believed that the tensile stress can be resisted and cracking near the edge can be controlled if the exterior region is reinforced by steel reinforcement that perpendicular to and crossing the interface surface.

3.5 Summary and conclusion

Longitudinal cracking in the joint between adjacent box beams has been a concern for decades. Many past research results pointed to the fact that an effective joint material should have small or zero shrinkage at the early-age and a small temperature induced self-volume change. It should able to achieve sufficient bond strength at the interface between the joint and the box beam starting from early-age through the entire bridge service life.

In this paper, two phases of laboratory material characterization tests were performed. During the Phase I, four potential joint materials were tested and evaluated based on the shrinkage, flexural tensile strength, and normal bond strength properties. The results indicate that epoxy grout is superior to construction grout for Type IV joint geometries and shrinkage compensated concrete is superior to the fiber reinforced concrete for Type V joint geometries. During Phase II, time dependent material testing was conducted on epoxy grout and shrinkage compensated concrete to characterize the nonlinear changes, bond strength, compressive and tensile strength with time. The compressive strength and split cylinder tensile strength data were used to calibrate Kanstad's (1990) time dependent material change equation. The bond strength test indicates that both epoxy grout and shrinkage compensated concrete with the same surface treatment show a similar bond strength. However, an interface reinforced by even a minimal amount of steel has a notably higher normal bond strength than with other surface treatment approaches at both the early-age and 28 days.

A finite element modeling approach which is capable of simulating the early-age joint behavior was developed and utilized for further evaluation. Two finite element models were developed for 4ft long beam-joint-beam structures with Type IV joint connected with epoxy

grout and Type V joint connected with shrinkage compensated concrete. The stress distribution in the joint was output from the analytical model and conclusions can be draw as follows:

1. Self-volume change of the joint material generate internal stress during the early-age.

2. The shear key within the Type IV joint induces stress concentrations.

3. An expansion material is better than shrinkage material since it forced a "compression-domain" joint. But the best option is the material without any early-age self-volume change, since the difference in the self-volume change between the joint material and box girder material is the cause of the early-age joint stress.

4. For the same reason, a material which has similar thermal expansion characteristic as the box girder concrete material is preferred (cement based concrete rather than epoxy grout) when considering the thermal stress changes when the structure is subject to daily temperature change.

Based on the conclusions above, the Type V joint filled with shrinkage compensated concrete is expected to perform superior to the Type IV joint with epoxy in resisting joint cracking and debonding at the interface. Although the FEM results indicated that Type V joint filled with shrinkage compensated concrete still induces tensile stress near the exterior of the interface, the placement of reinforcement near the edge will have sufficient capacity to resist the debonding at the interface during the early-age period when initial cracking has been found to occur.

3.6 References

Attanayake, U., and Aktan, H. (2008). "Issues with Reflective Deck Cracks in Side-by-Side Box Beam Bridges." Proceedings of the 2008 Concrete Bridge Conference, Federal Highway Administration, National Concrete Bridge Council, Missouri Department of Transportation, American Concrete Institute, 18p.

Bazant, Z. P. (1988). Mathematical Modeling of Creep and Shrinkage of Concrete. JOHN WILEY AND SONS.

Dong, H., Li Y., and Ahlborn T.M. (2007). "Performance of Joint Connections between Decked Prestressed Concrete Bridge Girders," PCI National Bridge Conference, Proceedings, Phoenix, Arizona.

El-Remaily, A., Tadros, M. K., Yamane, T., and Krause, G. (1996). "Transverse design of adjacent precast prestressed concrete box girder bridges." PCI Journal, 41, 96-113.

Grace, N. F., Jensen, E. A.,and Bebawy, M. R. (2012). "Transverse post-tensioning arrangement for side-by-side box-beam bridges." PCI Journal, 57(2), 48-63.

Kanstad, T., Hammer, T. A., Bjøntegaard, Ø., & Sellevold, E. J. (1999). Mechanical properties of young concrete: Evaluation of test methods for tensile strength and modulus of elasticity. Determination of model parameters. NOR-IPACS report STF22 A99762.

Lall, J., S. Alampalli, and E. F. DiCocco. (1998). "Performance of Full-Depth Shear Keys in Adjacent Prestressed Box Beam Bridges." PCI Journal, 43(2), 72-79.

L'Hermite, R. (1988). Mathematical modeling of creep and shrinkage of concrete. Z. P. Bazant (Ed.). New York: Wiley.

Ramakrishnan, V. "Expansion-Shrinkage, Creep, and Elastic Modulus of Shrinkage-Compensating Gap-Graded Concrete." Special Publication 64 (1980): 123-152.

Russell, H. G. (2009). Adjacent precast concrete box beam bridges: Connection details (Vol. 393). Transportation Research Board.

Sang, Z. (2010). "A Numerical Analysis of the Shear Key Cracking Problem in Adjacent Box Beam Bridges." Doctoral dissertation, The Pennsylvania State University.

Sharpe, G. P. (2007). "Reflective cracking of shear keys in multi-beam bridges", Doctoral dissertation, Texas A&M University.

Ulku, E., Attanayake, U., and Aktan, H. M. (2010). "Rationally Designed Staged Post-tensioning to Abate Reflective Cracking on Side-by-Side Box-Beam Bridge Decks."
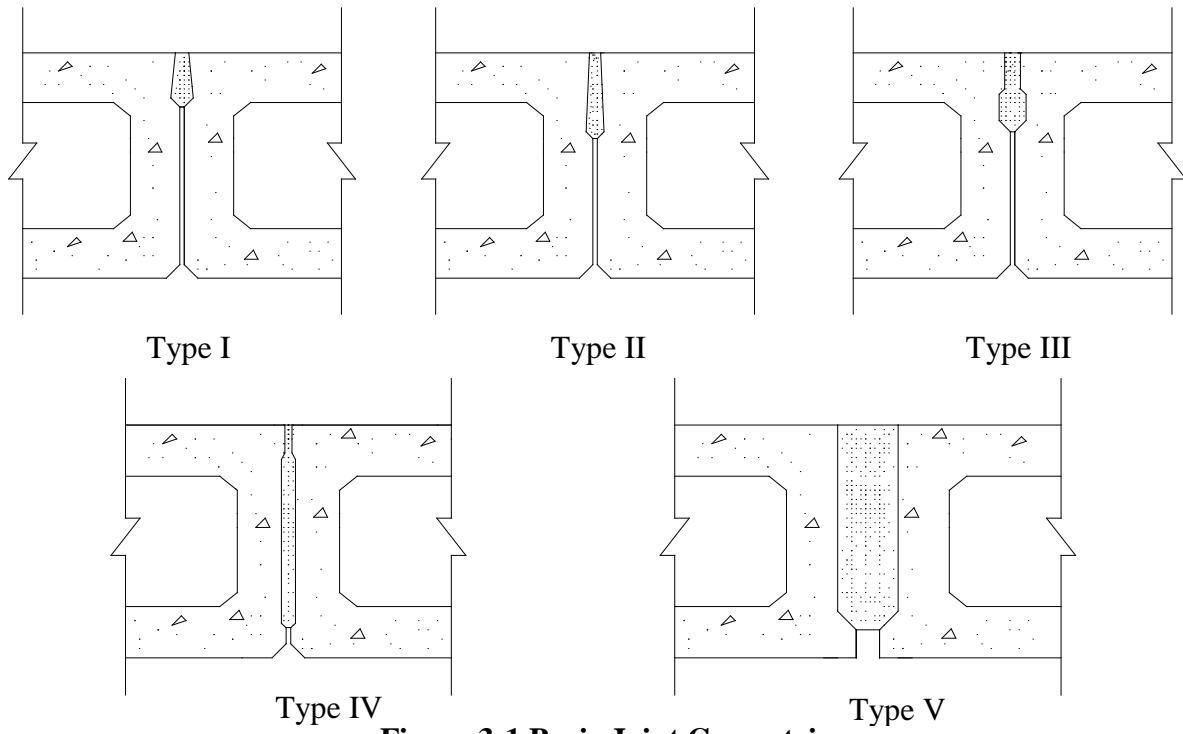
Type I   Type II   Type III

Type IV   Type V

Figure 3-1 Basic Joint Geometries

Table 3-1 Mix Design

Component (lb/yd^3)	Iowa DOT C4	Shrinkage compensated concrete	Fiber reinforced concrete
Portland Cement	474	403	474
Water	255	255	255
Fine Aggregate	1500	1500	1500
Coarse Aggregate	1517	1517	1517
Type K Cement		71	
Polypropylene Fiber			5

(a) 1"×1"×11.25" specimen (epoxy grout)

(b) 3"×3"×11.25" specimen (concrete)

(c) Flexural tensile strength (epoxy grout)

(d) Flexural tensile strength (concrete)

(e) Pull off test

(f) Split cylinder debonding test

Figure 3-2 Time Dependent Material Properties Test
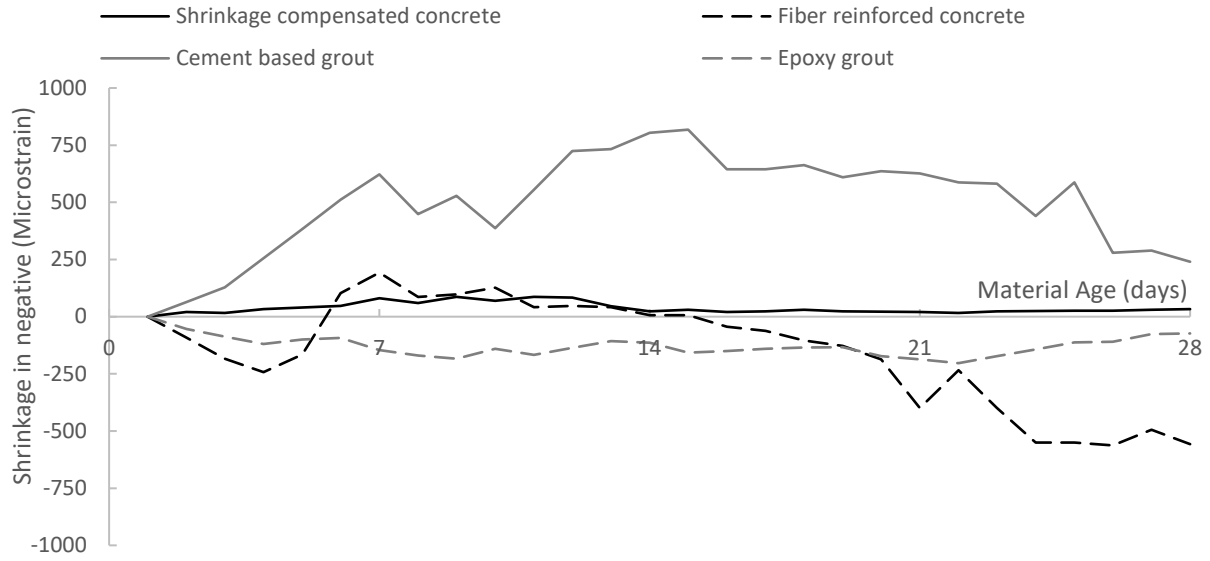
Figure 3-3 Shrinkage Test Results
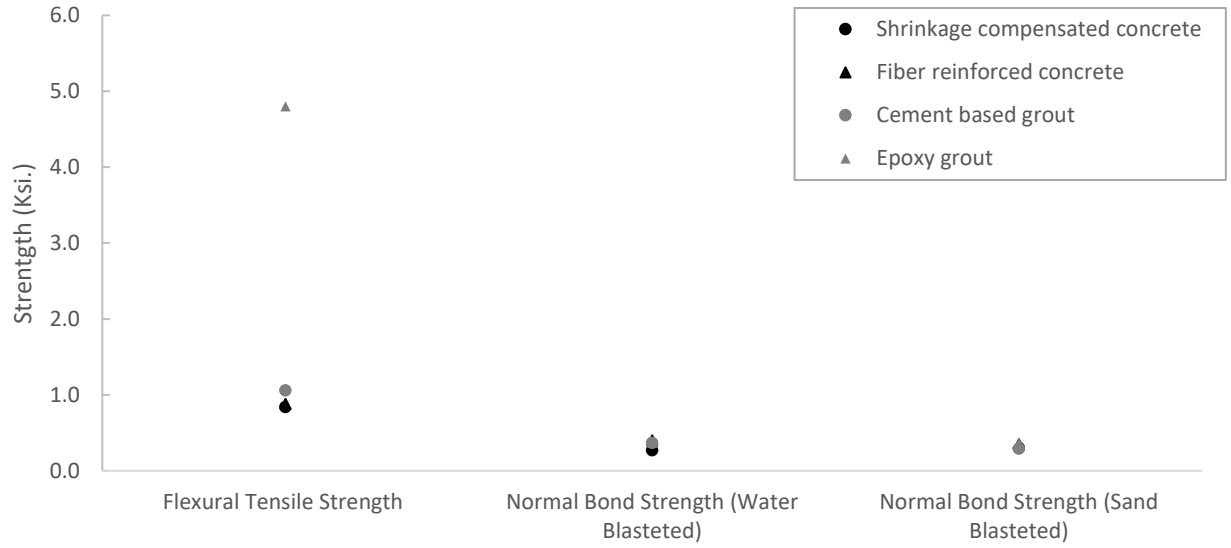
Figure 3-4 Flexural Tensile Strength and Bond Strength Tests Results
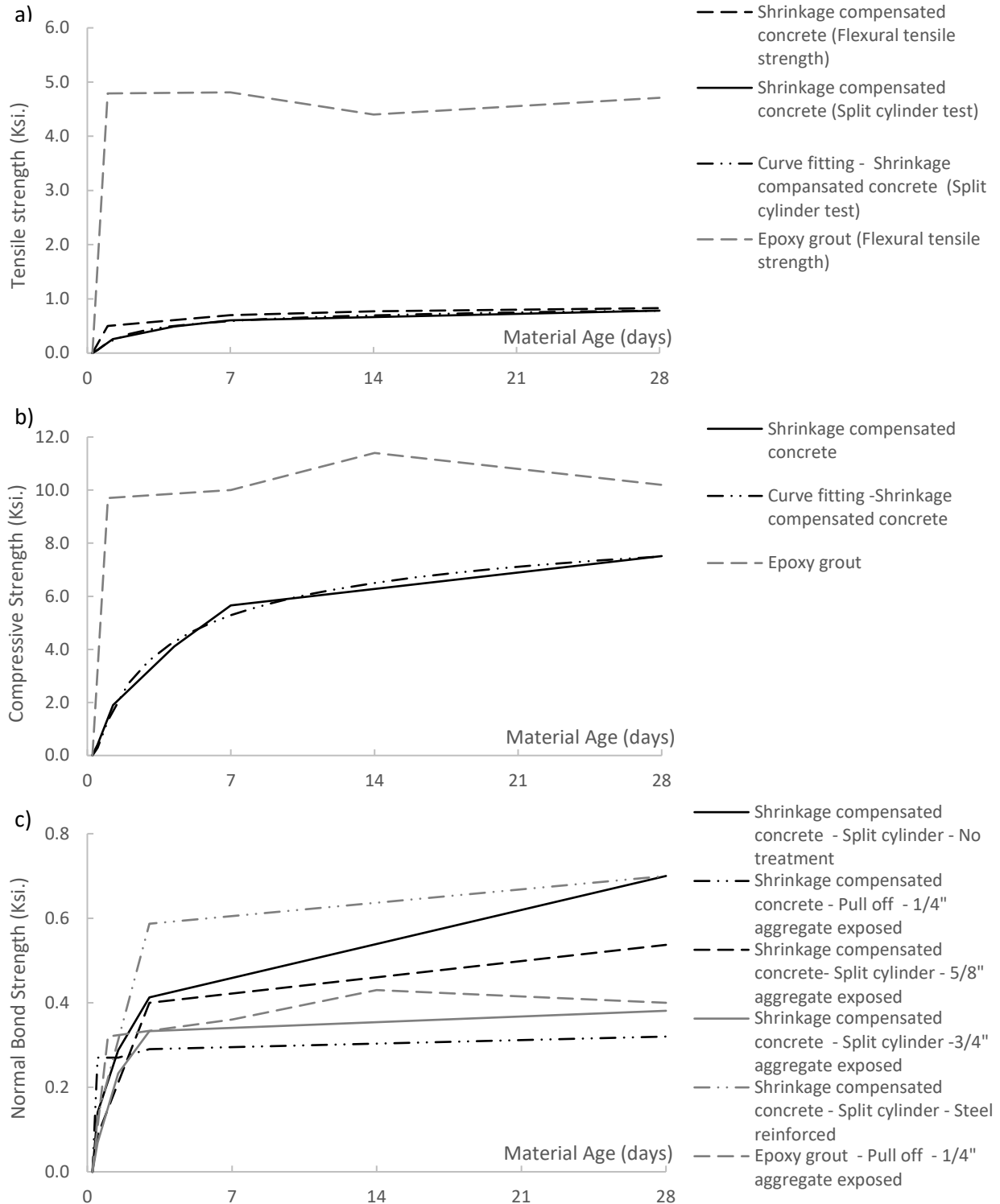
Figure 3-5 Time Dependent Material Properties Test Results: (a) Tensile strength; (b)

Compressive strength; (c) Normal bond strength
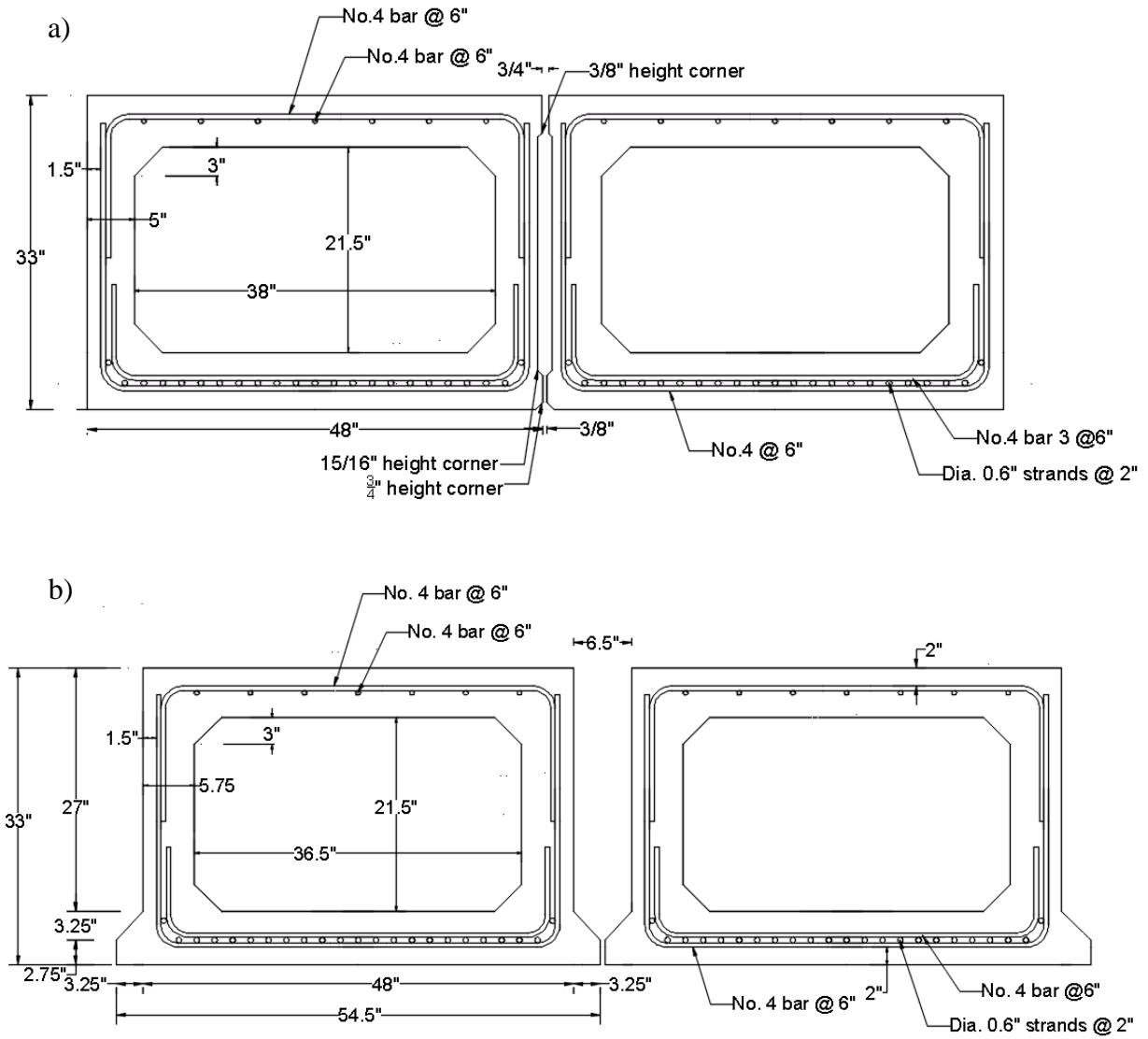
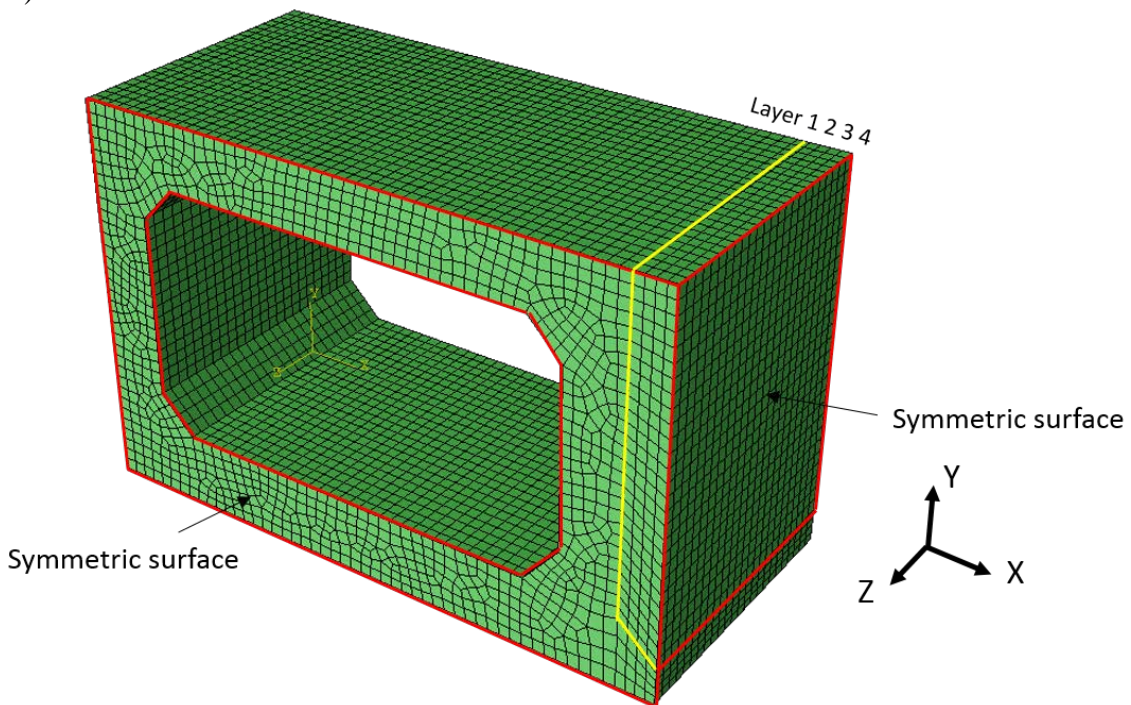**Figure 3-6 Cross Section Design: a) Type IV joint; b) Type V joint**

a)
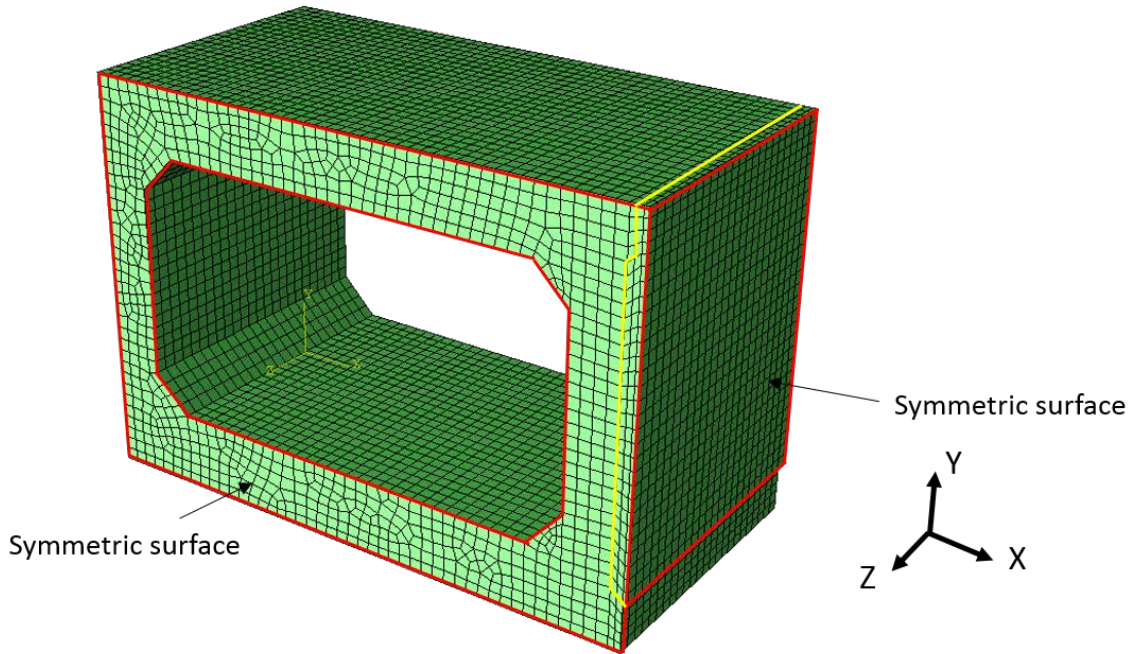
b)

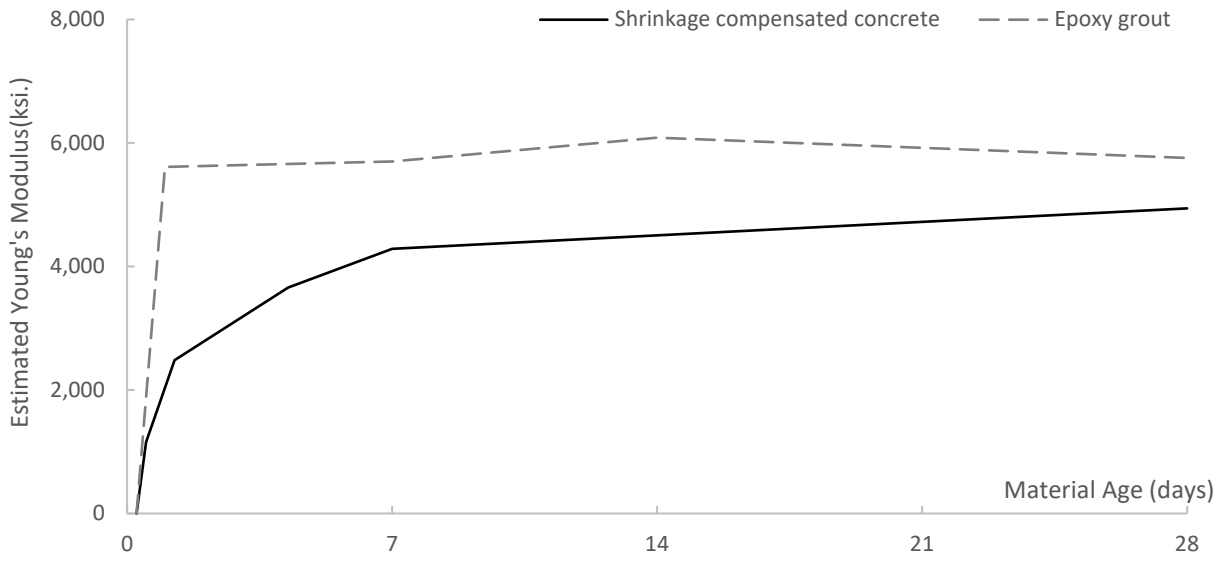**Figure 3-7 Finite Element Models: a) Type IV Joint; b) Type V Joint**

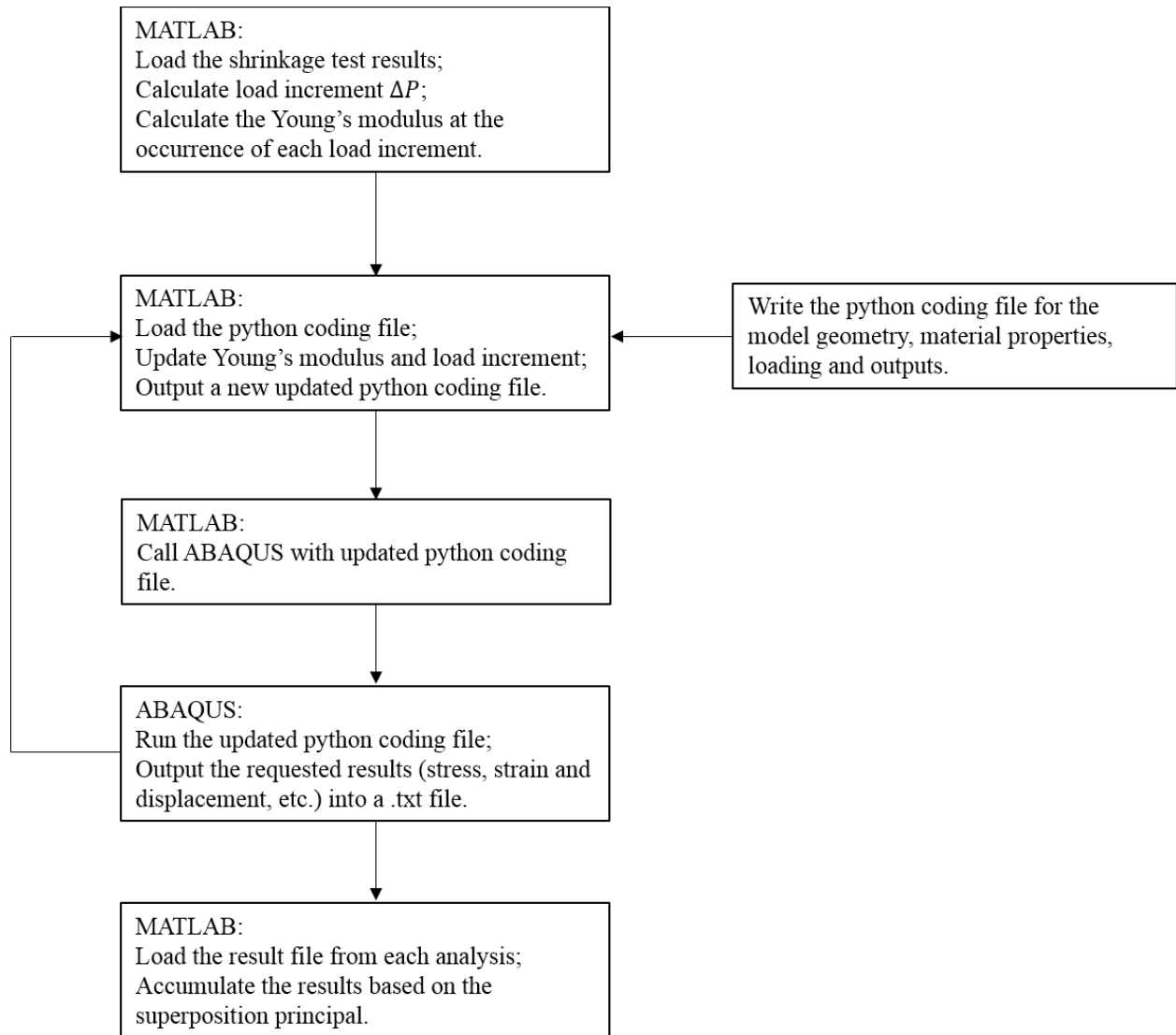**Figure 3-8 Estimated Time Dependent Young's Modulus**

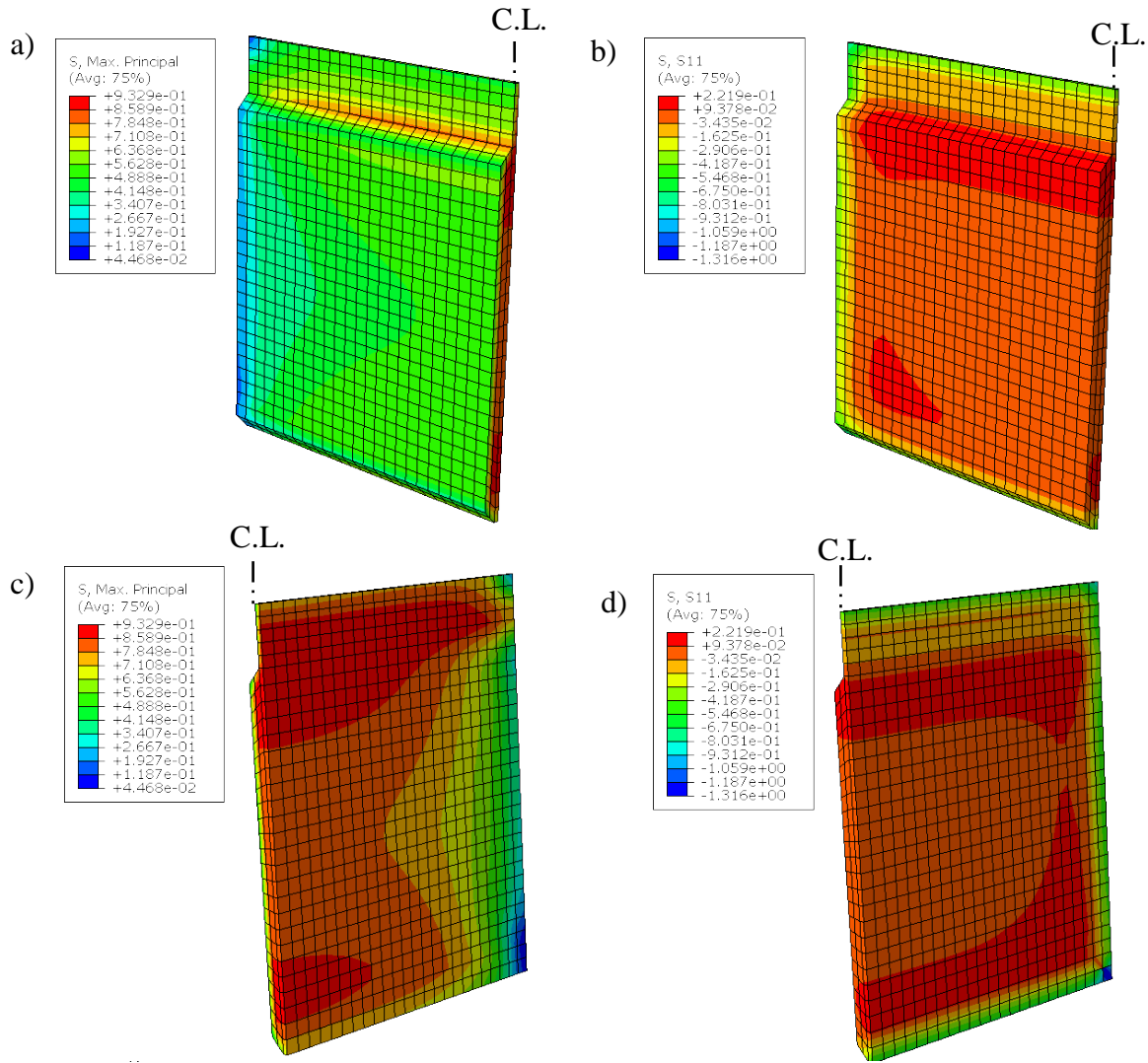**Figure 3-9 Flow Chart for Time Dependent Analysis**

Figure 3-10 Stress Distribution in Type IV Joint: a) First Principal Stress in the Joint near the Interface; b) Transverse Stress (σ_{xx}) in the Joint near the Interface; c) First Principal Stress at the Center of the Joint; d) Transverse Stress (σ_{xx}) at the Center of the Joint
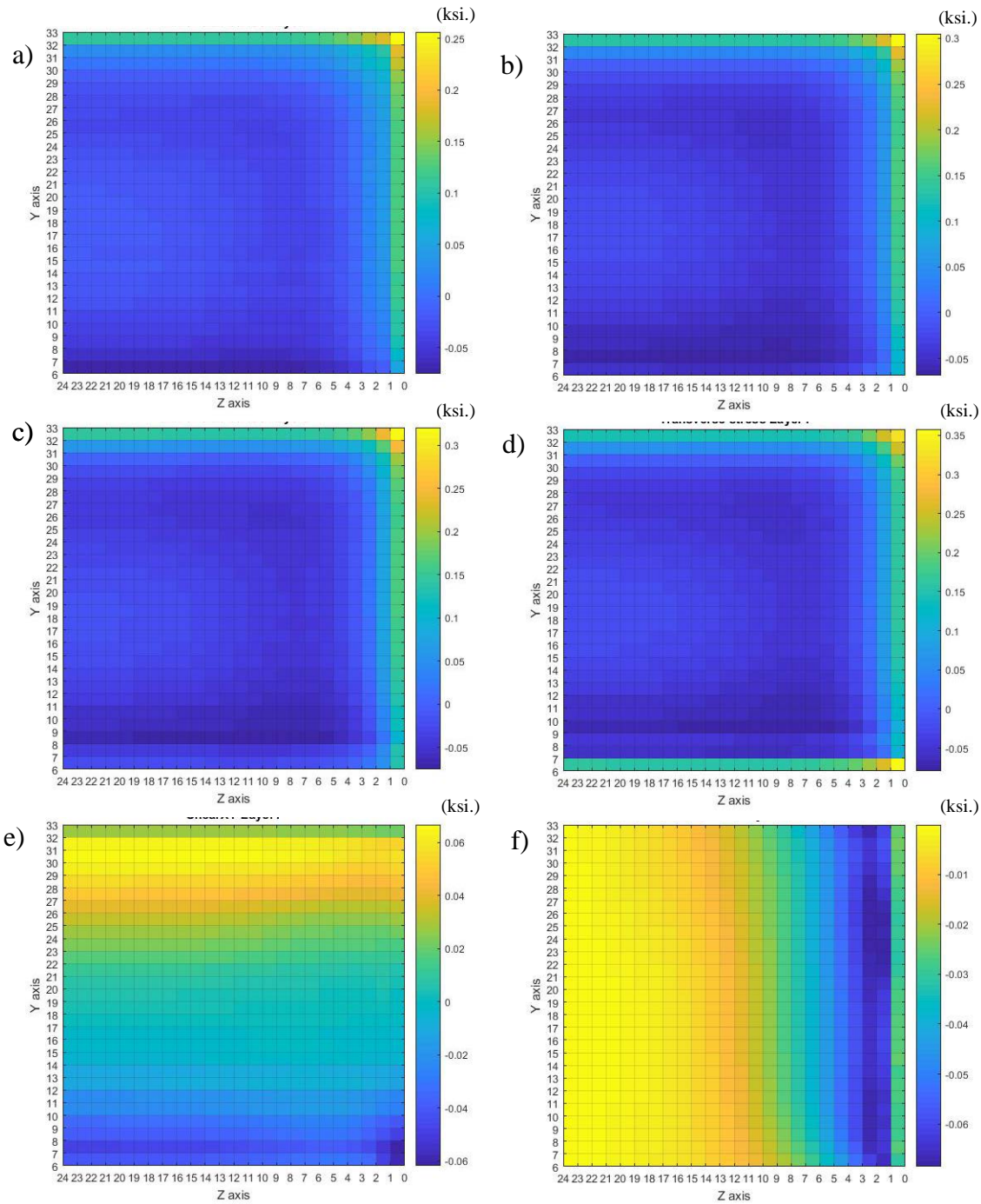
Figure 3-11 Stress Distribution in Type V Joint: a) Transverse Stress (σ_{xx}) in Layer 1; b) Transverse Stress (σ_{xx}) in Layer 2; c) Transverse Stress (σ_{xx}) in Layer 3; d) Transverse Stress (σ_{xx}) in Layer 4; e) Shear Stress XY in Layer 1; f) Shear Stress XZ in Layer 1;

CHAPTER 4. INNOVATIVE JOINT DESIGN FOR ADJACENT BOX BEAM BRIDGES

Liu, Zhengyu[3]; Phares, Brent M[4]

This paper is to be submitted to Engineering Structures, ELSEVIER

4.1 Abstract

Adjacent concrete box beam bridges constitute more than 15% of bridges built or replaced each year and have been in service for many decades. A recurring problem with this type of bridge is the cracking in the longitudinal joints between adjacent beams which allows water and salt leakage through the joint and reflective cracks in the wearing surface. In this paper, a comprehensive review of the literature over the past 20 years was conducted to identify the potential reasons that may induce the joint cracking. An innovative connection was then designed with wide joint, shrinkage compensating concrete, rough interface between the joint and box girder, and reinforcing steel that crosses the interface between the joint and box beam, to overcome the problems mentioned in the literature review. The design was evaluated on four small scale specimens with different transverse reinforcement amount. The specimens were monitored for early-age joint behavior and then tested for ultimate capacity. Finite element models were developed to simulate the early-age joint behavior to determine the stress distribution in the joint and at the interface between the joint and the box beam concrete. The shrinkage, temperature, strain data collected during the early-age monitoring was used to validate the finite element model. Both experimental and finite element analysis results indicated that the innovative joint showed good performance in resisting joint cracking when it subject to joint material expansion and heat of hydration. The results also indicated that the expansion of the

---

[3] Liu, Zhengyu, Ph.D. candidate, Graduate Research Assistant, Department of Civil, Construction and Environment Engineering, Iowa State University, Ames, Iowa 50010, zhengyu@iastate.edu.
[4] Phares, Brent M., PhD, P.E., Director, Bridge Engineering Center, Iowa State University, Ames, Iowa 50010, bphares@iastate.edu.

joint material formed a "compression-dominate-joint" which would naturally inhibit crack formulation. The transverse reinforcing steel across the interface resists the expansion of the joint material and results in some additional transverse compression into the joint.

Keywords: Shrinkage Compensating Concrete; Adjacent Box Beam; Finite Element Modeling; Early-age Joint Behavior

4.2 Introduction

Adjacent concrete box beam bridges constitute more than 15% of bridges built or replaced each year. This type of bridge is generally constructed by placing box beams next to one another, grouting a shear key, applying a transverse post-tensioning force, and then placing either a thin (3 in.) wearing surface or a thick (6 in.) structural deck on top. In some cases, the top of the box beams are left bare to serve as the riding surface. These bridges are attractive because of their relatively shallow superstructure depth, ease of construction, and simple aesthetic attributes.

NCHRP Synthesis 39 (Russell, 2009) reported a wide variety of practices used by state highway agencies for the connection details between adjacent box beams. These practices include partial depth or full depth grouted keyways (joint), keyways grouted before or after transverse post-tensioning, prepackaged or non-prepackaged grout materials, post-tensioned or non-tensioned transverse ties, a wide range of applied transverse post-tensioning forces, and cast-in-place concrete decks or no decks. NCHRP Synthesis 39 indicated that research to evaluate those practices at the design and construction phases could lead to connection details that prevent cracking and leakage at the joints and extend the service life of adjacent box beam bridges.

Russell (2009) indicated that the most common types of distress are longitudinal cracking along the grout and box beam interface, water and salt leakage through the joint, and reflective

cracks in the wearing surface. In the United States, three typically used generic partial depth keyway geometries are the Types I, II and III keyways and a generic full depth keyway geometry (Type IV keyway) shown in Figure 3-1. Conversely, the typically used Japanese keyway is the full depth keyway Type V shown in Figure 3-1. El-Remaily et al. (1996) reported that longitudinal cracking was seldom found in the adjacent box beam bridges with the Type V full-depth keyway.

Liu and Phares (2018) conducted multiple levels of material tests and developed a finite element modeling approach which is capable of simulating early-age joint behavior to select the best material associated with various joint geometries that can resists early-age joint cracking. Four materials including epoxy grout, cement based construction grout, fiber reinforced concrete and shrinkage compensated concrete were evaluated using a combination of modeling and material test results. The results indicated that the Type V joint (see Figure 3-1) filled with shrinkage compensated concrete is expected to perform superior to the Type IV joint (see Figure 3-1) filled with epoxy. It was also found that the Type V joint filled with shrinkage compensated concrete still induces tensile stress near the exterior of the interface, and that the placement of reinforcement near the edge will have sufficient capacity to resist the debonding at the interface during the early-age period when initial cracking has been found to occur. It should be noted that the results from the finite element model represents the structure behavior due to only the joint material self-volume change during 24hr to 7th day, the structural response induced by other loadings, such as temperature change, self-weight, etc. were not included.

In this paper, a comprehensive literature review focusing on the relevant research from the past twenty years was conducted to identify the reasons that cause cracking in the joint between the adjacent box beams. An innovative joint was designed based on the results from the

literature review and proposed to eliminate joint cracking. The design was evaluated with a series of small scale tests and analytical models. The small scale tests were conducted on four 3-ft. long specimens with different joint reinforcement ratios to study the effect of the joint reinforcement. The early-age joint behavior was monitored and an ultimate load test was performed. The finite element modeling approach, which is capable of simulating the early-age joint behavior developed by Liu and Phares (2018), was used to calculate the time-dependent stress development in the joint and at the interface between the joint and the box beam concrete. The finite element model was validated by the experimental results. The behaviors of the joints with different reinforcement ratio were evaluated based on both experimental and analytical results.

4.3 Literature review

Huckelbridge et al. (1995) conducted field testing of several adjacent box girder bridges and the test results from two of these bridges were reported. A dump truck was used to conduct on-site, controlled tests. According to the results from the finite element analysis and field tests, the authors pointed out that intact shear keys should not permit relative deflection of more than 0.001 in. between adjacent girders. Reflective cracks were found around the shear keys on both bridges. They concluded that the partially fractured shear keys still displayed adequate lateral live load distribution characteristics.

Gulyas et al. (1995) conduct three types of tests on a box beam joints: a direct vertical shear test; a direct transverse tension test; and a direct longitudinal shear test to study the performance of grouted keyways using non-shrink grouts and magnesium ammonium phosphate mortars. They found that the composite keyway specimens using magnesium ammonium phosphate mortars showed higher direct tensile bond strengths, vertical shear strength, and

longitudinal shear strength than those of the non-shrink grout keyway specimens. The authors recommended not using non-shrink grouts for the keyway unless the tensile and shear strengths satisfy the requirements in their study.

El-Remaily, et al. (1996) compared the American and Japanese design approaches and reported that longitudinal cracking was very rarely associated with Japanese box beam bridges (Type V joint shown in Figure 3-1). It was found that the primary differences between American and Japanese designs were: (1) the size and shape of longitudinal joints and (2) the amount of transverse post-tensioning.

Huckelbridge and El-Esnawi1 (1997) investigated shear key failure and developed new types of keyway connection details. A 3D finite element model on a full-scale bridge and small scale experimental test were conducted. The analytical results indicated that transverse tensile stresses in the beam top flange are the main factor causing many shear key failures. FE results showed that the proposed shear key sustained much smaller tensile stresses that would not cause shear key cracking nor failure. The experimental results showed that the mid-depth shear key design (only the shear key was grouted instead of the entire keyway) had significantly improved the static load carrying capacity and provided a longer fatigue life than the previous shear key design.

Lall et al. (1998) compared the long-term performance of a partial depth shear key system and a modified, full-depth shear key/transverse tie system. The modified full-depth shear key/transverse tie system was developed based on the results of bridge inspections in the State of New York and information from other states. The new system possesses two post-tensioning ties located at the third points of the girder depth. Survey results indicated that the new full-depth shear key/transverse tendon system showed superior cracking prevention ability and reduced the

frequency of reflective cracking in the deck. As a result of the work, the authors recommended using the new full-depth shear key for future adjacent box beam bridges.

Miller et al. (1999) evaluated the performance of three types of specimens, fabricated with a top shear key with non-shrink grout, a mid-depth shear key with non-shrink grout, and a top shear key with epoxy grout. The specimens were made of four box beams, fabricated and tested outside under normal environmental conditions. Both cyclic load test and live load test were also performed. The test results indicated that temperature induced stresses were consistently high enough to cause significant cracking of the shear key material. These cracks propagated from the two ends near the supports toward the bridge mid-span after cyclic loads. They also found that live loads did not cause new cracking but appeared to propagate existing thermally induced cracks. In addition, static load test results showed that cracking in the shear key had no remarkable effect on the live load distributions among box beams but did cause leakage in the joints. A grout material with high bond strength for the joints of the adjacent box girders was recommended.

Greuel et al. (2000) studied the field performance of a bridge constructed with a mid-depth shear key. Only the shear key was grouted and the gap above the shear key was filled with compacted sand with a sealant encapsulating the exposed longitudinal joint. Non-prestressed tie rods were used to connect the box beam together before grouting. Static and dynamic (50 mph) field testing was conducted using four dump trucks located at various transverse positions. The results indicated that there was no appreciable differential displacement between girders and the shear key and transverse rod system adequately resisted the applied live loads.

Issa et al. (2003) conducted small scale tests of keyway specimens to investigate the performance of four grout materials using direct shear, direct tension, and flexural tests. The

chloride permeability and shrinkage of the four grouts were also measured. The test results indicated that the polymer concrete showed the highest shear, tensile and flexural strengths. The polymer concrete also had superior chloride resistance and less shrinkage compared to the other grouts, while the grout had significant shrinkage due to its high water content. Finite element analysis of the tension test specimens showed that the polymer concrete specimens sustained the highest load with a minimum of cracking and crushing compared to others.

Badwan and Liang (2007a) performed a grillage analysis to determine the required transverse post-tensioning for a precast adjacent, solid, multi-beam deck. The results indicated that the required post-tensioning stress decreases with an increase in the deck width, deck thickness, and skew angles. The authors noted that the influence of skew is due to the fact that transverse bending in the skew direction decreases with skew angle. The span length affects the needed post-tensioning stress when the bridge skew is very large.

Badwan and Liang (2007b) implemented field testing and associated FE analysis of a post-tensioned adjacent solid box girder bridge with full depth keyways, mid-depth shear keys, and transverse post-tensioning. A 3D FE model was established and validated using the field collected longitudinal strain data. The authors concluded that the lateral load distribution was not affected as long as no cracks were induced in the shear keys. It should be noted that serviceability issues caused by shear key cracking were not addressed.

Dong et al. (2007) established 3D finite element models to investigate and compare the behavior of three different types of joints. The results showed that radical changes in shear key geometry (i.e., very sharp corners) may result in higher stress levels. In addition, they also found that a higher strength grout material does not reduce the cracks.

Sharpe (2007) conducted extensive 3D finite element analyses on box girder bridges to investigate the performance of the shear keys. Finite element models were established and loaded with the AASHTO HS-25 truck load, strains due to shrinkage, and a temperature gradient. Two types of failure in the shear keys were considered: debonding and cracking (with different failure stresses). The FE analysis results indicated that reflective cracking was due to high tensile stresses in the shear keys caused by temperature gradients and shrinkage strains instead of live loads. The cracks usually initiated near the supports instead of at the bridge mid-span.

Attanayake and Aktan (2008) monitored an adjacent box-beam bridge starting from construction (the bridge has narrow, full depth keyways with top shear keys) to identify the main source of the formation of longitudinal reflective cracks. Inspection results revealed that cracks were found at the interfaces between beams and keyways three days after pouring of the joint and before the post-tensioning and live load was applied. They concluded that reflective cracks are due to effects such as hydration heat and drying shrinkage.

Ulku et al. (2010) proposed a rational design procedure to calculate the transverse moments along the transverse joints and thus determine the required transverse post-tensioning. A 3D FE model was established using solid elements for the beams, keyways, diaphragms and deck. They found that the temperature gradient is the main factor causing the cracks which developed at the interface of the top shear keys. Another cause of cracks is that the post-tensioning is not uniformly distributed at the keyway because of shear lag.

Sang (2010) performed grillage analysis of adjacent box girder bridges subjected to live loads to determine shear forces and moments that must be sustained by the shear keys. Shear tests were conducted to examine the failure modes of the keyway joints grouted with cementitious grout and epoxy grout. Parametric studies were performed using finite element

models to investigate the influence of keyway geometry, grouting materials, post-tensioning, and bearing locations on the performance of the shear key. The authors concluded that cracks developed in both the full depth and partial depth keyways using cementitious grout while cracks were found in the partial depth keyways but not in the full depth shear key using the epoxy grout and fiber reinforced cementitious grout. They also found that the vertical locations of the shear key did not affect its behavior.

Fu et al. (2011) proposed an approach to design the required post-tensioning for solid, multi-beam bridge system based on the shear friction concept and 3D finite element modeling techniques. The adequacy of the finite element models were validated against the strain data measured during field tests using an onsite controlled dump truck. Based on the FE results, the authors recommended different levels of post-tensioning for bridges with different span lengths. They found that the post-tensioning does not affect the live load distribution until cracks develop in the keyway and/or the concrete topping.

Hanna et al. (2011) and Hansen et al. (2012) developed and evaluated multiple transverse connection details (the wide joint system and the narrow joint system) without diaphragms nor a structural concrete deck. All the joints were reinforced by the top and bottom reinforcement placed in the top and bottom flanges of the box beams. 3D finite element models were established. Two beam specimens using the two systems were fabricated and tested under cyclic loads and for water leakage. Test results indicated that neither cracks nor water leakage were found in the keyway. However, in their study, no apparent consideration was given to performance under thermal loads and shrinkage effects.

Grace et al. (2012) inspected a bridge in Michigan and conducted an experimental laboratory test to find the source of longitudinal reflective cracks in the joint. They concluded

that traffic loads are not the main condition causing reflective cracking in the deck. A 3D finite element model was established and validated against the results from the experimental tests. FE analyses of real bridges were performed considering dead and live loads and temperature gradients. The authors found that post-tensioning effects are mainly localized at the diaphragm regions and the temperature induced effects may be the primary source of crack development.

A significant amount of information related to adjacent box beams was presented and summarized. Cracking in the joint between adjacent box beams appears to principally be a service-related problem as multiple sources indicate that even with a cracked joint, a bridge can continue to effectively distribute loads throughout the primary load carrying members. With regards to cracking, it appears that cracking tends to be most prominent at the interface between the joint material and the box beam due to apparent low bond strength. Use of a shear key may induce stress concentrations in the joint. Consistent throughout the literature is the conclusion that the joints that use full-depth keyways have the best performance. The use of transverse post-tensioning can induce transverse tensile stress and cracks since uniform distribution of the post-tension force at the keyway cannot be always guaranteed. Cracking does not seem to be first initiated by the application of live loads. There are, however, differing opinions on the relative contribution to cracking from shrinkage and temperature. Nevertheless, once cracking is initiated by either shrinkage and/or temperature, cracks can continue to grow with subsequent live load application.

4.4 Innovative joint design

Based on the findings of the literature review, joint cracks are suspected to be caused by low bond strength between the joint material and box girder, large shrinkage of joint material, stress concentrations near the shear key, and temperature changes. With consideration of these

potential cracking mechanisms and other concepts, an innovative connection (shown in Figure 4-2) was designed with the following features: wide joint (6-1/2in.) without shear key, shrinkage compensating concrete mixed with Type K cement, form retarder used to create a rough surface on the sides of the box girder to increase the shear resistance, and reinforcing steel that crosses the interface between the joint and box girder.

Consistent with the work conducted by Zhengyu and Phares (2018), the shrinkage compensated concrete was developed based on the standard Iowa DOT C4 concrete with 15% of the traditional Portland cement was replaced by Type-K shrinkage-compensating cement to minimize/eliminate the shrinkage typically associated with normal concrete. Note that the shrinkage/expansion magnitude can be controlled by adjusting the amount of the Portland cement replaced by Type K cement. To enhance the shear transfer capability, the flat interface was roughened using form retarder and water blasting with aggregate protruding about ¾ to 1 in. To provide transverse restraint and generate a large compression zone associated with the expanding material in the early-age joint, transverse reinforcing steel across the interface was included as shown in Figure 4-3. Longitudinal reinforcing steel and stirrups are placed in the joint to create an internal reinforced beam within the joint.

4.5 Small scale test

To investigate the performance of the innovative joint and study the effect of the joint reinforcement, the design was first evaluated with a small-scale laboratory test. Figure 4-4 shows the cross-section view of the small-scale test specimen consisting of two 20in. wide beams and a 6-1/2 in. wide joint. The specimens were approximately 3 ft. long and 2-1/4 ft. high. Four specimens were fabricated with different transverse reinforcement size and spacing across the interface: 1) no reinforcement; 2) No.4 bar at 9 in. spacing (reinforcement ratio 0.79‰); 3) No.6

bar at 9 in. spacing (reinforcement ratio 2.32‰); 4) No.4 bar at 6 in. spacing (reinforcement ratio 1.59‰). Figure 4-5 shows the specimen-4 innovative joint before placement of the joint material. The shrinkage (expansion) strain of the joint material was measured for each specimen following ASTM C157 and shown in Figure 4-6. The first data were collected at 0.5day and the results indicate that all of four joints experienced expansion from 0.5day to 1day of about 150 to 200 microstrain. Data from specimen-1 after first 4days were lost. The compressive strength test and split cylinder tensile strength test were conducted at 28 days following ASTM C39 and ASTM C469, respectively, and the results are shown in Table 4-1.

The joint behavior during the first seven days was monitored with vibrating wire strain gages (VWSG) mounted on the top surface (Figure 4-7a), thermal couples embedded in the joint (Figure 4-7b) and at the bottom of the specimen, and foil strain gages attached to the joint reinforcement (Figure 4-7c). The deformation on the top of the specimen was measured using VWSG which have a good performance on the long-term monitoring. The gages were placed across the interface between the concrete block and the joint to capture relative movement between the joint and the concrete block (although no cracks occurred in the specimens during the early-age monitoring). Figure 4-8 shows the temperature data measured from specimen-1. The temperature in the joint increased due to heat of hydration until twelve hours after placement when it is about 10°F to 15°F higher than the bottom and top surface temperature. Internal temperature then starts to decrease until 3 days after placement when it is similar to the exterior temperature. A careful observation indicates that the temperature at the center of the joint is slightly (2 to 4°F) higher than that at the interface. The temperature data for the other three specimens show very similar trend and distribution. Four foil gages were attached on each of the specimen 2, 3 and 4 (see Figure 4-7c) to measure the transverse reinforcement strain during

early-age monitoring and evaluate the efficiency of the transverse reinforcing. The foil gages were installed on both top and bottom transverse joint reinforcement and placed a 2in. from the interface between the joint and box beam. No foil gages were used on specimen-1 since there is no transverse reinforcing steel in the joint.

The specimens were tested to an ultimate load with one beam tied-down and the other loaded. The tie-down force and the loading force were applied 1.5ft from the centerline of the specimen as is shown in Figure 4-9. During the test, displacement transducers were used to measure the vertical movement of the loaded beam. Figure 4-10 shows the load vs. displacement curves from the four specimens. The specimen-1, without any joint reinforcement, failed with a brittle failure when the load reached 75 kips, while the specimen 2 and 3 yielded with a similar loading but show more ductile behaviors. It was a surprise that the specimen-4, with intermediate reinforcement ratio but more uniform distribution, yielded with a lower loading about 55kips. Comparing specimen-4 to specimen-3, it is obvious that even with lower reinforcement ratio, the smaller reinforcement size and spacing results into a more ductile bending behavior. However, considering that the longitudinal joint between the adjacent box beams were designed to transfer shear and moment in service level without cracking and yielding, a minimum reinforcement ratio 0.79‰ (No.4 at 9in. spacing) is sufficient for the service performance.

4.6 Analytical study on early-age joint

Since many past research projects indicated that longitudinal joint cracking are initiated by either shrinkage and/or temperature, the early-age joint behavior is of concern. Since the internal joint stress distribution during early-age is difficult to be measured from the laboratory test, the finite element approach was adopted to simulate the early-age joint behavior to determine the stress distribution in the joint and at the interface between the joint and concrete

blocks. A finite element model which is capable of simulating the early-age joint behavior as illustrated by Liu and Phares (2018) was used in the calculation. Note that creep behavior was not included since the joint stress tends to be in relaxation form and reduces with time when it is subject to a constant loading. The model without creep results in a higher stress in the joint and is more conservative.

The model was established using 3D solid element for the concrete blocks and the joint (shown in Figure 4-11) with an average element size about 2 in, and beam element for the transverse reinforcing steel. The longitudinal steel and stirrups in the concrete block and joint were not modeled since they contribute minimally to the transverse stress in the joint and at the interface. Since the concrete blocks were more than two months old when the joint material was placed and only the first three days of joint behavior is of interest, the time-dependent effect of the concrete blocks was not included in the model. The time-dependent finite element analysis started from 0.25 day after joint material placed and it is assumed that zero joint stress and strength existed prior to that. The expansion of the joint material measured shrinkage testing (shown in Figure 4-6) and the temperature measured with the thermal couples (shown in Figure 4-8) were applied to the model. The temperature field between the temperature measurement points was assumed using linear interpolation. Since the shrinkage data in Figure 4-6 starts from 0.5 day, an 80 microstrain expansion was estimated based on the initial slope of the shrinkage curve of each joint for the 0.25 to 0.5 day period.

The load was divided into load increments with a time step of 0.05day (1.2hr). A linear elastic analysis was performed with each load increment and the Young's Modulus at the occurrence of each load increment continually updated. Young's Modulus in each elastic analysis was updated to account for the concrete hardening effect. Kanstad's (1990) time-

dependent Young's Modulus equation calibrated by Liu and Phares (2018) was used and scaled based on the square root of compressive strength at 28day (shown in Table 4-1). The structural response including displacement, strain and stress results, etc. from each elastic analysis were accumulated based on the superposition principal.

4.6.1 Model validation

The finite element model was developed for all four specimens and validated with the collected experimental data. Since each VWSG crosses two different materials, the strain data was multiplied by the gage length and compared with the corresponding displacement results from FEM as shown in Figure 4-12 for Joint 2. Both experimental and FEM results indicate that the concrete blocks move apart during the 0.25 day to 1 day period. This is because the Type K cement in the joint concrete expanded as previously discussed (see shrinkage data in Figure 4-6). Both experimental and analytical results show similar magnitude of the movement on the top surface. Figure 4-13 compares the analytical elastic strain on the transverse reinforcing steel to the experimental data for Joint 2. The gage in Section-2 near the bottom lost signal during the test. Comparing the experimental data from the top gages in Section 1 and 2, it is obvious that the reinforcement near the corner (in Section 1) shows higher tensile strain than the reinforcement in the middle. Although the analytical result is about 20 to 100 percent higher than the experimental results due to the absence of creep effect in FEM, the analytical result still shows higher elastic strain on the reinforcement near the corner and lower elastic strain in the middle. Both the analytical and experimental results indicate that joint transverse reinforcement starts to carry the load before the joint material gains full strength. Both Figure 4-12 and Figure 4-13 indicated that the experimental data achieved the yield point earlier than the FEM results.

This is because the material finished most of the expansion in Figure 4-6 earlier than the data collected time point -1 day.

4.6.2 Stress distribution in the joint

The finite element analysis results indicate that the highest tensile stress occurs at the corner of the joint (see location in Figure 4-11). The first principal stress at the corner from four joints were plotted in Figure 4-14 and compared with the time dependent tensile strength. The time dependent tensile strength curve was established based on Kanstad's (1990) equation calibrated by Liu and Phares (2018) and scaled based on the tensile strength at 28th day shown in Table 4-1. Figure 4-14 shows that the highest stress in the joint is very close to the strength from 0.25 day to 1 day but it should be noticed that the stress on the laboratory specimen should be smaller than the analytical results due to the concrete creep (relaxation) characterization.

To evaluate the bond sufficiency at the interface between the joint and the concrete blocks, the normal and shear stress at the interface element (see location in Figure 4-11) were output. The bond strength was calculated based on the Coulomb failure criterion

$$\tau_u = c' - \sigma \tan\Phi' \tag{1}$$

where c' is cohesion and Φ' is friction angle. Espeche (2011) estimated the bond strength envelopes for old-to-new concrete interfaces based on the cylinders splitting test and proposed that cohesion c' can be calculated using tensile strength obtained by concrete cylinder tests as

$$
\begin{aligned}
c' &= \left(\frac{2 - \sin\Phi'}{\cos\Phi'}\right) f_t' && \text{for} \quad \Phi' > 30^o \\
c' &= \sqrt{3} f_t' && \text{for} \quad \Phi' \leq 30^o
\end{aligned}
\tag{2}
$$

Espeche (2011) indicated that the friction angle Φ' ranges from 43 to 53. A value of 50 was adopted in this analysis. The shear stress versus strength ratio was used to evaluate the bonding safety and debonding occurs when the ratio is larger than 1. The normal stress and shear

resultant in the interface plane at the center of each element were output and used to calculate the shear strength and shear resultant. The interface shear stress versus strength ratio were checked for all four specimens. The highest ratio (0.45) occurs near the corner at joint age 1day and is lower than one, which corresponds to the experimental results which indicates that no debonding occurs during the early-age. Figure 4-15 shows the shear stress versus strength ratio on the elements at the interface for Joint 2 at 1day.

Figure 4-16 shows the normal stress contour for the interface element at joint age 1day. Most of the interface is subject to compression which results in a "compression-dominate-joint". Although the region that near the exterior edge is subject to tension, the stress magnitude (about 0.11 ksi.) is small compared to the concrete tensile strength 0.2ksi at 1day (see Figure 4-14). It can be seen that the contours become darker as the reinforcement ratio increases, which indicates that as increasing of the joint reinforcement more compression was generated in the joint. This result validates the expectation that as the joint material expanding and pushing the concrete blocks moving apart during the early-age, the transverse reinforcing steel across the interface resists the movement and results in additional transverse compressive stress into the joint. A line was drawn on each contour plot to mark the edge between the compression zone and the tension zone. Comparing specimen-1 to specimen 2, 3 and 4, the specimen without reinforcement has a larger area that is subject to tension. Comparing specimen 2, 3 and 4, there is no significant difference on the area under tension. It can be concluded that on the new innovative joint, the transverse reinforcing steel placed at 9 in. spacing is sufficient to resist early-age joint crack development.

4.7 Summary and conclusion

Adjacent concrete box beam bridges constitute more than 15% of bridges built or replaced each year and have been in service for many decades. A recurring problem with this type of bridge is the cracking in the longitudinal grouted joints between adjacent beams, which then allows water and salt leakage through the joint and reflective cracks that are commonly observed in the road surface. A comprehensive review of literature from the past 20 years indicates that the joint cracks are suspected to be caused by low bond strength between the joint material and box girder, large shrinkage of the joint material, stress concentrations near the shear key, and temperature changes. To overcome these problems, an innovative connection was designed that has a wide width, shrinkage compensating concrete, rough interface between the joint and box girder, and reinforcing steel that crosses the interface.

Four small scale specimens with different transverse reinforcement amount crossing the interface was designed, constructed and monitored for early-age behavior and tested to ultimate live load capacity. A finite element model was developed to simulate the early-age joint behavior and to determine the stress distribution in the joint and at the interface between the joint and the box beam concrete. Shrinkage, temperature, strain data collected during early-age monitoring was used to validate the FEM. The time-dependent stresses in the joint were compared to the time-dependent tensile strength and the Coulomb failure criteria was adopted to evaluate the bond sufficiency at the interface between the joint material and concrete. Both experimental and FEM results indicate that,

1) The expansion of the joint material generates a compression stress in the most of the joint and formed a "compression-dominate-joint".

2) Transverse reinforcing steel can resist early age loadings before the joint material gains full strength.

3) Compared with the joint without reinforcement, transverse reinforcement resists the expansion of the joint material and creates a large compressive field.

4) No significant improvement in shear or moment capacity was found during the live load test. However, the specimen with smaller rebar size, but closer spacing, shows better ductility.

5) No.4 transverse rebar placed with 9in. spacing is sufficient for the new innovative joint to resist early-age joint cracking.

4.8 References

Attanayake, U., and Aktan, H. (2008). "Issues with Reflective Deck Cracks in Side-by-Side Box Beam Bridges." Proceedings of the 2008 Concrete Bridge Conference, Federal Highway Administration, National Concrete Bridge Council, Missouri Department of Transportation, American Concrete Institute, 18p.

Attanayake, U., and Aktan, H. M. (2009). "Side-by-side Box-beam Bridge Superstructure: Rational Transverse Post-tension Design." Transportation Research Board Annual Meeting, Washington D.C.

Badwan, I. Z., and Liang, R. Y. (2007a). "Transverse Post-Tensioning Design of Precast Concrete Multi-beam Deck." PCI Journal, 52(4), 84-92.

Badwan, I. Z., and Liang, R. Y. (2007b). "Performance evaluation of precast post-tensioned concrete multibeam deck." Journal of Performance of Constructed Facilities, 21(5), 368-374.

Dong, H., Li Y., and Ahlborn T.M. (2007). "Performance of Joint Connections between Decked Prestressed Concrete Bridge Girders," PCI National Bridge Conference, Proceedings, Phoenix, Arizona.

El-Remaily, A., Tadros, M. K., Yamane, T., and Krause, G. (1996). "Transverse design of adjacent precast prestressed concrete box girder bridges." PCI Journal, 41, 96-113.

Espeche, A. D., & León, J. (2011). Estimation of bond strength envelopes for old-to-new concrete interfaces based on a cylinder splitting test. Construction and building materials, 25(3), 1222-1235.

Fu, C. C., Pan, Z., and Ahmed, M. S. (2010). "Transverse Post-tensioning Design of Adjacent Precast Solid Multibeam Bridges." Journal of Performance of Constructed Facilities, 25(3), 223-230.

Grace, N. F., Jensen, E. A.,and Bebawy, M. R. (2012). "Transverse post-tensioning arrangement for side-by-side box-beam bridges." PCI Journal, 57(2), 48-63.

Greuel, A., Baseheart, T. M., Rogers, B. T., Miller, R. A., and Shahrooz, B. M. (2000). "Evaluation of a high performance concrete box girder bridge." PCI journal, 45(6), 60-71.

Gulyas, R. J., Wirthlin, G. J., & Champa, J. T. (1995). "Evaluation of keyway grout test methods for precast concrete bridges." PCI Journal, 40(1), 44-57.

Hanna, K. E. (2008). "Behavior of Adjacent Precast Prestressed Concrete Box Girder Bridges." PhD diss., University of Nebraska, Lincoln, NE.

Hanna, K.E., G. Morcous, and M. K. Tadros (2007). "Transverse Design and Detailing of Adjacent Box Beam Bridges," PCI National Bridge Conference, Proceedings, Phoenix, Ariz.

Hanna, K. E., Morcous, G., & Tadros, M. K. (2009). Transverse post-tensioning design and detailing of precast, prestressed concrete adjacent-box-girder bridges. PCI journal, 54(4), 160-174.

Hanna, K., Morcous, G., & Tadros, M. K. (2011). Adjacent box girders without internal diaphragms or post-tensioned joints. PCI journal, 56(4), 51-64.

Hansen, J., Hanna, K., and Tadros, M. K. (2012). "Simplified transverse post-tensioning construction and maintenance of adjacent box girders." PCI journal, 57(2), 64-79.

Harries K.A. (2006). "Full-scale Testing Program on De-commissioned Girders from the Lake View Drive Bridge," Report No. FHWA-PA-2006-008-EMG001, Pennsylvania Department of Transportation, Harrisburg.

Huckelbridge Jr, A. A., and El-Esnawi, H. H. (1997). "Evaluation of Improved Shear Key Designs for Multi-beam Box Girder Bridges." No. FHWA/OH-97/009, report to Ohio Department of Transportation, Case Western Reserve University, Cleveland, OH.

Huckelbridge Jr, A. A., El-Esnawi, H., and Moses, F. (1995). "Shear key performance in multibeam box girder bridges." Journal of Performance of Constructed Facilities, 9(4), 271-285.

Illinois DOT (2008). "Concrete Deck Beams," Guide Bridge Special Provisions (GBSP), No. 62, Illinois Department of Transportation, Springfield.

Issa, M. A., do Valle, C. L. R., Abdalla, H. A., Islam, S., and Issa, M. A. (2003). "Performance of transverse joint grout materials in full-depth precast concrete bridge deck systems." PCI Journal, 48(4), 92-103.

Kim, J. H. J., Nam, J. W., Kim, H. J., Kim, J. H., & KEUN, J. B. (2008). "Overview and applications of precast, prestressed concrete adjacent box-beam bridges in South Korea." PCI Journal, 53(4), 83-107.

Lall, J., E.F. DiCocco, and S. Alampalli (1997). "Full-Depth Shear-Key Performance in Adjacent Prestressed-Beam Bridges." Special Report No. 124, Transportation Research and Development Bureau, New York State Department of Transportation, Albany.

Lall, J., S. Alampalli, and E. F. DiCocco. (1998). "Performance of Full-Depth Shear Keys in Adjacent Prestressed Box Beam Bridges." PCI Journal, 43(2), 72-79.

Liu, Zhengyu and Brent M. Phares. (2018) "Material Selection for the Joint between Adjacent Box Beams."

Macioce, T.P., H.C. Rogers, R. Anderson, and D.C. Puzey (2007). "Prestressed Concrete Box Beam Bridges—Two DOTs'Experience," PCI National Concrete Bridge Conference, Proceedings, Phoenix, Ariz.

Miller, R. A., Hlavacs, G. M., Long, T., and Greuel, A. (1999). Full-scale testing of shear keys for adjacent box girder bridges. PCI Journal, 44(6), 80-90.

Nottingham, D. (1995). Discussion of "Evaluation of Keyway Grout Test Methods for Precast Concrete Bridges," by R.J. Gulyas, G.J. Wirthlin, and J.T. Champa, PCI Journal, 40(4), 98–103.

Precast/Prestressed Concrete Institute (PCI) (1997; 2004), PCI Bridge Design Manual, Precast/Prestressed Concrete Institute, Chicago, IL, 1997 (updated July 2004).

Precast/Prestressed Concrete Institute (PCI). (2003). PCI bridge design manual, 2nd Ed., Precast/Prestressed Concrete Institute, Chicago, IL.

Russell, H. G. (2009). Adjacent Precast Concrete Box Beam Bridges: Connection Details (Vol. 393). Transportation Research Board.

Sang, Z. (2010). "A Numerical Analysis of the Shear Key Cracking Problem in Adjacent Box Beam Bridges." Doctoral dissertation, The Pennsylvania State University.

Sharpe, G. P. (2007). "Reflective cracking of shear keys in multi-beam bridges", Doctoral dissertation, Texas A&M University.

Ulku, E., Attanayake, U., and Aktan, H. M. (2010). "Rationally Designed Staged Post-tensioning to Abate Reflective Cracking on Side-by-Side Box-Beam Bridge Decks." Transportation Research Record: Journal of the Transportation Research Board, 2172(-1), 87-95.

Yamane, T., M.K. Tadros, and P. Arumugasaamy (1994). "Short to Medium Span Precast Prestressed Concrete Bridges in Japan," PCI Journal, 39(2), 74–100.
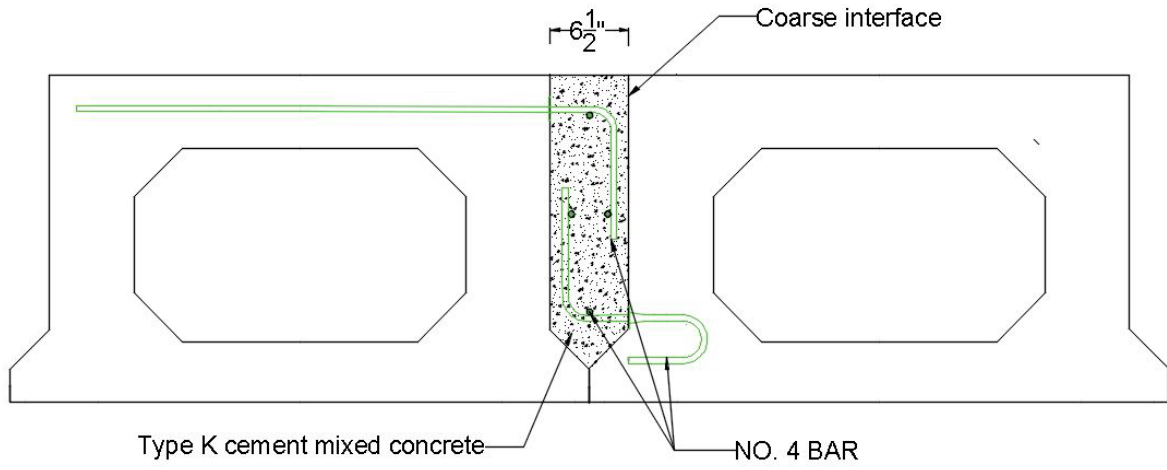
Figure 4-1 Basic Keyway Geometries
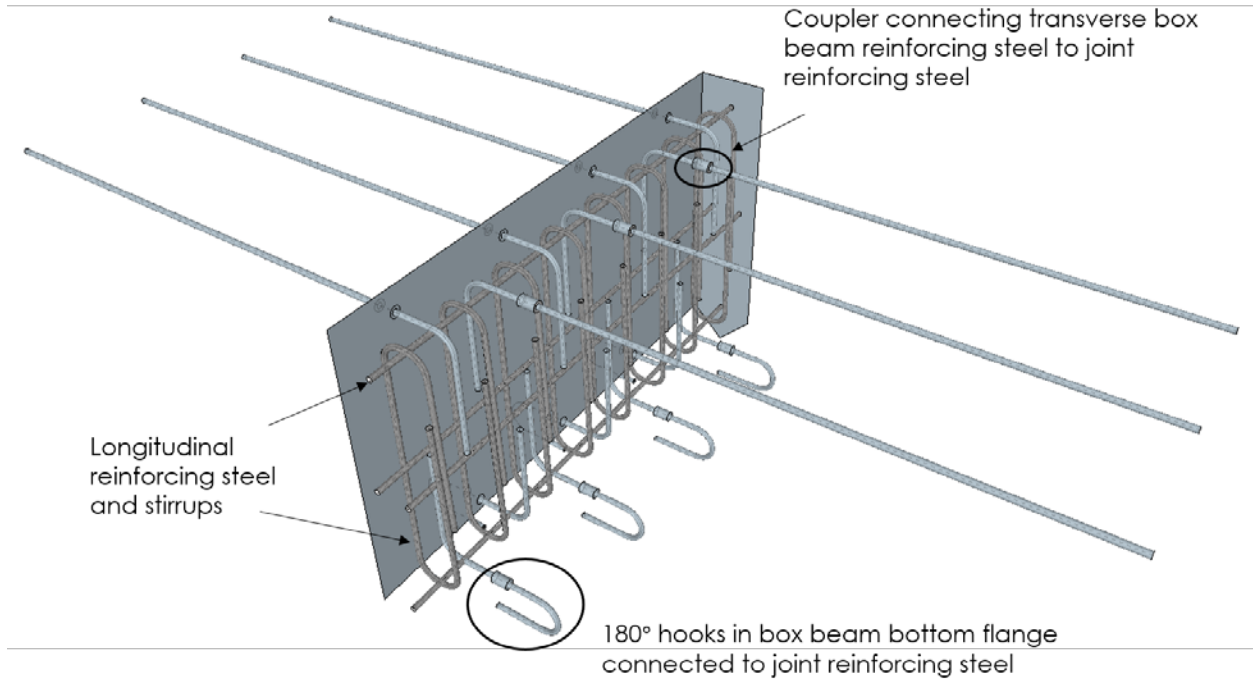
Figure 4-2 Innovative Joint Design

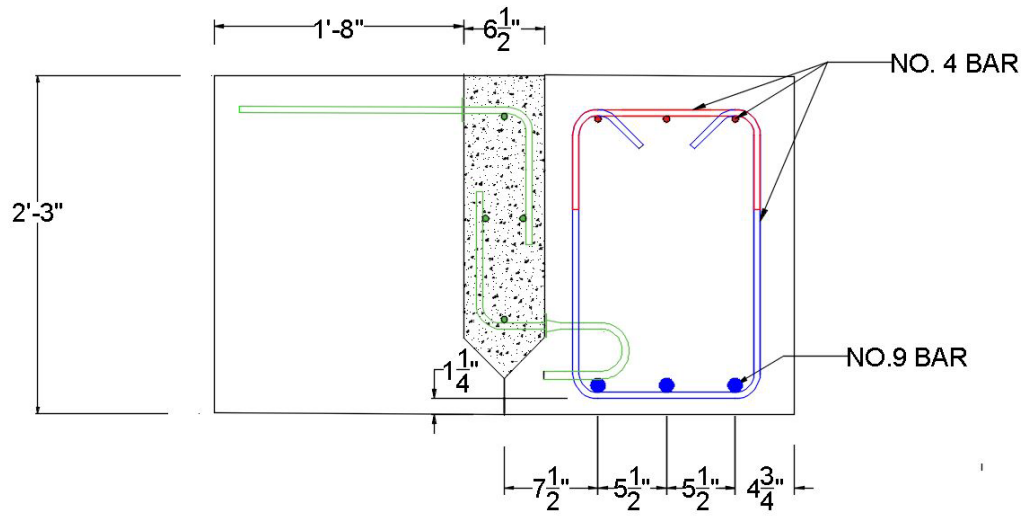**Figure 4-3 3D View of Joint Reinforcement Design**

Figure 4-4 Cross Section View of the Specimen

Figure 4-5 Innovative Joint on Specimen-4

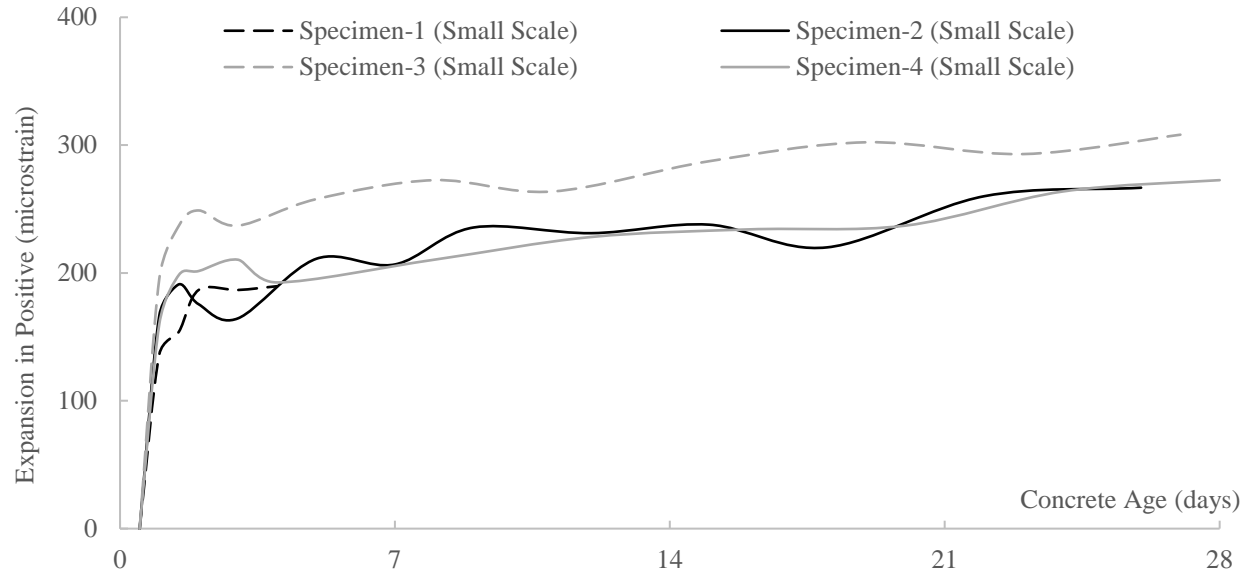**Figure 4-6 Shrinkage Data of Four Joints**

Table 4-1 Results of Material Testing

	Compressive Strength (ksi.)	Tensile Strength (ksi.)
Box Girder	5.60	0.50
Specimen-1	7.25	0.76
Specimen-2	7.75	0.79
Specimen-3	7.70	0.75
Specimen-4	7.70	0.82

a.

b.

c.
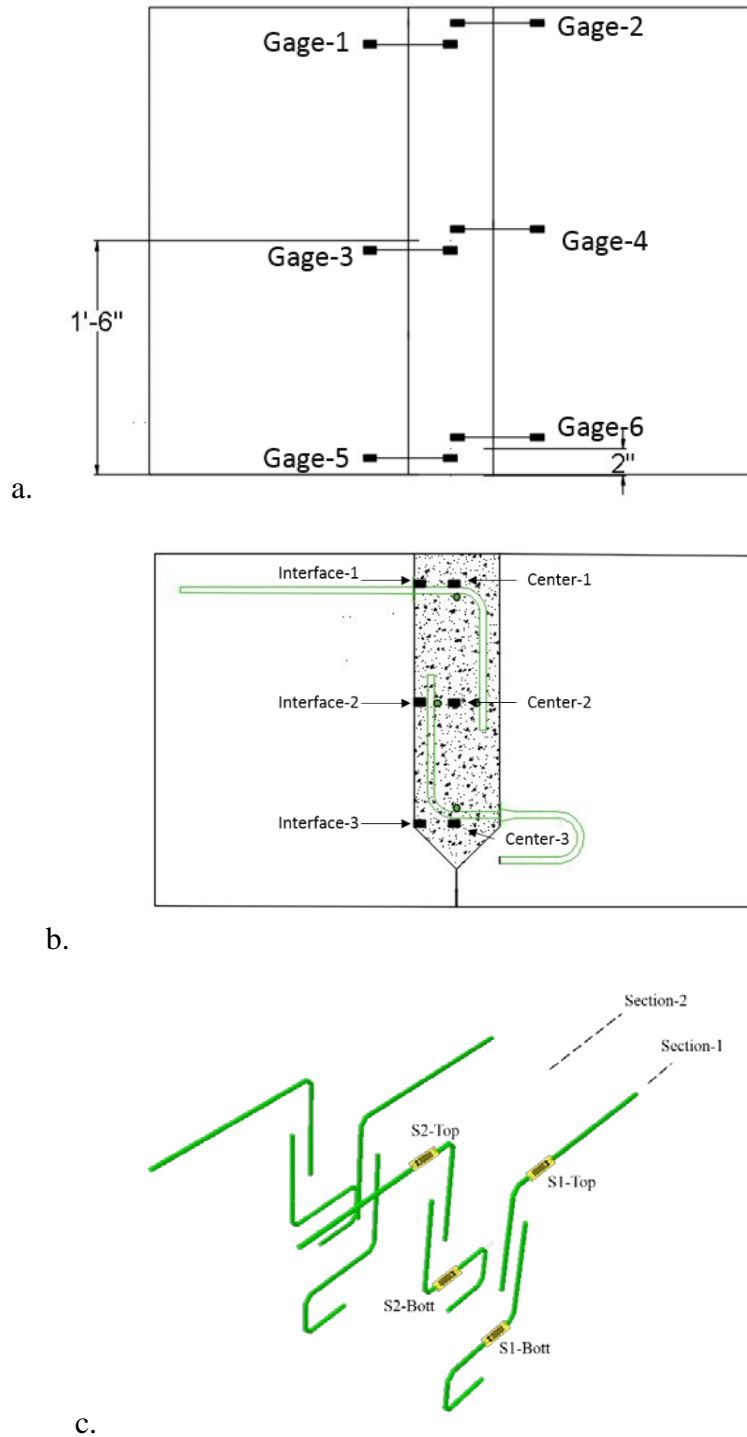
Figure 4-7 Instrumentation during the Early-age Monitoring: a) Vibrating Wire Strain

Gage (VWSG); b) Thermal Couple; c) Foil Gage
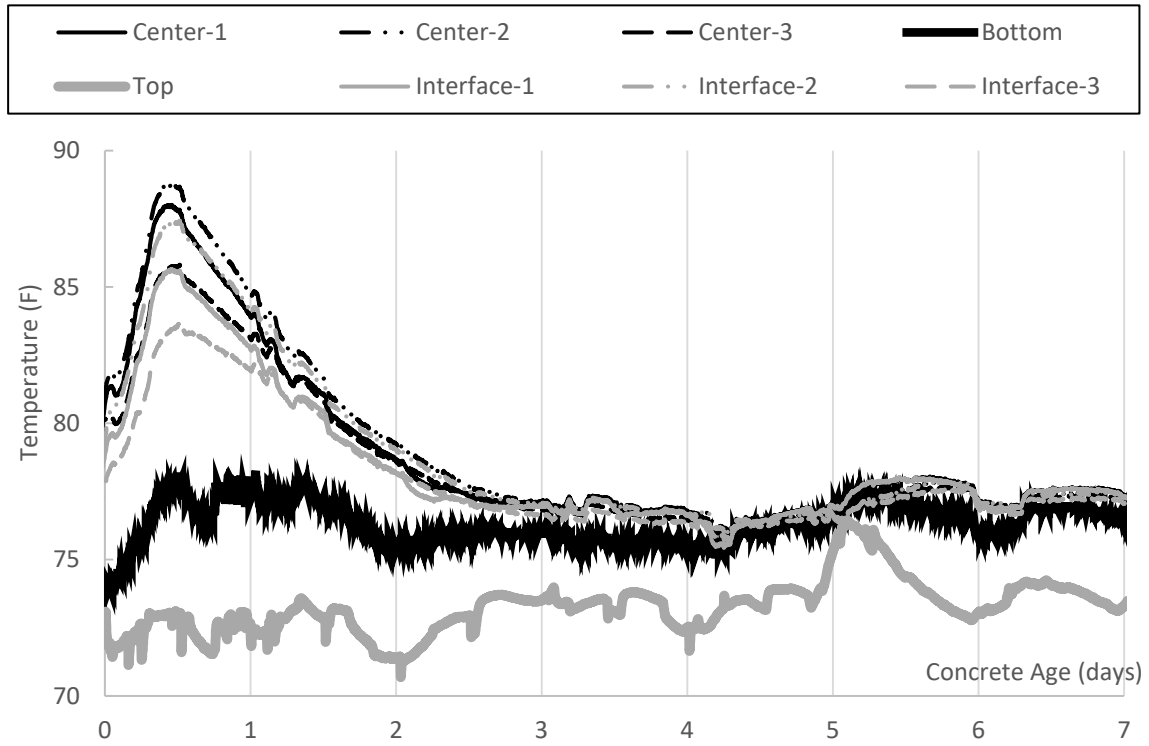
Figure 4-8 Temperature Distribution from Specimen-1
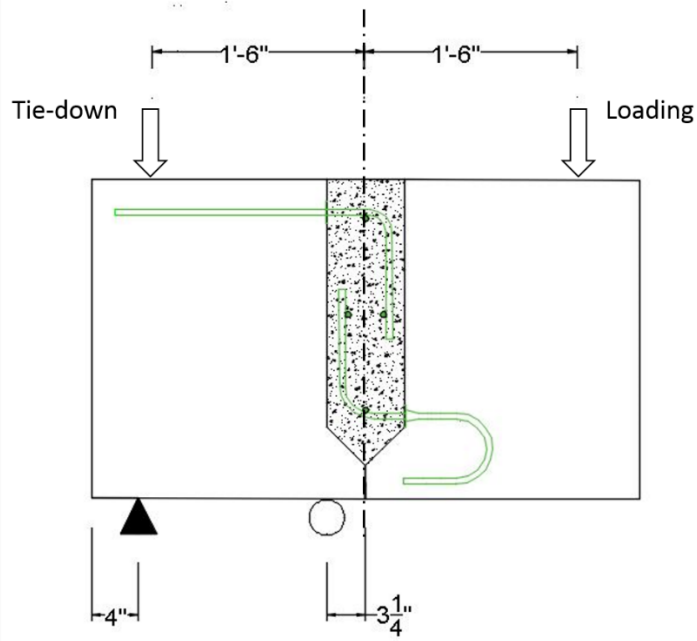
Figure 4-9 Ultimate Load Test Configuration
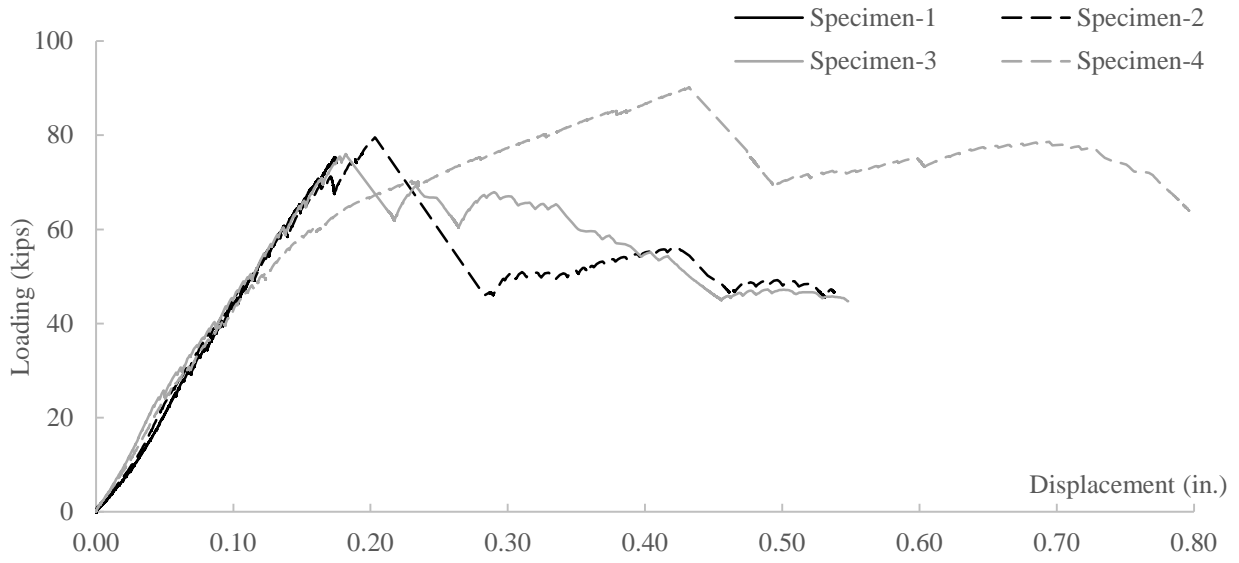
Figure 4-10 Load-Displacement Curves
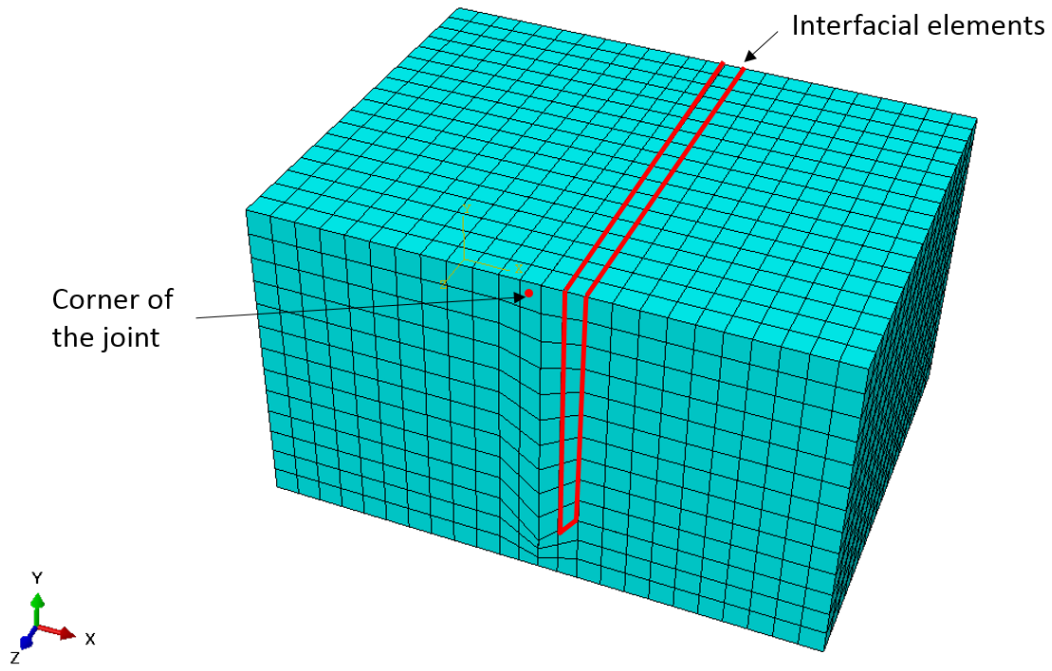
Figure 4-11 Finite Element Model
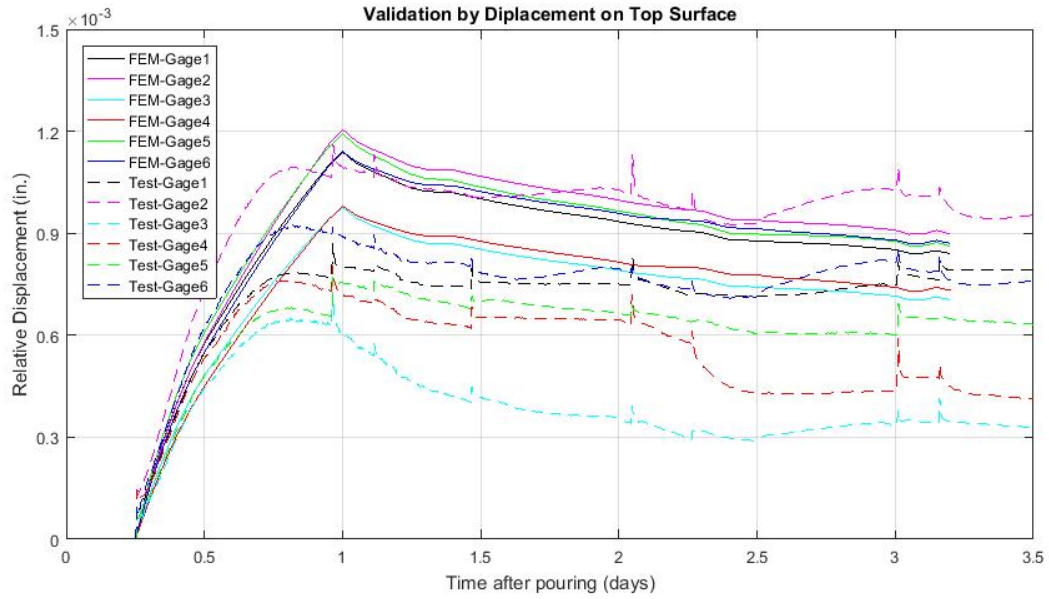
Figure 4-12 Validation by Displacement Data on Top Surface (Joint-2)
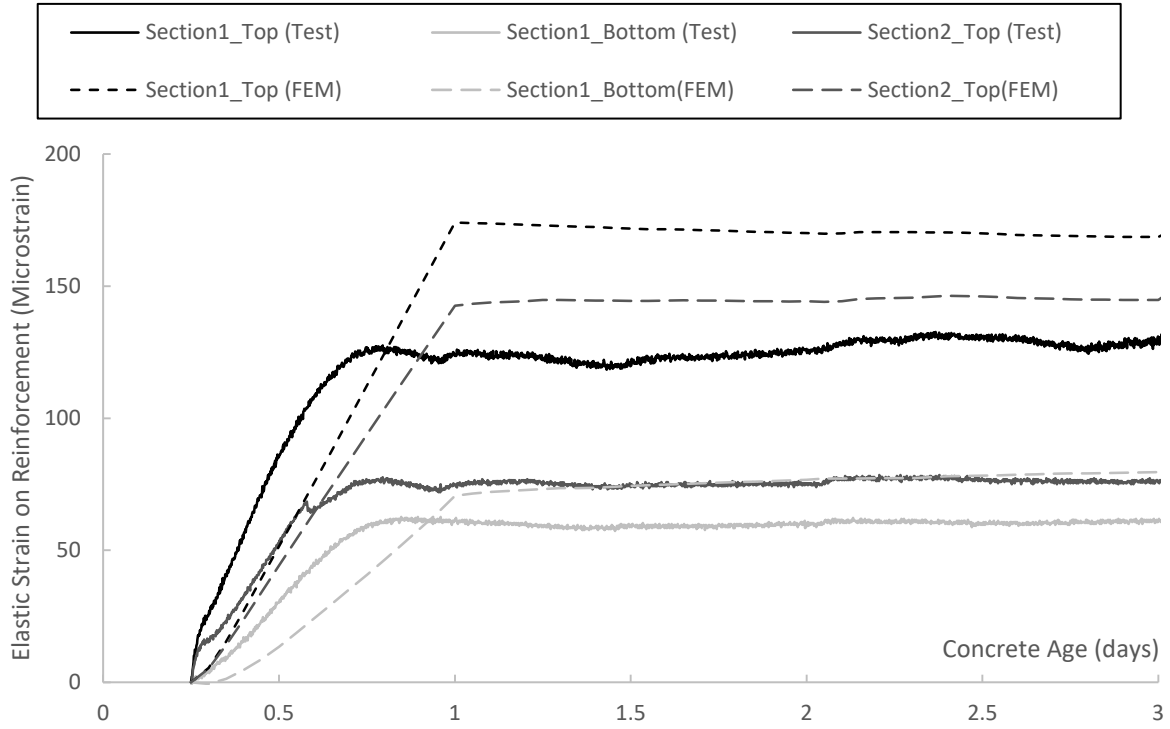
Figure 4-13 Validation by Reinforcement Strain (Joint-2)
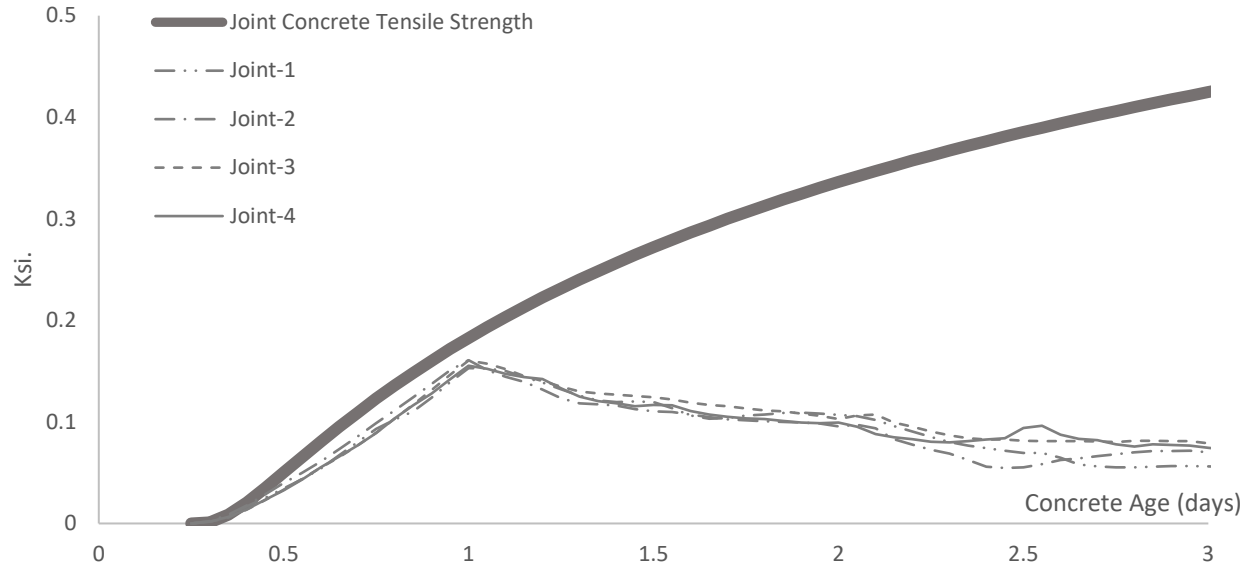
Figure 4-14 First Principal Stress at the Joint Corner
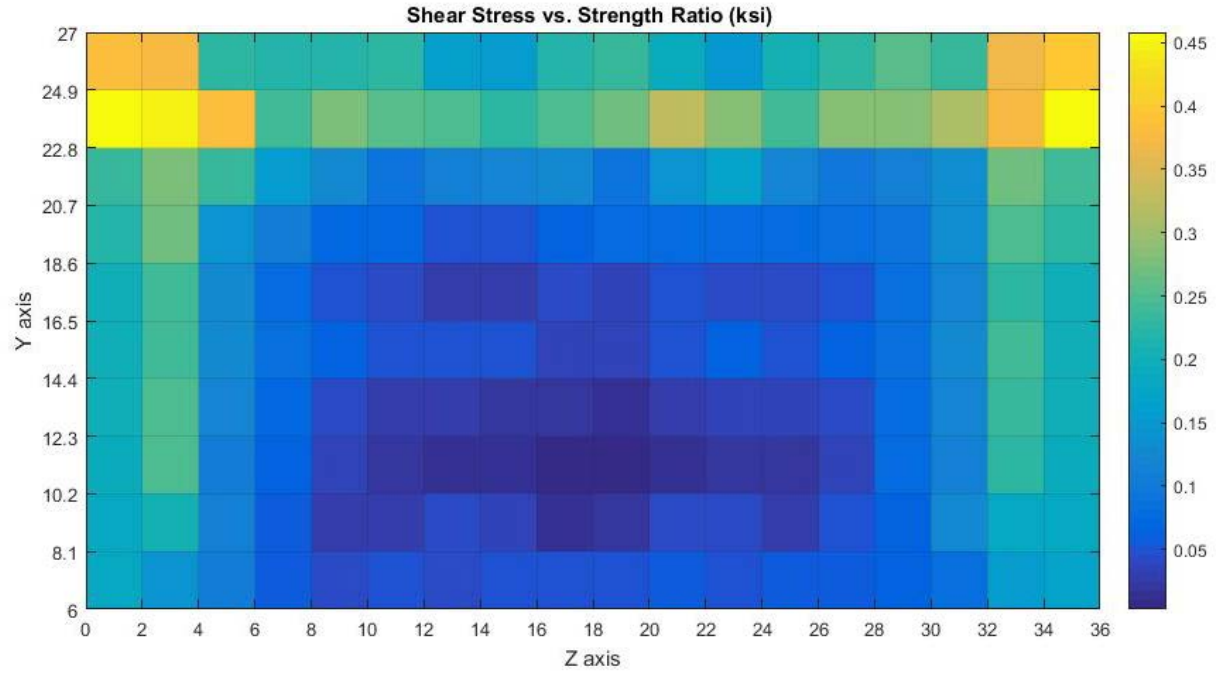
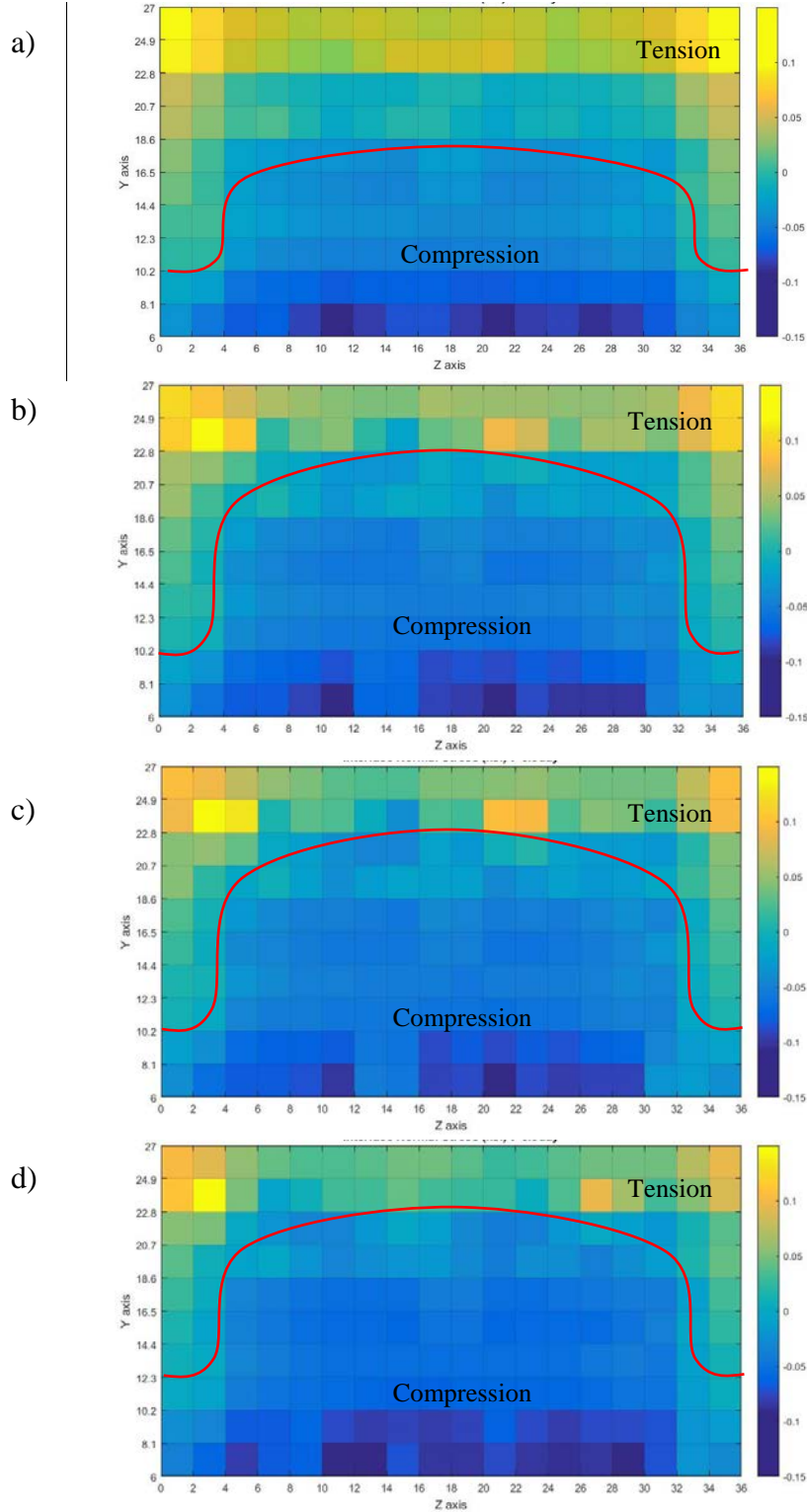**Figure 4-15 Shear Stress/Strength Ratio at the Interface (Joint-2)**

Figure 4-16 Interfacial Normal Stress: a) Specimen 1; b) Specimen 2; c) Specimen 3; d)

Specimen 4

CHAPTER 5. FULL SCALE EVALUATION OF AN INNOVATIVE JOINT DESIGN BETWEEN ADJACENT BOX BEAMS

Liu, Zhengyu[5]; Phares, Brent M[6]; Shafei, Behrouz[7]; Shi, Weizhuo[8];

5.1 Abstract

Adjacent precast, prestressed box beam bridges have suffered cracking in the material used to connect the beams. These cracks provide a direct path for chlorides and water to enter the structural system causing corrosion of the mild and prestressing steel that can lead to significant maintenance costs and/or safety concerns. Liu and Phares[2] (2018) reviewed a large amount of the past literature and designed an innovative connection as a 6-1⁄2in. wide joint between the roughened interface surface, filled with shrinkage compensating concrete, and reinforced by reinforcing steel. The innovative joint was evaluated on a small scale basis and showed a good performance on resisting the early-age cracking. In this paper, the innovative joint design was further evaluated on a 31ft long specimen during the joint early-age, and subject to multiple level of the cyclic loadings. A finite element model which is capable of simulating the early age concrete hardening was developed and validated by the experimental data. The early-age time-dependent stress development in the joint and at the interface between the joint and box beam was investigated from the analytical model. Based on the results of laboratory tests, the innovative connection can create a crack-free joint without the utilization of a shear key nor

---

[5] Liu, Zhengyu, Ph.D. Candidate, Graduate Research Assistant, Department of Civil, Construction and Environment Engineering, Iowa State University, Ames, Iowa 50010, zhengyu@iastate.edu.

[6] Phares, Brent M., Ph.D., P.E., Director, Bridge Engineering Center, Iowa State University, Ames, Iowa 50010, bphares@iastate.edu.

[7] Shafei, Behrouz, Ph.D., Assistant Professor, Department of Civil, Construction and Environment Engineering, Iowa State University, Ames, Iowa 50010, shafei@iastate.edu.

[8] Shi, Weizhuo, Ph.D. Student, Graduate Research Assistant, Department of Civil, Construction and Environment Engineering, Iowa State University, Ames, Iowa 50010, wzshi@iastate.edu.

transverse post-tensioning. Both experimental and analytical results from the full scale evaluation indicated that the innovative joint showed a good performance in resisting joint cracks in both early-age and the long-term service life of the bridge. The "compression-dominate-joint" created by the expansion joint material associate with transverse reinforcing steel across the interface is expected to overcome the difficulties in predicting the early-age internal forces during the design phase stated by AASHTO (2014). To further investigate the performance of this joint detail, it is recommended that a field trial, including the monitoring beginning from early age to at least two years following the construction, should be completed.

Keywords: Shrinkage Compensating Concrete; Adjacent Box Beam; Finite Element Modeling; Early Age Joint Behavior

5.2 Introduction

Adjacent precast, prestressed box beam bridges have been used by multiple Departments of Transportation (DOT) with varying levels of success. Historically, they have suffered from differential displacements, which cause cracking in the material used to connect the boxes (or, in some cases, cast-in-place topping material). Generally, these cracks do not pose a safety hazard. However, these cracks provide a direct path for chlorides and water to enter the structural system causing corrosion of the mild and prestressing steel that can lead to significant maintenance costs and/or safety concerns.

Traditional joints between adjacent box girders in the U.S are narrow joints (3/4 to 1-1/2 in.) wide and can either be partial or full depth. The joints were usually designed with one or more shear keys near the top, middle or bottom of the joint. These shear keys are thought to provide better transfer of transverse moment and shear between adjacent box girders. Past studies indicate that shear keys in the joint can introduce stresses high enough to induce cracking (Miller

et al., 1999). El-Remaily (1996) indicates that the wide joints (about 6in.) used in Japan are seldom associated with cracking. Based on the results from an analytical study conducted by Sharp (2007) and field inspection by Attanayake etc. (2008), shrinkage of the cement-based grout, which is usually used to fill the traditional narrow joint, is regarded as a possible source of cracking. Dong et al. (2007) also pointed out that radical changes in shear key geometry (i.e., very sharp corners) may result in higher stress levels. Ulku et al. (2010) found that the temperature gradient caused by weather changes is the main factor that causes cracks to develop near the top of shear key interfaces. Another cause of cracks is that post-tensioning forces are not uniformly distributed at the keyway because of shear lag.

Yuan and Graybeal (2016) developed two joint designs filled with Ultra-High Performance Concrete (UPHC). The joint was reinforced at the interface between the joint material and the box girder by steel reinforcement extending from the box girders into the joint. During testing daily temperature change was simulated by pumping steam through a copper tube embedded in the beams. Traffic load was simulated by four-point cyclic bending. The results of this work have resulted in a connection detail that appears to perform well. However, the main drawback associated with this connection detail as pointed out by Phares (2017) is that UHPC is needed and tends to be very expensive and requires a high level of expertise for proper mixing and placement.

Considering the above summarized literature findings, Liu and Phares[1] (2018) conducted multiple levels of material tests and developed a finite element modeling approach which is capable of simulating early-age joint behavior to select the most crack resistant material associated with various joint geometries. The results indicated that the 6-1/2 in. wide joint filled with shrinkage compensated concrete is expected to perform superior to all the other choices.

Continuing the work by Liu and Phares[1] (2018), Liu and Phares[2] (2018) designed an innovative

6-1⁄2in. wide joint without a shear key (shown in Figure 4-2) incorporating other concepts:

shrinkage compensating concrete mixed with Type K cement, form retarder used to create a

rough surface on the sides of the box girder to increase shear and bond capacity, and reinforcing

steel that crosses the interface between the joint and box girder. The design was evaluated with a

series of small scale tests and analytical models with different joint reinforcement ratios to study

the effect of the joint reinforcement. The early-age joint behavior was monitored and an ultimate

load test was performed. Both experimental and FEM results indicated that the innovative joint

with No.4 transverse rebar placed at 9in. spacing showed good performance in resisting early-

age joint cracking.

In this paper, the innovative joint design was further experimentally and analytically

evaluated. A 31ft long specimen consisting of two box beams and one innovative joint was

fabricated and tested in the laboratory. The early-age joint behavior subject to daily temperature

change, heat of hydration and material self-volume change was monitored. The joint was then

tested under multiple levels of cyclic loadings and an ultimate horizontal transverse loading. To

investigate the early-age joint behavior and to study the time-dependent stress development in

the joint, a three-dimensional (3D) finite element model was developed based on the modeling

approach proposed by Liu and Phares[1] (2018) and validated with the early-age experimental test

results.

AASHTO (2014) states that the differential shrinkage due to differences in age, concrete

mix, environmental conditions etc., have been observed to cause internal force effects that are

difficult to predict at the design phase. To date, most researchers have analytically studied long-

term joint behavior or experimentally investigated the early-age joint, but only a few have

analytically studied the stress development in the early-age. This paper not only demonstrates the efficiency of an innovative joint detail but also provides details for the modeling of early-age joint between adjacent box beams and opens the door for predicting internal stress in fresh concrete on bridge structures.

5.3 Full scale test

The box girders utilized in this work were designed based upon standard Iowa DOT (2018) drawing and only minor changes were made to facilitate the geometric features of the joint. Two 31ft long box girders were constructed with No.5 stirrups and No.9 longitudinal non-prestressed bar reinforced as shown in Figure 5-2. Five diaphragms were cast in each beam (at the two ends, mid-span and two quarter spans). In each diaphragm, two transverse plastic ducts were placed near the top and bottom sized to accommodate transverse post-tensioning rods. However, during the testing, the specimen was never post-tensioned because good performance was observed without the post-tensioning.

The joint was design and constructed in an approach as in Liu and Phares[2] (2018). The details of the innovative joint are repeated here. The standard Iowa DOT C4 concrete was selected as the basic joint material. To minimize/eliminate the shrinkage typically associated with normal concrete, 15% of the traditional Portland cement was replaced by Type-K shrinkage-compensating cement. To enhance the shear transfer capability, the box beam interface was roughened using form retarder and water blasting. After water blasting, the aggregate protruded about ¾ in., creating a rough surface. To further enhance the load transfer capabilities of the innovative joint, as well as to provide resistance to shrinkage induced early age cracking, reinforcing steel was detailed and included. The spacing of reinforcing steel across the interface was designed to match the spacing of the stirrups in the box girders, i.e., narrow

spacing (8 in.) near the end regions and wide spacing (1ft.) in the middle region. The transverse interface-crossed reinforcing steel in-and-out of the box beam were connected by couplers. Figure 5-3-a and b shows roughen side surface of the box girder with hook bars installed and longitudinal reinforcing steel and stirrups in the joint. To further enhance the strength and serviceability of the joint, the longitudinal reinforcing steel and stirrups were placed in the joint.

The compressive strength of the box beam concrete was tested in accordance to ASTM C39 for the box girder concrete on the day the joint material was placed. The compressive strengths were 5.9 ksi. for Beam 1 and 8.2 ksi. for Beam 2. A time-dependent test was conducted on the joint material, for the compressive strength following ASTM C39 and for the flexural tensile strength test following ASTM C78 at 6hr., 18hr., 24hr., 3day, 14day and 28day. Joint shrinkage was tested following the provisions outlined in ASTM C157 with the first data collected at 24hr. The material test results are shown in Figure 5-4.

During testing of the box beam, strain, displacement and temperature were measured by multiple types of measuring devices: vibrating wire strain gages (VWSG), displacement transducers, and thermocouples. In total, 36 VWSGs were attached on both top and bottom surfaces (shown in Figure 5-5a) in three typical and symmetric cross-sections: Sections 1 and 5 are about 1ft from each end; Sections 2 and 4 are at the quarter span; and Section 3 is at the middle span. For each label, "S" represents the strain gage, the first number is the section number, the second number is the gage number in that section and the last letter "T" (or "B") refers to top (or bottom) surface. The temperature data were measured by thermocouples and the thermal gages embedded in the VWSGs. The temperature measured from the surface mounted VWSGs were assumed to be the temperature of the top and bottom surfaces. Within the joint, Sections 3 and 5 were instrumented with six thermal couples (see Section 3 in Figure 5-5b).

Three thermal couples (I1, I2, and I3) were embedded at the interface between the joint and box girder at three levels; another three (J1, J2, J3) were placed in the middle of the joint. The temperature distribution at the exterior of the specimen were also measured. Four displacement transducers were placed at the bottom of the mid-span as shown in Figure 5-5b (D3-1B, D3-2B, D3-3B and D3-4B). Several transverse displacement transduces were placed at the top and bottom of the specimen crossing the entire joint and two of them are shown in Figure 5-5b (D3-1T and D3-5B).

5.3.1 Early-age loading test

The early-age testing was designed to simulate the changing environmental conditions occurring after place of the joint material that may influence the joint material behavior, including daily temperature variation, joint material expansion, concrete hardening and heat of hydration. Before placing the joint material, a temporary temperature isolation room made of plastic foam panels (Figure 5-3c) was built on top of the specimen, in which twenty heat lamps and two electric heaters were placed to generate heat. During a typical sunny day in the midwest, the extreme high and low temperatures usually occur at around 4:00 pm and 6:00 am, respectively. To simulate these temperature changes, the application of heat to the specimen was conducted to replicate these condition (i.e., uniform temperature through the depth of the girder at 6:00 am and the largest temperature gradient of 30°F at 4:00 pm).

The joint material was placed on August 23, 2016 starting at 1:30 pm and finished at 3:00 pm when the temperature on the top of the specimen was relatively high. The placement of joint material caused a slight temperature drop in the temperature isolation room and took 1½ hr. to complete. After placement, the joint concrete was covered with wet burlap and plastic as maintenance during the first seven days. The temperature on the top and bottom surface tends to

be uniform and the average top and bottom temperature during the first several days is shown in Figure 5-6a. Figure 5-6b shows the temperature distribution in the joint at Section 3. The effect from heat of hydration can be observed during the first 48 hours after placement of the joint material. Comparing the temperature from the gages in the center of the joint (J1, J2 and J3 in Figure 5-5 b) to those attached at the interface (I1, I2 and I3 in Figure 5-5 b), there was no significant temperature difference between the center and interface. The thermal couples in Section 5 indicates very similar temperature distribution as at Section-3.

5.3.2 Cyclic loading test

After 28 days of curing of the joint concrete, a cyclic loading protocol was initiated. The cyclic loading was applied at a frequency of 2Hz and the beams were tested with two different boundary conditions: both beams simply supported and one beam restrained. The specimen was first tested with simply supported conditions, as shown in Figure 5-7a. The load was applied by two actuators, one on each beam. The load was transferred to each box beam by a spreader beam and two 8×8 in. steel plates between the spreader beam and the specimen. The spacing between the two steel plates in the longitudinal direction was approximately 6 ft. Figure 5-7b shows the transverse location where the load was applied. On each beam, the load was applied 6 in. off center. Figure 5-8 shows the cyclic loading applied to the specimen, subjected to the simply supported condition. To keep the specimen stable, a minimum of 5 kips was placed on both beams throughout the test. Regardless of the load magnitude. Regardless of load magnitude that was applied, one beam was loaded to the maximum level while the other was loaded to the minimum level.

Table 5-1 shows a summary of the cyclic loading protocol that was followed. The specimen was first tested at a maximum of 18 kips, 36 kips and 42 kips on each actuator in the

117

simply supported condition with hand tightened transverse post-tensioning ties. The maximum

load of 42kips generated a moment on the 30ft long simply supported beam approximately equal

to that induced by a HL-93 design truck (AASHTO, 2014). For each of the loading level, one

million cycles were applied. The wrench tightened transverse post-tensioning was then removed

and another 400,000 cycles of 42 kips was performed in the simply supported condition. The

specimen was then tested with Beam 1 restrained (shown in Figure 5-7c) and without transverse

post-tensioning force, subjected to 18kips (200,000 cycles), 36kips (400,000 cycles) and 42kips

(1 million cycles). During the test period, a static load test with three load applications was

performed after each 200,000 cycles for both the simply supported and restrained test. Strain and

displacement data were collected during the static load tests.

Figure 5-9 shows the vertical displacement data at mid span during the 42kips cyclic load

with simply supported condition. While the two beams were subjected to different loading, the

measured displacements from both beams are very close, which indicates that the joint was fully

functional and transferring the load from one beam to the other and maintaining this integrity

throughout testing. The displacement was similar before and after each one million cycles with

no significant increase in displacement, which indicates that there is no evidence that the joint

functionality changed with time. The displacement data from D3-1 and D3-4, which are at the

center of each beam, was used to calculate the Load Distribution Factors (LDF). Since there was

a large difference in the compressive strength of the two box girders, the LDF of Beam-1 can be

calculated with the following equation:

$$LDF_1 = \frac{E_1\Delta_1}{E_1\Delta_1 + E_2\Delta_2}$$

where LDF_1 is the load distribution factor for Beam-1; E_1 (4380 ksi.) and E_2 (5160 ksi.) are the

Young's modulus of Beam 1 and Beam 2, respectively, and estimated by $57000\sqrt{f_c'}$; Δ_1 and Δ_2

are the vertical displacement under Beam 1 and Beam 2, respectively. Figure 5-10 shows the LDF changes during the first three million cycles in simply supported condition. During the simply supported test, LDF_1 is always smaller than LDF_2, which could be caused by the lower compressive strength and Young's Modulus of Beam 1.

During the restrained test, the loading on the beam 1 was held at 5 kips and Beam 2 was loaded as shown in Figure 5-8. Figure 5-11 shows the displacement data before and after one million cycles of 42kips loading. The results shows that there is no increasing displacement after one million cycles which indicates that the joint integrity had not deteriorated in any way.

During each static test, only VWSG S3-5B and S3-6B that measured the longitudinal strain at the bottom of the box girder, and S3-1T, S3-2T, S3-3T and S3-4T that measured transverse strain on the top surface had significant readings. However, there is no increasing strain during the test. During the cyclic load test no cracks occurred in the joint.

5.4 Analytical study on early-age joint behavior

A finite element model was developed using the same approach as the early-age simulation in Liu and Phares[1,2] (2018) to study the stress distribution in the joint and at the interface between the joint and box beam during the first 3days after joint material palced. Figure 5-13 and Figure 5-14 show the finite element model of the full scale specimen and the transverse reinforcing steel across the interface. The element size used within the model was about 2 to 4in with an aspect ratio less than 2. The model was simply supported along the longitudinal direction and constrained at the other two directions to prevent rigid motion. The simulation starts was initiated at 0.25 days after joint material placed and before that zero joint stress and strength was assumed to exist. Because of the high temperature gradient illustrated in Figure 5-6a, a refined time step 0.0125day (0.3hr.) was used instead of the 0.05day used in Liu and Phares[2] (2018).

Kanstad's (1990) time-dependent Young's Modulus equation calibrated by Liu and Phares[1] (2018) were used for joint material and scaled based on the square root of compressive strength at 28day (shown in Figure 5-4-a).

Since the shrinkage data in Figure 5-4-c starts at 1 day and the same mix design as in Liu and Phares[2] (2018) was used on the full scale specimen, a 160 microstrain expansion was estimated for the period of 0.5 to 1 day based on results of small scale material tests. Similar to the simulation in Liu and Phares[2] (2018), an 80 microstrain expansion was assumed for the period 0.25 to 0.5day. The temperature field was established using the temperature data in Figure 5-6 at the locations (marked with white and black dots) in Figure 5-15 with linear interpolation in between. The temperature at the block dot was measured during the test. The temperature at white dots inside the box beam was calculated as the sum of 25% of the bottom surface temperature and 75% of the top surface temperature to account for a positive temperature gradient outlined by AASHTO (2014). The 25% and 75% were calculated based on the temperature gradient data for Zone 2 in AASHTO (2014).

5.4.1 Model validation

The data from all 36 VWSGs and vertical displacement transducers were used to validate the FEM, the results from eight VWSGs and two exterior displacement transducers in the Section 3 are shown in the paper. The other gages show the similar results. The strain data from VWSGs was temperature compensated and results shown in this paper are the stress induced strain. Although the monitoring started before placement of joint concrete and ended when the joint was seven days old, the data for the first three days (zeroed at 0.25 day) was shown here because the data for day 4 to 7 just repeat the cycles in the first three days with no significant changes found.

Figure 5-16a and Figure 5-16b compare the FEM model results to the longitudinal strain on the top and bottom surface at Section 3, respectively. Figure 5-17a and Figure 5-17b compare the FEM model results to the experimental transverse strain. The results indicates that small elastic strains were induced at the bottom surface in transverse and longitudinal direction. Compare to the temperature data shown in Figure 5-6a, both experimental and analytical results indicate that the top surface is subject to compression when the temperature rises and tension when the temperature decreases. During the day, the high temperature on the top surface induced expansion and compressive stresses on the top surface.

Figure 5-18 compares the analytical results to the vertical displacement from the two displacement transducers D3-1B and D3-4B at mid-span of the specimen. The results indicate that both beams had the same displacement and maintained structural integrity during the early-age. The daily temperature rise during the day time caused the mid-span of the beam to move upward, as shown by the measured displacements. Both FEM results and experimental data show small transverse displacements across the joint on the top surface (such as D3-1T) but they do show an expansion during the day time and a contraction at night. The results also indicate that the developed FEM predicts the behavior of the specimen under the early-age loading.

5.4.2 Stress distribution in the joint

Since Liu and Phares[1,2] (2018) indicated that the corner of the joint (see Figure 5-13) is the critical location where stress concentration occurs during joint material expansion, the first principal stress at the corner was output from the FEM and compared with the time dependent concrete splitting cylinder tensile strength and flexural tensile strength shown in Figure 5-19. The splitting cylinder tensile strength was obtained from Liu and Phares[1,2] (2018) since the same mix design was used for both tests. The flexural tensile strength was from the material test

results in Figure 5-4b. Figure 5-19 indicates that the concrete expansion during 0.25 to 1 day induced tensile stress at the corner of the joint as expected. The stress development was highly impacted by the concrete placement time and the daily temperature change after the first day when the joint material completed the majority of its self-volume change. The stress calculated from the FEM was lower than both tensile strength test results.

Figure 5-20 shows the calculated elastic strain in the transverse reinforcing steel across the interface. The output location and labels can be found in Figure 5-14. Generally speaking, tensile stress is induced in these transverse reinforcing steel. The reinforcing steel in Section 1 is continuously subject to tensile stress which are caused by the joint material expansion while in section 2 (8 in. from the Section 1), the stress in the reinforcing steel are influenced by the temperature change. It is obvious that joint transverse reinforcing steel starts to carry the load well before the joint material gains its full strength.

The bond at the interface between the joint and the box beam was evaluated using Coulomb failure criterion (Espeche, 2011). More details can be found in Liu and Phares[2] (2018). The shear stress versus strength ratio was used to evaluate the bond sufficiency noting that debonding occurs when the ratio is larger than 1. The shear stress versus strength ratio on each element in the plane of interface (see Figure 5-13 for element location) was calculated and plotted in Figure 5-21a for concrete age 1.2day when the highest ratio (0.26) occured near the corner. The value is much lower than one, which corroborants the experimental result that no debonding occurs during the critical early age. The normal stress and shear resultant in the interface plane at each element center was output and plotted in Figure 5-21b and Figure 5-21c for joint age 1.2 day. Figure 5-21b indicates that the expansion of the joint material generates

normal compressive stress at the majority of the interior region which creates a "compression-dominate-joint".

5.5 Summary and conclusion

Adjacent precast, prestressed box beam bridges have suffered cracking in the material used to connect the beams. These cracks provide a direct path for chlorides and water to enter the structural system causing corrosion of the mild and prestressing steel that can lead to significant maintenance costs and/or safety concerns. Based on the research results in Liu and Phares[1] (2018) and other historical literature, Liu and Phares[2] (2018) designed an innovative connection with a 6-1⁄2in. wide joint between a roughened interface surface, filled with shrinkage compensating concrete, and reinforced by reinforcing steel. The innovative joint was evaluated on a small scale basis and showed good performance resisting early-age cracking.

In this paper, the innovative joint design was further evaluated experimentally and analytically on a full scale basis. A 31ft long specimen was fabricated and monitored during the joint early-age and tested under multiple levels of the cyclic loadings. A finite element model which is capable of simulating concrete hardening was used and validated by the experimental data. The stress in the joint and the bond at the interface between the joint and box beam was investigated from the analytical model. Some valuable findings are as follow:

1) The temperature gradient induced by the daily temperature change generates stress gradient through the height of the beam and joint. When the temperature rises on the top surface, expansion and compressive stresses induced on the top surface.

2) Stress development in the joint is affected by the joint concrete placement temperature.

3) Since the shrinkage compensated concrete expanded during the early-age, most of the joint is subject to compression except the exterior region. The stress in the joint induced by the

daily temperature change, heat of hydration, and joint concrete self-volume change is lower than the both flexural and splitting cylinder tensile strength.

4) The transverse reinforcing steel across the interface started to carry the load before the joint material gains its full strength, thereby credits a mechanism to resist cracking.

5) The bond status at the interface was evaluated by calculating the shear stress versus strength ratio based on the Coulomb failure criterion. The highest ratio (0.26) is less than 1, which matches the experimental results indicating that no debonding occurs during the early age.

6) In total, more than 5,000,000 cycles of live loading were applied during the cyclic load testing. The maximum applied load was 42kips which is equivalent to a design truck load based on AASHTO code, and at no time was cracking in the joint observed.

Based on the results of laboratory tests, the innovative connection can create a crack-free joint without the utilization of a shear key nor transverse post-tensioning. Both experimental and analytical results from the full scale evaluation indicate that the innovative joint showed good performance in resisting joint cracks in both the early-age and the long-term service life of the bridge. The "compression-dominate-joint" created by the expansive joint material combined with transverse reinforcing steel across the interface is expected to overcome the difficulties in predicting the early-age internal forces during the design phase stated by AASHTO (2014).

<h2 style="text-align:center">5.6 References</h2>

AASHTO. (2014). *AASHTO LRFD bridge design specifications*, 3rd Ed., Washington, DC.

Attanayake, U., and Aktan, H. M. (2009). "Side-by-side Box-beam Bridge Superstructure: Rational Transverse Post-tension Design." Transportation Research Board Annual Meeting, Washington D.C.

Dong, H., Li Y., and Ahlborn T.M. (2007). "Performance of Joint Connections between Decked Prestressed Concrete Bridge Girders," PCI National Bridge Conference, Proceedings, Phoenix, Arizona.

El-Remaily, A., Tadros, M. K., Yamane, T., and Krause, G. (1996). "Transverse design of adjacent precast prestressed concrete box girder bridges." PCI Journal, 41, 96-113.

Espeche, A. D., & León, J. (2011). Estimation of bond strength envelopes for old-to-new concrete interfaces based on a cylinder splitting test. Construction and building materials, 25(3), 1222-1235.

Iowa DOT Standard Drawing (2018). https://iowadot.gov/projectdev/standard-drawings

Liu, Zhengyu and Brent M. Phares.[1] (2018) "Material Selection for the Joint between Adjacent Box Beams."

Liu, Zhengyu and Brent M. Phares.[2] (2018) "Innovative Joint design for Adjacent Box Beam Bridges."

Miller, R. A., Hlavacs, G. M., Long, T., and Greuel, A. (1999). Full-scale testing of shear keys for adjacent box girder bridges. PCI Journal, 44(6), 80-90.

Phares, B., Greimann, L., Liu, Z., & Freeseman, K. (2017). Context Sensitive Designs: Testing of Multi-Performance Level Box Beam Standards (No. IHRB Project TR-681).

Sharpe, G. P. (2007). "Reflective cracking of shear keys in multi-beam bridges", Doctoral dissertation, Texas A&M University.

Ulku, E., Attanayake, U., and Aktan, H. M. (2010). "Rationally Designed Staged Post-tensioning to Abate Reflective Cracking on Side-by-Side Box-Beam Bridge Decks." Transportation Research Record: Journal of the Transportation Research Board, 2172(-1), 87-95.

Yuan, J., & Graybeal, B. (2016). Full-scale testing of shear key details for precast concrete box-beam bridges. Journal of Bridge Engineering, 21(9), 04016043.
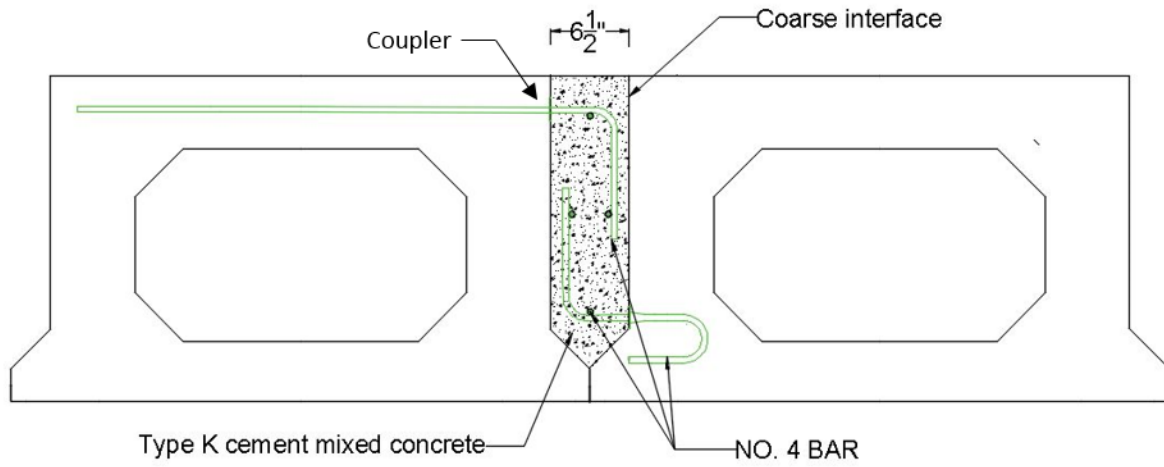
Figure 5-1 Innovative Joint Design
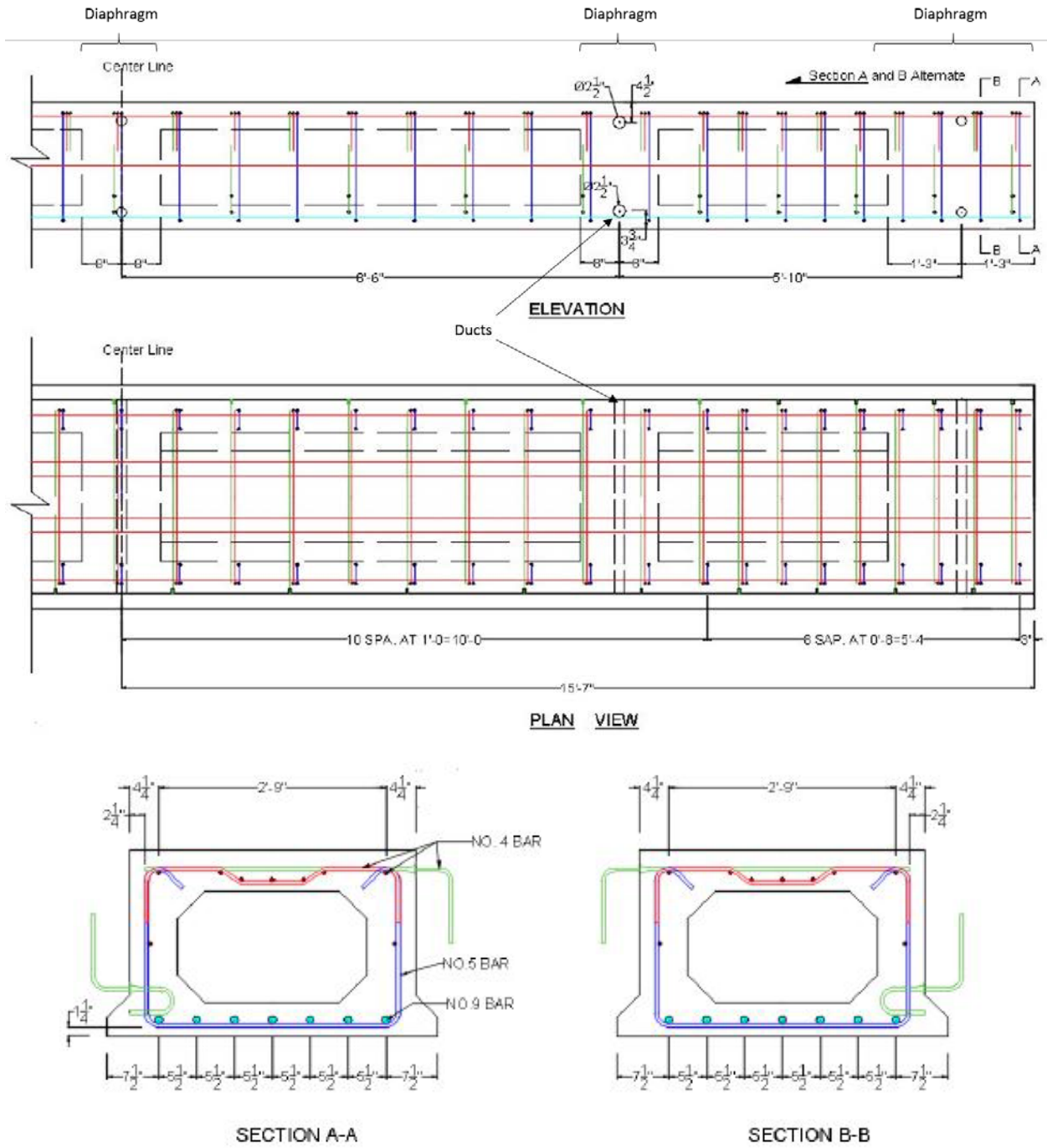
Figure 5-2 Box Beam Construction Drawing
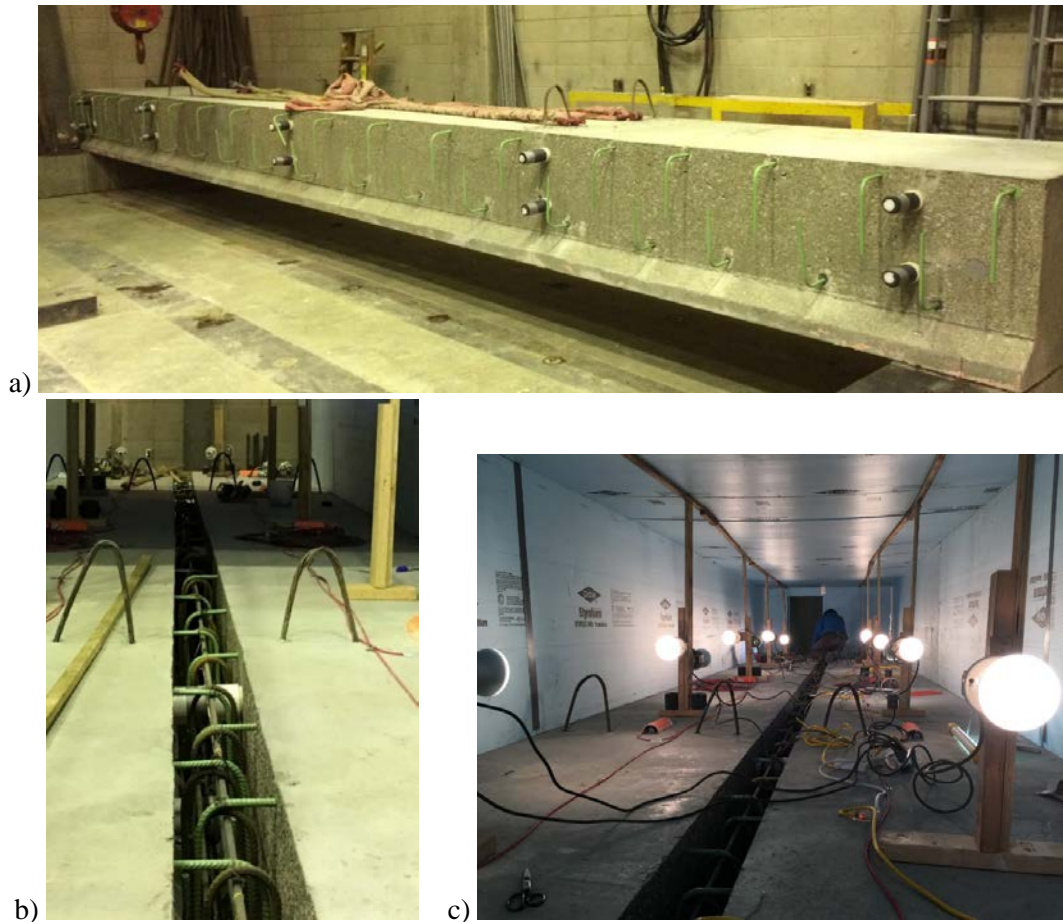
Figure 5-3 Experimental Test: a) Side of the Box Girder with Hook Bar Installed; b) Joint Reinforcement with Longitudinal Reinforcing steel and Stirrups c) Heating Devices in the Temperature Isolation Room
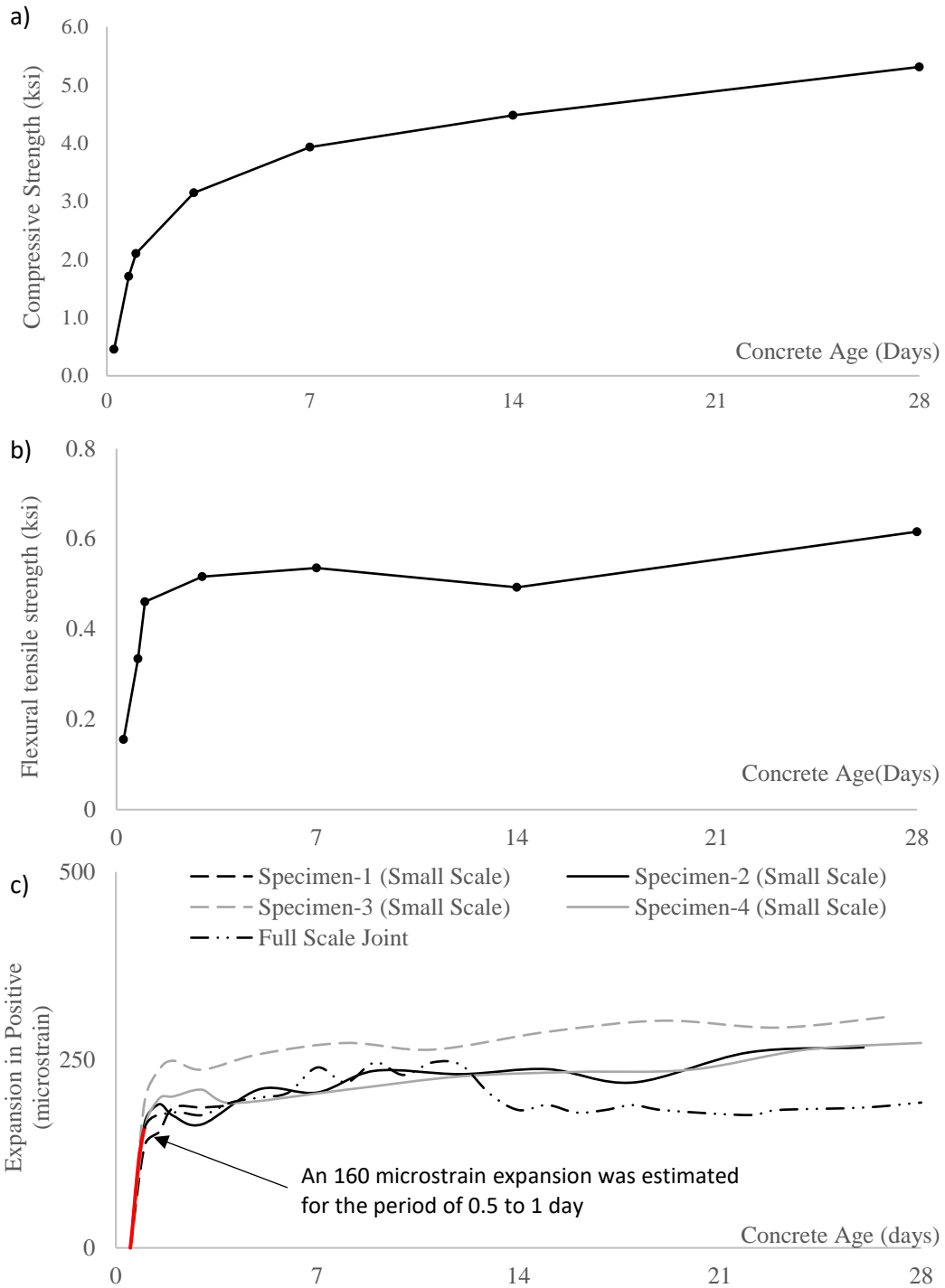
Figure 5-4 Joint Material Test Results: (a) Compressive Strength; (b) Flexural Tensile
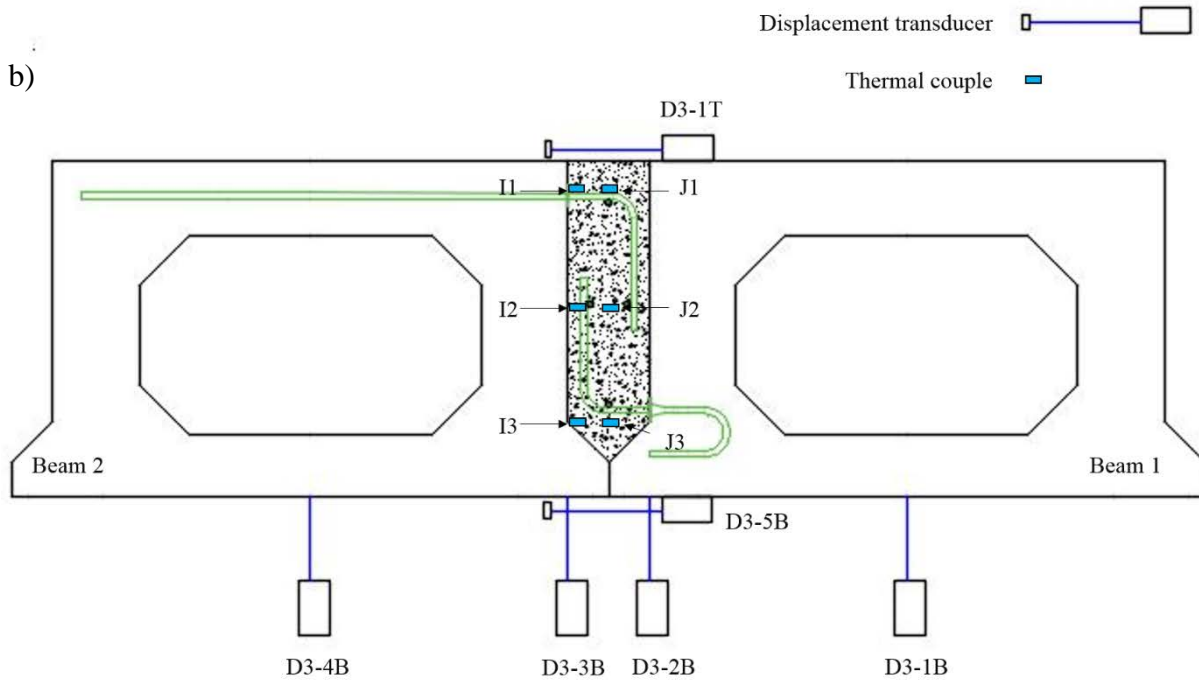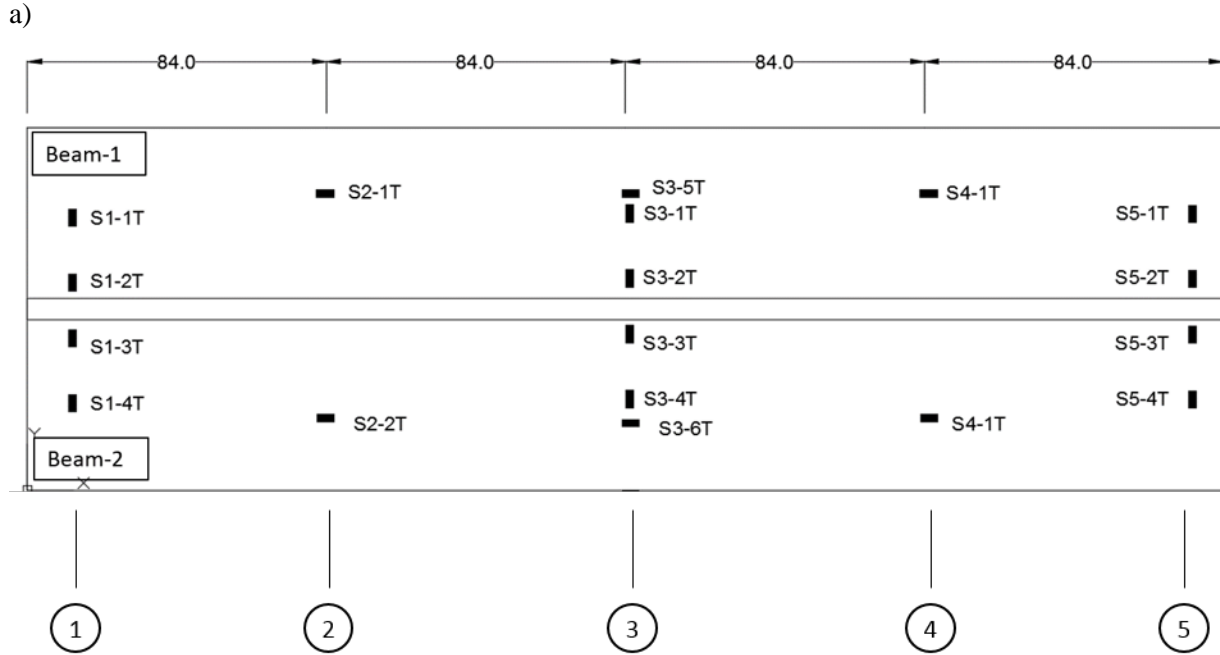
Strength; (c) Shrinkage

a)

b)

Figure 5-5 Instrumentation: a) Vibrating Wire Strain Gage Map on Top Surface (Similar for bottom surface; b) Instrumentation in Section 3;

a)

b)
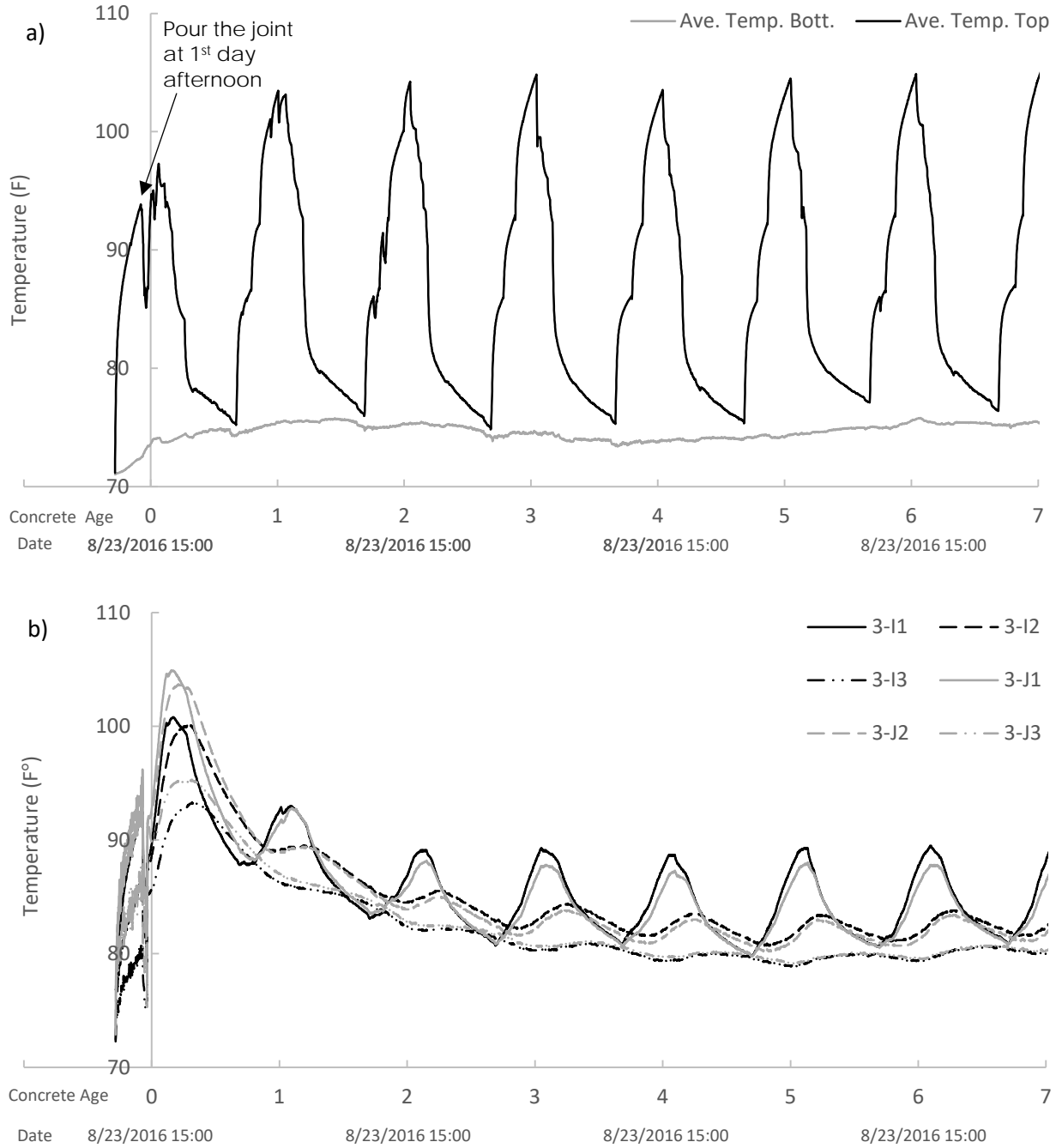
Figure 5-6 Temperature Data: a) Average Temperature on the Top and Bottom Surface; b)

Joint Temperature at Section 3
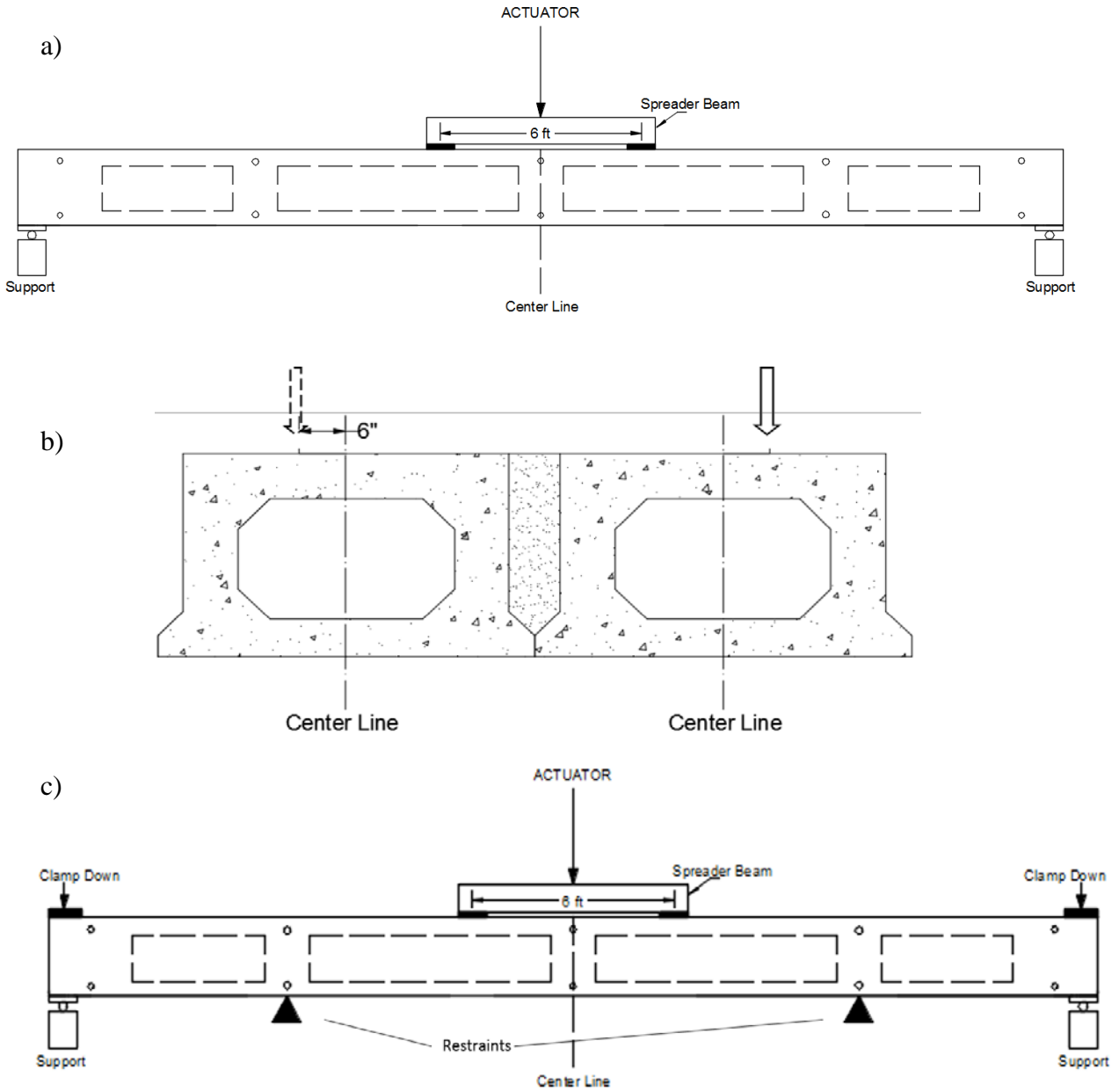
Figure 5-7 Schematic of Cyclic Load Test: (a) Test Schematic with Simply Support Condition; (b) Load Application on Cross-section View; (c) Test Schematic with One Beam Restrained

132
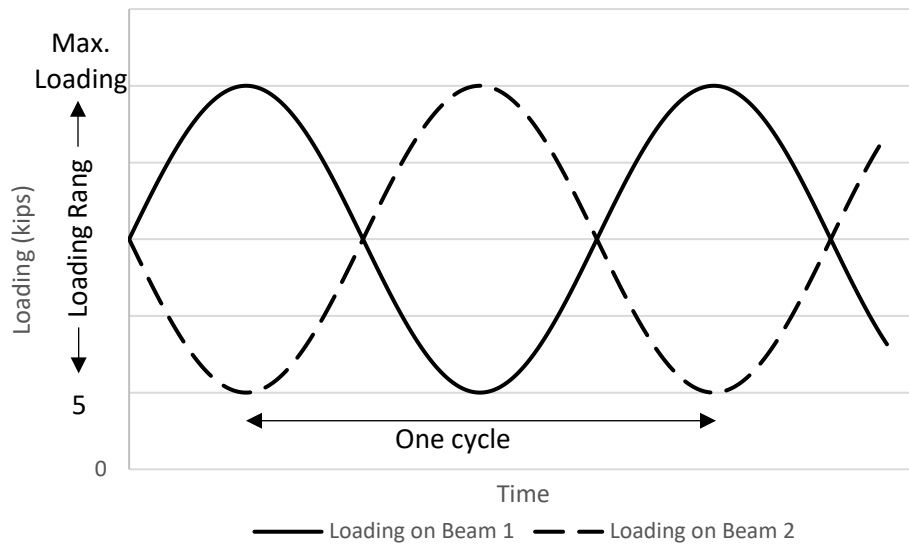
Figure 5-8 Cyclic Loading under the Simply Supported Condition

Table 5-1 Summary of Cyclic Loading Test

Support Condition	Max. Loading (kips) Applied Through Actuator	Post-tension	Number of Cycles
Simply supported	18	Snug tight	1 million
Simply supported	36	Snug tight	1 million
Simply supported	42	Snug tight	1 million
Simply supported	42	None	400,000
Beam 1 restrained	18 on Beam 2	None	200,000
Beam 1 restrained	36 on Beam 2	None	400,000
Beam 1 restrained	42 on Beam 2	None	1 million
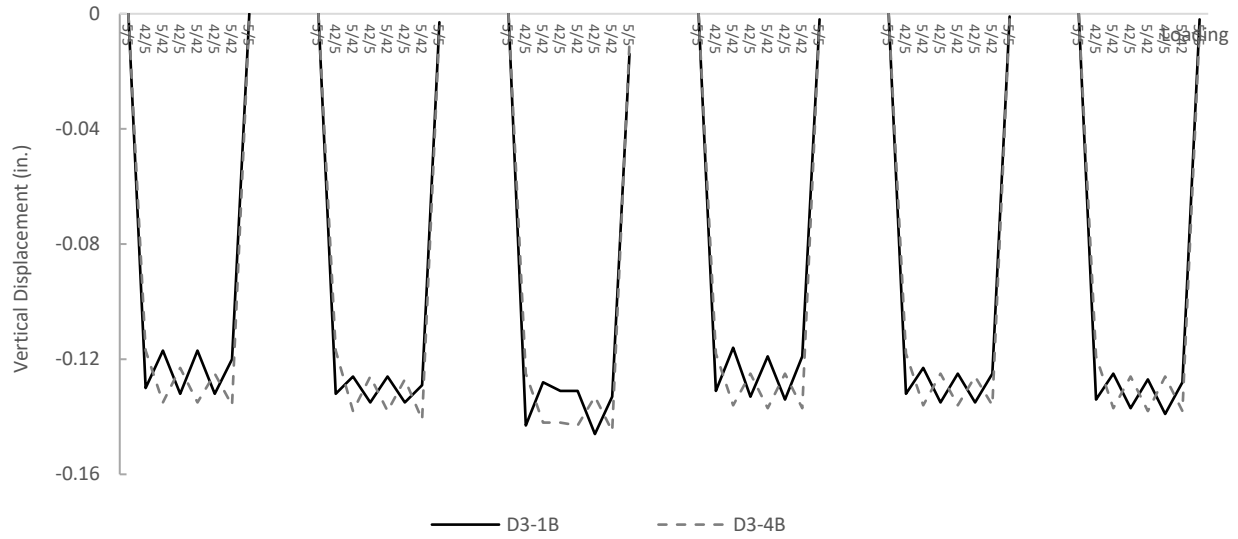
Figure 5-9 Displacement from 42kips Static Tests with Simply Supported Condition
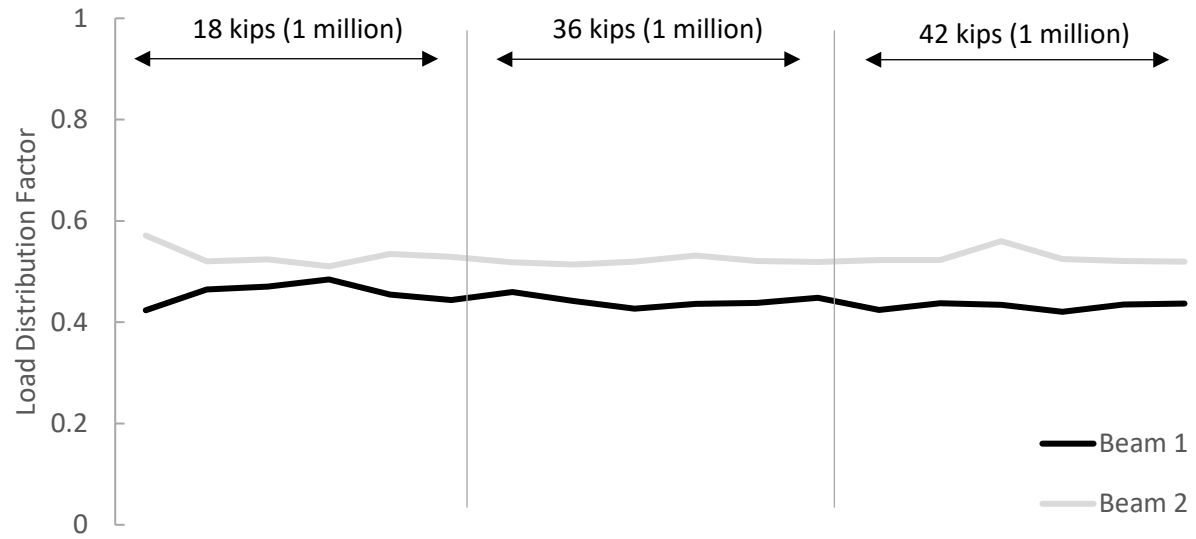
Figure 5-10 Distribution Factor Change during the first three Million Cycles with Simply

Supported Condition
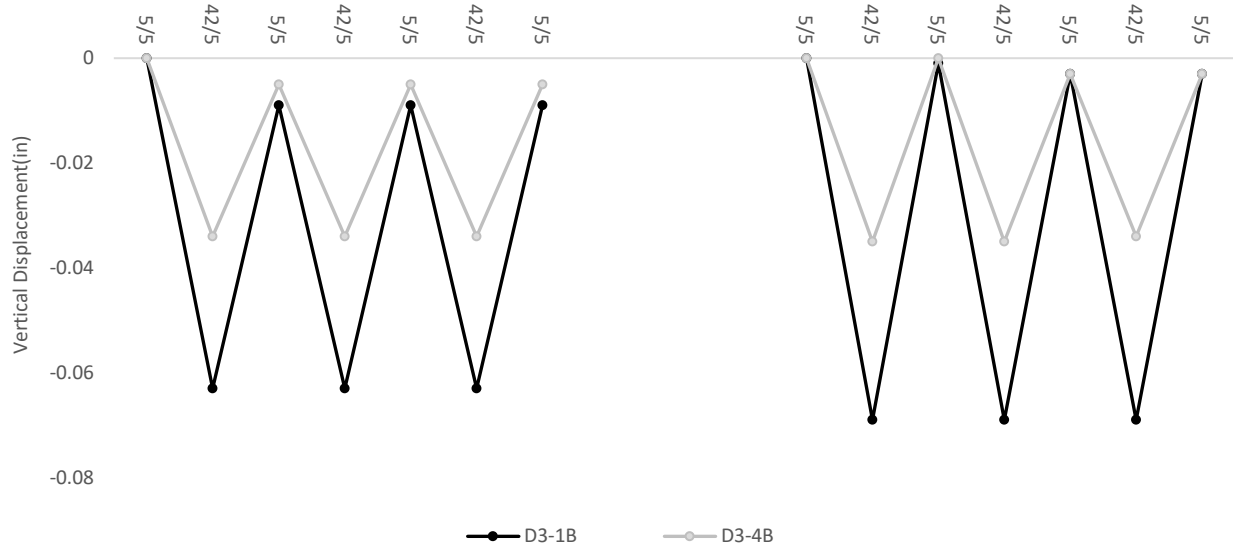
Figure 5-11 Displacement from 42kips Static Tests with Beam 1 Restrained

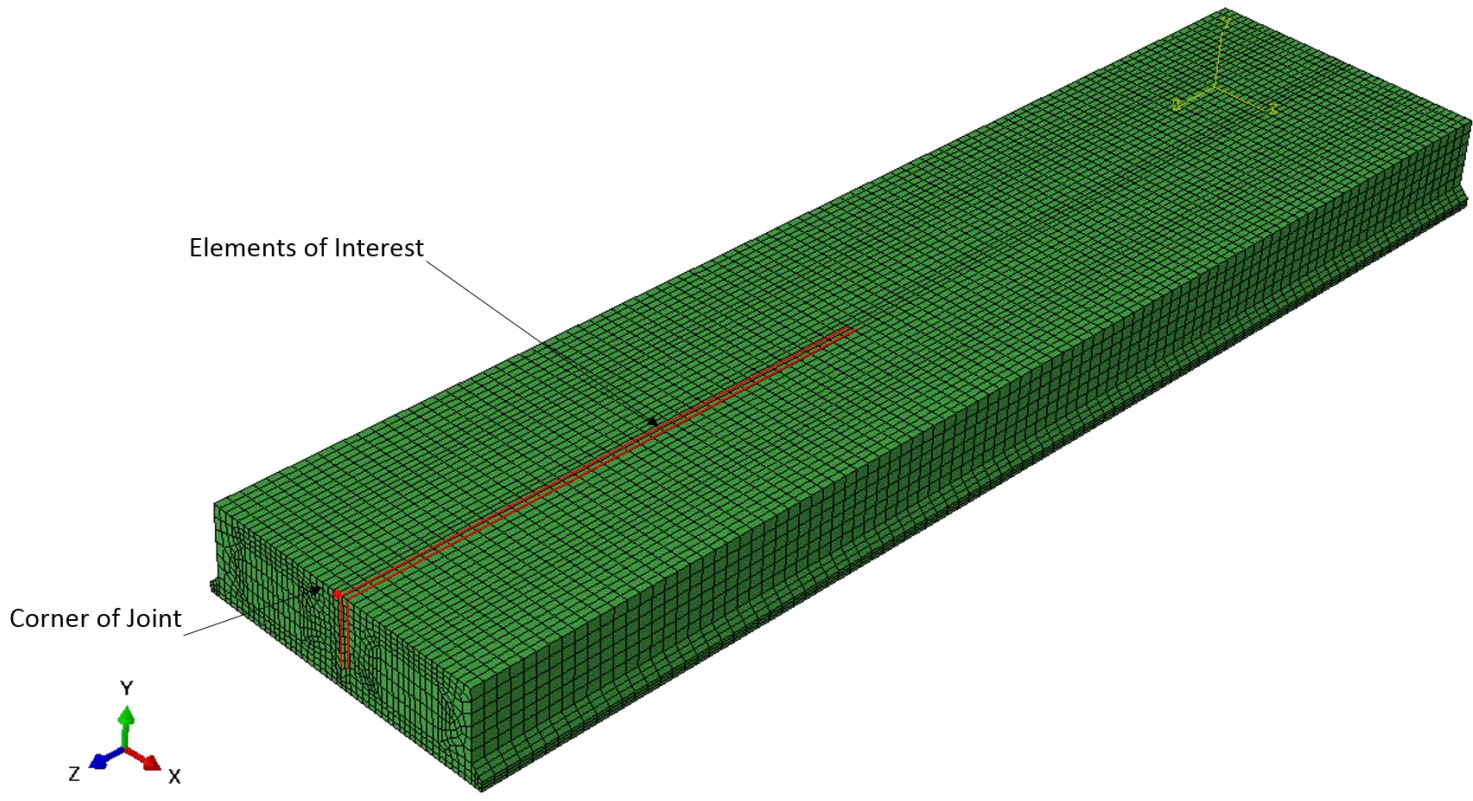**Figure 5-12 Crashed Box Girder due to Horizontal Load**

Elements of Interest

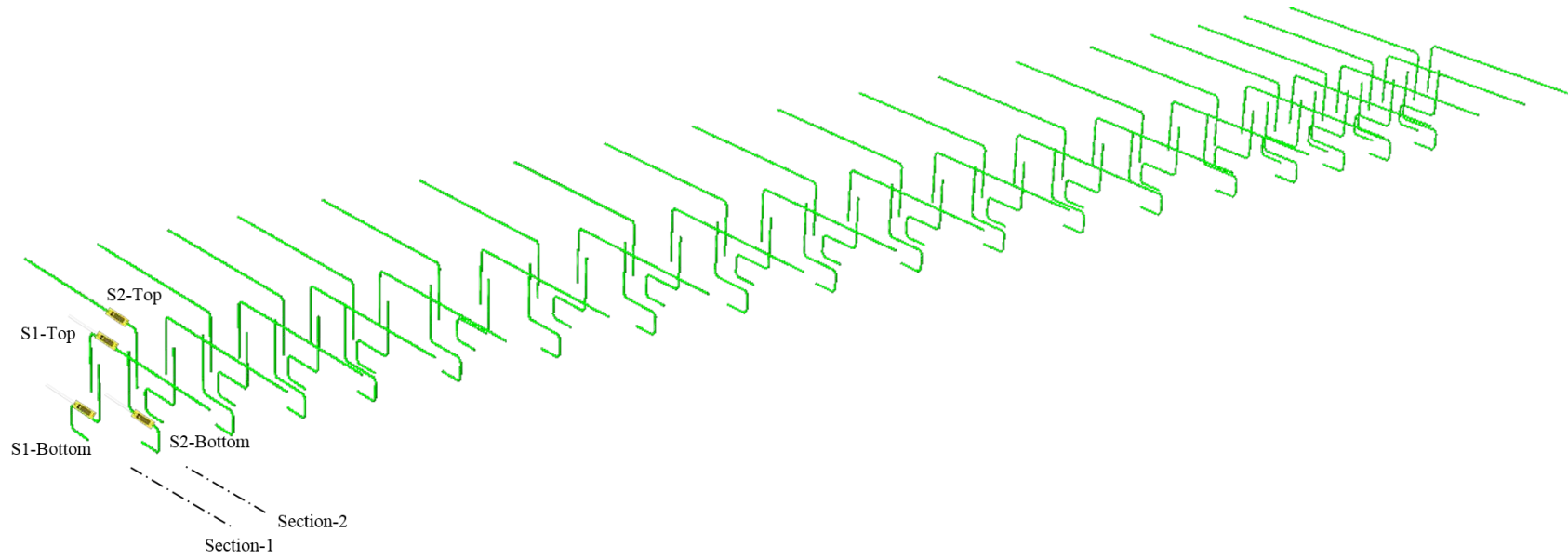Corner of Joint

Figure 5-13 Finite Element Model

Figure 5-14 Joint Reinforcing steel
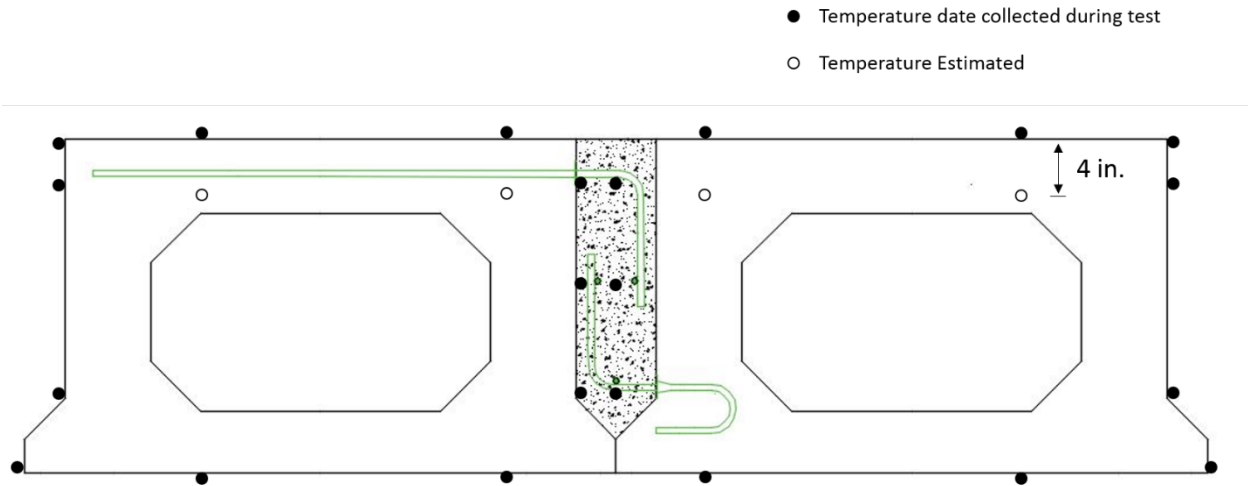
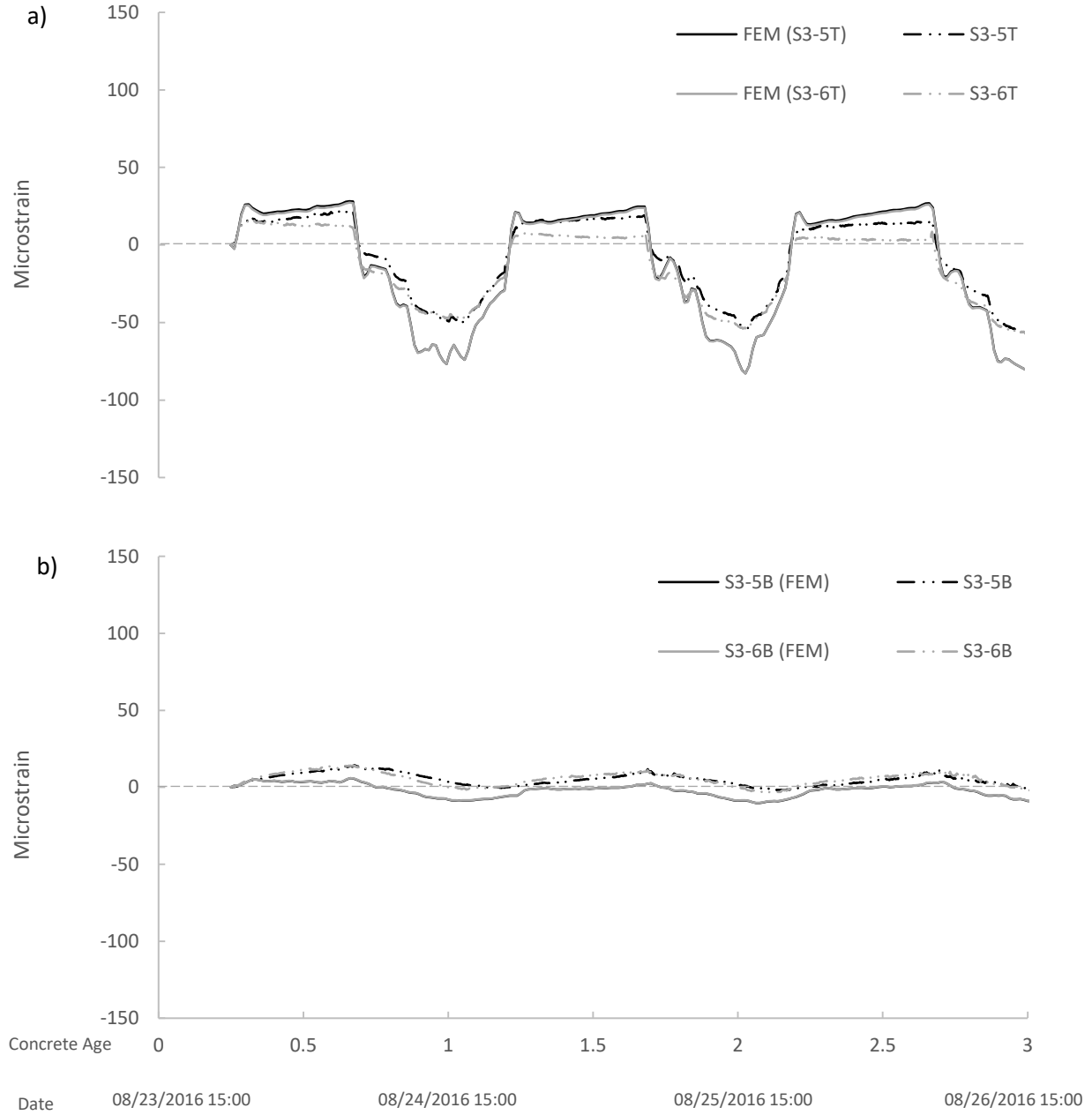**Figure 5-15 Temperature Data Input into FEM**

Figure 5-16 Model Validation by Longitudinal Strain in Section 3: a) Bottom Surface 3; b)
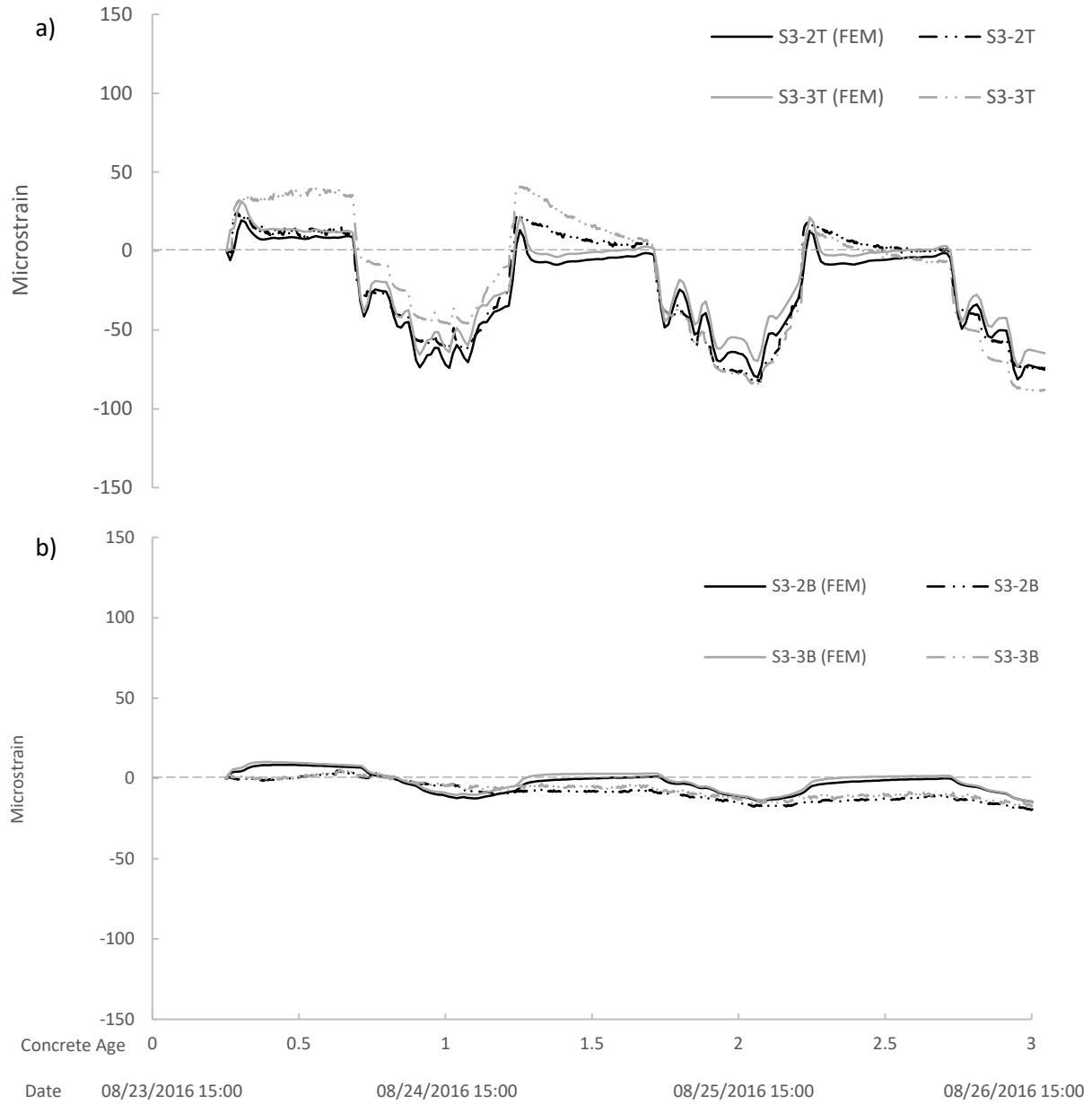
Top Surface

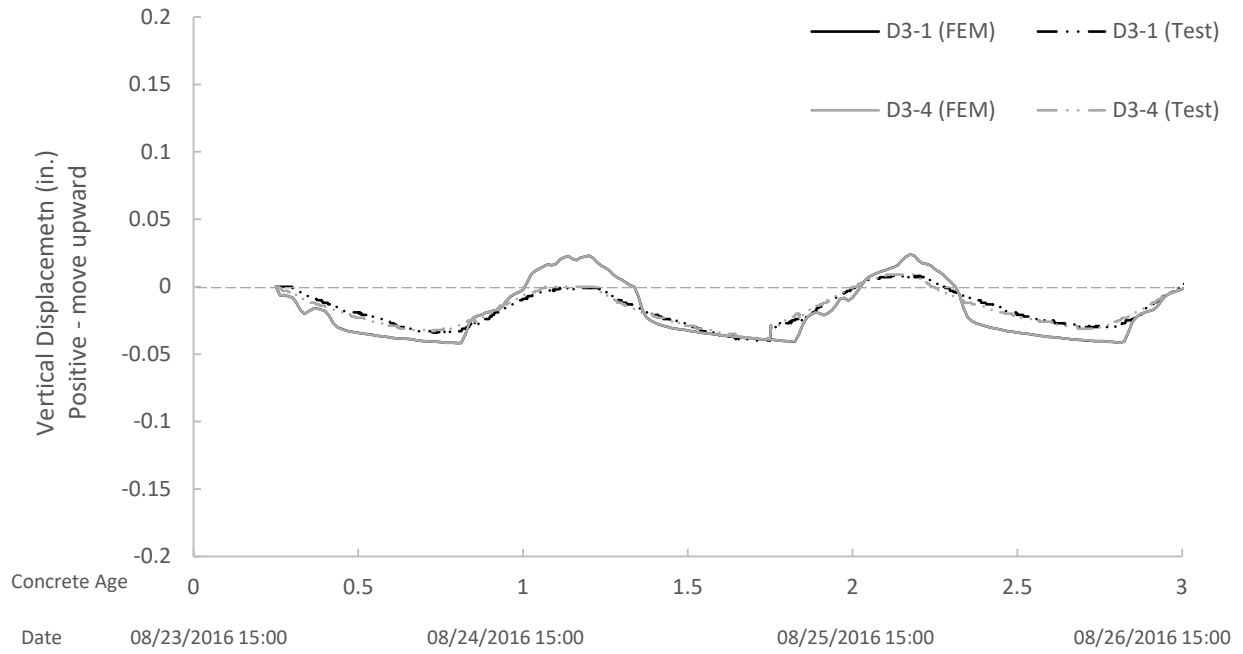**Figure 5-17 Model Validation by Transverse Strain in Section 3: a) Bottom Surface 3; b) Top Surface**

143

Figure 5-18 Model Validation by Vertical Displacement in Section 3
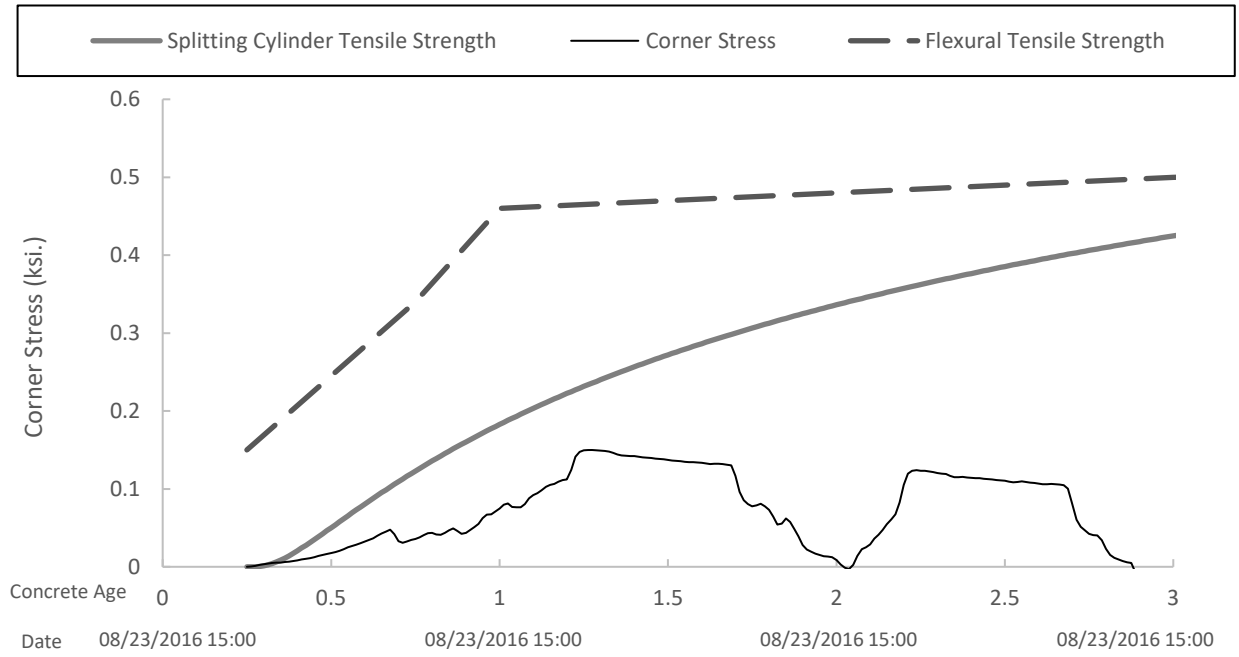
144

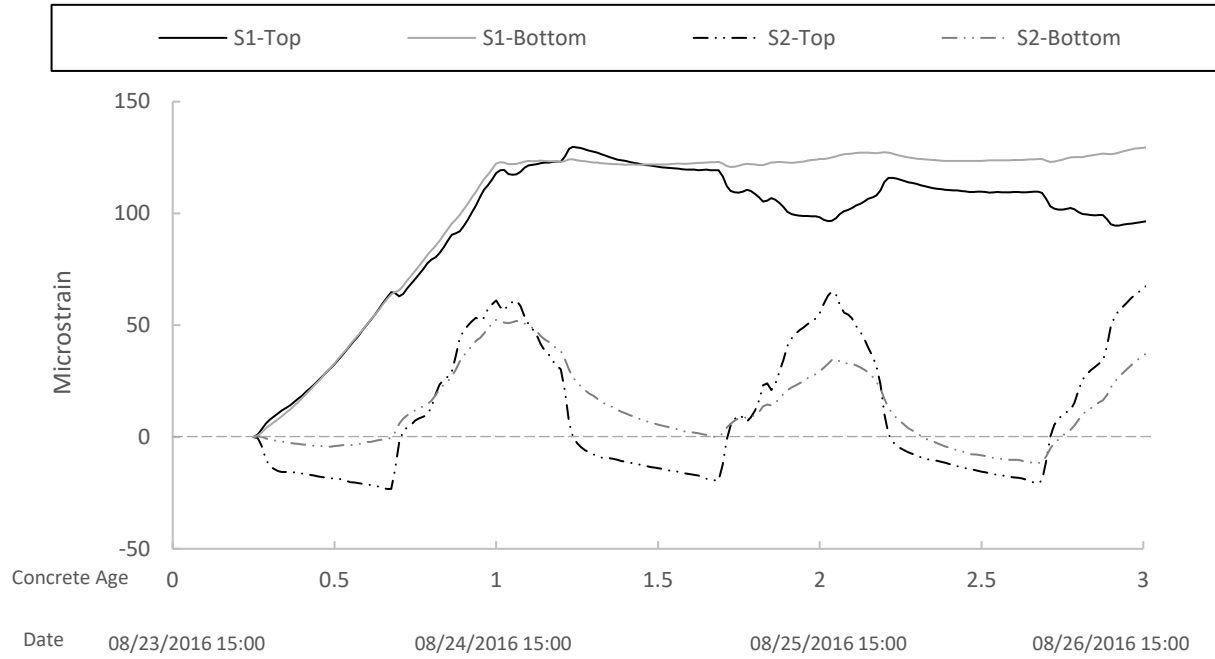**Figure 5-19 First Principal Stress Compare to Concrete Tensile Strength**

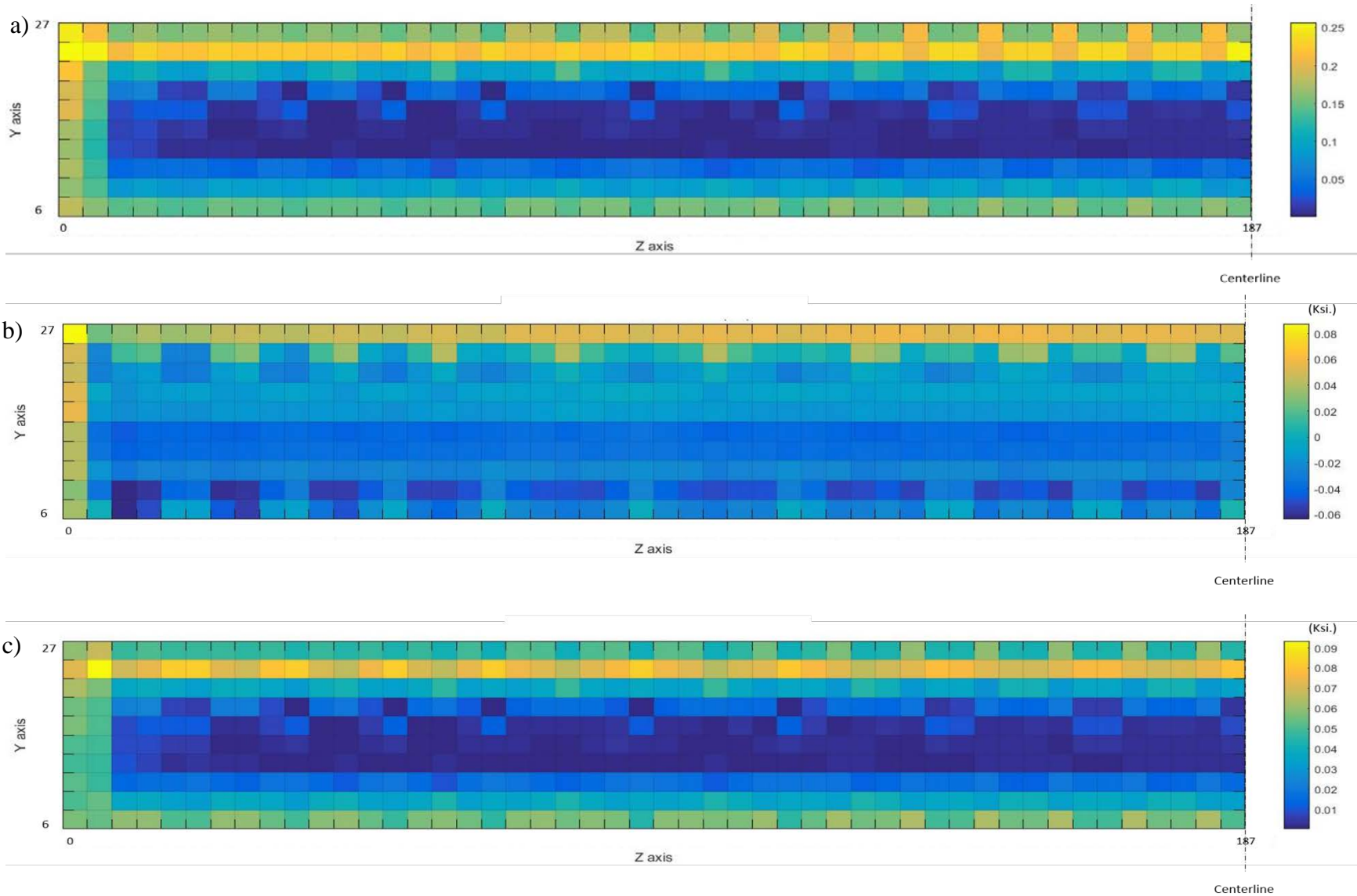**Figure 5-20 Reinforcing steel Elastic Strain**

Figure 5-21 Interface Contour Plot at 1.2day: a) Shear Stress/Strength Ratio; b) Normal Stress; c) Shear Resultants;

CHAPTER 6. SUMMARY AND CONCLUSIONS

6.1 Summary

Adjacent concrete box beam bridges constitute more than 15% of bridges built or replaced each year and have been in service for many decades. Longitudinal cracking in the joint between adjacent box beams has been a concern for decades. These cracks provide a direct path for chlorides and water to enter the structural system causing corrosion of the mild and prestressing steel that can lead to significant maintenance costs and/or safety concerns. A comprehensive review of literature from the past 20 years indicates that joint cracks are suspected to be caused by low bond strength between the joint material and box girder, large shrinkage of the joint material, stress concentrations near the shear key, and temperature changes. Many past research results pointed to the fact that an effective joint material should have small or zero shrinkage at the early-age and a small temperature induced self-volume change. It should able to achieve sufficient bond strength at the interface between the joint and the box beam starting from early-age through the entire bridge service life.

In the first step of this research, two phases of laboratory material characterization tests were performed. During Phase I, four potential joint materials were tested and evaluated based on the shrinkage, flexural tensile strength, and normal bond strength properties. The results indicate that epoxy grout is superior to construction grout for Type IV joint geometries and shrinkage compensated concrete is superior to the fiber reinforced concrete for Type V joint geometries. During Phase II, time dependent material testing was conducted on epoxy grout and shrinkage compensated concrete to characterize the nonlinear changes, bond strength, compressive and tensile strength with time. The compressive strength and split cylinder tensile

strength data were used to calibrate Kanstad's (1990) time dependent material change equation. The bond strength test indicates that both epoxy grout and shrinkage compensated concrete with the same surface treatment show a similar bond strength. However, an interface reinforced by even a minimal amount of steel has a notably higher normal bond strength than with other surface treatment approaches at both the early-age and 28 days. A finite element modeling approach which is capable of simulating the early-age joint behavior was developed and utilized for further evaluation. Two finite element models were developed for 4ft long beam-joint-beam structures with Type IV joint connected with epoxy grout and Type V joint connected with shrinkage compensated concrete. The stress distribution in the joint was output from the analytical model.

In the second step, based on the research results in the first step and the past literature, an innovative connection was designed within a 6-1⁄2in. wide joint between a roughened interface surface, filled with shrinkage compensating concrete, and reinforced by reinforcing steel. Four small scale specimens with different transverse reinforcement amount crossing the interface were designed, constructed and monitored for early-age behavior and tested to ultimate live load capacity. A finite element model was developed to simulate the early-age joint behavior and to determine the stress distribution in the joint and at the interface between the joint and the box beam concrete. Shrinkage, temperature, strain data collected during early-age monitoring was used to validate the FEM. The time-dependent stresses in the joint were compared to the time-dependent tensile strength and the Coulomb failure criteria was adopted to evaluate the bond sufficiency at the interface between the joint material and concrete.

In the third step, the innovative joint design was further evaluated experimentally and analytically on a full scale basis. A 31ft long specimen was fabricated and monitored during the

joint early-age and tested under multiple levels of the cyclic loadings. A finite element model which is capable of simulating concrete hardening was used and validated by the experimental data. The stress in the joint and the bond at the interface between the joint and box beam was investigated from the analytical model.

6.2 Conclusions and limitations

The detailed conclusions for each step were presented at the end of Chapter 3 through 5. The general conclusions have been drawn as follow:

- Self-volume change of the joint material generate internal stress during the early-age. An expansion material is better than shrinkage material since it forced a "compression-domain" joint. But the best option is the material without any early-age self-volume change, since the difference in the self-volume change between the joint material and box girder material is the cause of the early-age joint stress.

- For the same reason, a material which has similar thermal expansion characteristic as the box girder concrete material is preferred (cement based concrete rather than epoxy grout) when considering the thermal stress changes when the structure is subject to daily temperature change.

- The wide (6-½ in.) joint without shear key filled with shrinkage compensated concrete is expected to perform superior to the traditional used narrow (3/4 to 1-1/2 in.) joint with shear key filled with epoxy in resisting joint cracking and debonding at the interface. The shear key within the Type IV joint induces stress concentrations.

- Compared with the joint without reinforcement, transverse reinforcement resists the expansion of the joint material and creates a large compressive field. Transverse reinforcing steel can resist early age loadings before the joint material gains full strength, thereby

creating a mechanism to resist cracking. No.4 transverse rebar placed with a 9in. spacing is sufficient for the new innovative joint to resist early-age joint cracking.

- The temperature gradient induced by the daily temperature change generates stress gradient through the height of the beam and joint. When the temperature rises on the top surface, expansion and compressive stresses are induced on the top surface. Stress development in the joint is affected by the joint concrete placement temperature.

- Under the daily temperature change, heat of hydration, and joint concrete self-volume change, the stress in the joint is lower than the both flexural and splitting cylinder tensile strength and the time-dependent bond stress versus strength ratio is less than 1, which matches the experimental results indicating that no debonding occurs during the early age.

- The live load is not the reason that induces the joint cracks. No significant improvement in shear or moment capacity was found during the live load test. However, the specimen with smaller rebar size, but closer spacing, shows better ductility.

Based on the results of laboratory tests, the innovative connection can create a crack-free joint without the utilization of a shear key nor transverse post-tensioning. Both experimental and analytical results indicate that the innovative joint showed good performance in resisting joint cracks in both the early-age and the long-term service life of the bridge. The "compression-dominate-joint" created by the expansive joint material combined with transverse reinforcing steel across the interface is expected to overcome the difficulties in predicting the early-age internal forces during the design phase stated by AASHTO (2014).

During the investigation of the performance of this joint detail, several limitations of the evaluation were also recognized. The limitations and how additional studies might address these limitations are as below:

- Since the early-age self-volume change of the shrinkage compensated concrete can be controlled by adjusting the amount of the type K cement, a further study should be conducted to find the best mix design that can results in the minimum early-age material expansion.

- Although the effect of the transverse reinforcement in the joint was studied on small scale specimen with four different reinforcement ratio, the minimum reinforcement ratio that can keep the joint functional is unknown. The next level study could focus on the further study of the reinforcement ratio and the best reinforcing steel shape.

- The early-age time dependent model, although shows conservative results and is sufficient for the evaluation, a further analytical study could be conducted to develop a more decent model with creep and contact element at the interface between the joint material and box beams.

- The forgoing tests indicated the good performance of the innovative joint on small and full scale specimen under the lab condition. It is recommended that a field trial should be completed to study the joint performance on full bridge subject to the field environmental condition. During this field trial, the bridge should be monitored and evaluated during early age concrete curing as well as for a period of at least two years following construction.

6.3 Reference

Kanstad, T., Hammer, T. A., Bjøntegaard, Ø., & Sellevold, E. J. (1999). Mechanical properties of young concrete: Evaluation of test methods for tensile strength and modulus of elasticity. Determination of model parameters. NOR-IPACS report STF22 A99762.